2011

Resonance Raman Spectral Calculations of Organic Semiconductor Molecules

MohammadAmin Torabi
University of Windsor

Resonance Raman Spectral Calculations of Organic Semiconductor Molecules

by

Mohammad Amin Torabi

A Thesis
Submitted to the Faculty of Graduate Studies
through the Department of Physics
in Partial Fulfillment of the Requirements for the Degree of
Master of Science
at the University of Windsor

Windsor, Ontario, Canada
2011

Resonance Raman Spectral Calculations of Organic Semiconductor Molecules

by

Mohammad Amin Torabi

Approved By:

Dr.Iain Samson
Department of Earth & Environmental Sciences

Dr.Gordon Drake
Department of Physics

Dr.Chitra Rangan, Advisor
Department of Physics

Dr.Ricardo Aroca, Co–Advisor
Department of Chemistry & Biochemistry

Dr.William Baylis, Chair of Defence
Department of Physics

November 16, 2010

Author's Declaration of Originality

I hereby certify that I am the sole author of this thesis and that no part of this thesis has been published or submitted for publication.

I certify that, to the best of my knowledge, my thesis does not infringe upon anyone's copyright nor violate any proprietary rights and that any ideas, techniques, quotations, or any other material from the work of other people included in my thesis, published or otherwise, are fully acknowledged in accordance with the standard referencing practices. Furthermore, to the extent that I have included copyrighted material that surpasses the bounds of fair dealing within the meaning of the Canada Copyright Act, I certify that I have obtained a written permission from the copyright owner(s) to include such material(s) in my thesis and have included copies of such copyright clearances to my appendix. I declare that this is a true copy of my thesis, including any final revisions, as approved by my thesis committee and the Graduate Studies office, and that this thesis has not been submitted for a higher degree to any other University or Institution.

Abstract

Organic semiconductors have received a great deal of attention in recent years due to their optoelectronical properties and their potential applications in industry. In this thesis, resonance Raman calculations of a family of organic semiconductor dyes: perylene tetracarboxylic diimides (PTCD) derivatives, are presented. Also the UV/vis, infrared and normal Raman spectra, structures and molecular orbitals, excitation energies, dipole moments, (hyper) polarizabilities and charge population analyses of these molecules are calculated. The calculations in this thesis are performed using a Time-Dependent Density Functional Theory (TDDFT) method, and for that, the Amsterdam Density Functional program package (ADF2009) is used. The molecular properties calculated for the molecules in this thesis are then compared with experimental data and the main spectroscopic characteristics are found to be, for the most part, due to the perylene plane and therefore, the same for all of its derivatives.

A theoretical treatment of Raman scattering and computational chemistry methods are also reviewed in this thesis.

Acknowledgement

First and foremost, I am heartily thankful to my parents and my siblings who have been a constant source of encouragement and reassurance, while I am away from them. My love for them is eternal and what is best in me, I owe it to them.

I am thankful to my advisor *Dr.Chitra Rangan* for accepting me as her student, and for allowing me to pursue my studies in the direction I have chosen. It was a great opportunity for me to be here and interact with people from all around the globe in a friendly and safe environment, and I owe it all to her. I also thank her for her financial support.

I would like to express my sincere gratitude to my co-advisor *Dr.Ricardo Aroca* for providing me with invaluable resources and knowledge. This work would not be possible without his guidance. I am deeply indebted to him and I cannot thank him enough.

I should also thank *Dr.Matt Kundrat, Dr.Alexei Yakovlev* and *Dr.Erik van Lenthe* from the Scientific Computing and Modelling (SCM) company for guiding me in working with ADF. I should also thank *Dr.Jochen Autschbach* from SUNY at Buffalo for his advice on excitation energy and resonance Raman calculations, and *Dr.Jemmy Hu*, Sharcnet HPC Analyst, for helping me in debugging my calculations in Sharcnet.

I also had the benefit to discuss and learn concepts in computational chemistry from two chemistry graduate students: *Bahareh Khalili* from the University of Western Ontario and *Ariel Guerrero* from the University of Windsor, and I want to take the opportunity to thank them.

Furthermore, I want to thank my friend *Erfan Baghani* who helped me greatly in my first days in Windsor.

Contents

List of Figures

List of Tables

Nomenclature

ADF	Amsterdam Density Functional
AO	Atomic Orbital
CI	Configuration Interaction
DFT	Density Functional Theory
GGA	Generalized Gradient Approximation
GTO	Gaussian-Type Orbitals
HF	Hartree-Fock
HK	Hohenberg-Kohn
HOMO	Highest Occupied Molecular Orbital
HPA	Hirshfeld Population Analysis
KHD	Kramers-Heisenberg-Dirac
KS	Kohn-Sham
LDA	Local Density Approximation
LUMO	Lowest Unoccupied Molecular Orbital
MO	Molecular Orbital
MPA	Mulliken Population Analysis
NRS	Normal Raman Scattering
PES	Potential Energy Surface
RRS	Resonance Raman Scattering
SERS	Surface Enhanced Raman Scattering
STO	Slater-Type Orbitals
TDDFT	Time Dependent Density Function Theory
VDD	Voronoi Deformation Density
XC	Exchange-Correlation

Preface

While the cornerstone of the electronics industry in the past was limited to metals, insulators and inorganic semiconductors, the emergence and development of organic semiconductors, with many advantages over their inorganic analogues, has been revolutionary. The great development in this research area is driven by many industrial applicaitons, such as in large area flat displays, light emitting diodes and thin layers of transistors [1]. Among these organic compounds are the perylene derivatives, which are archetypal semiconductor molecules that have been commonly utilized for the fabrication of such organic devices.

A deeper knowledge of the optoelectronic properties of these organic semiconductors would lead to an improved design and performance of these devices. To obtain such a knowledge, vibrational spectroscopy is commonly practiced. Infrared absorption and Raman scattering are famous for being complementary versatile tools for the investigation and identification of these materials [2]. Moreover, interpretation of resonance Raman spectra provides detailed information about the internal vibrational modes elongated between the electronic ground and excited states.

A number of quantum ab-initio methods, having roots in the Hartree-Fock theory, have become available in the past decades for calculating the spectroscopic characteristics of electronic systems. However, due to their large computational cost, their applications have been restricted to small molecules. For molecules in which the cost of these ab-initio methods is restrictive, an effective computational approach with lower cost was required. For this purpose, Density Functional Theory has received a great deal of attention in recent years, and has provided a cost-effective method for the investigation of the molecular properties of large electronic systems [3].

In this thesis, infrared, UV/Vis, noraml and resonance Raman calculations of some perylene derivatives, using time-dependent density functional theory method of the Amsterdam density functional program package are presented, to yield detailed insight into their structure. Chapter One contains a brief summary of the theory of infrared absorption and Raman scattering. Chapter Two deals with a description of some computational chemistry methods, with an emphasis on density functional theory. Chapter Three contains a brief explanation of the essential settings of ADF calculations, and also the presentation and discussion of the main spectroscopic results from the calculations done on one of the perylene derivatives (PTCDA). Chapter Four summarizes the main results and extends some suggestions for future development of this research. Appendix

A presents an analytical derivation of the irreducible representation of BBIP-PTCD. Appendix B reviews some charge population analysis, and finally, detailed information about all of the calculations done on PTCDA and other perylene derivatives are presented in Appendix C.

1 Theoretical Treatment of Raman Scattering

1.1 Introduction

Vibrational spectroscopy, mainly infrared absorption and Raman scattering [4] [5] are versatile complementary tools which are widely used to reveal valuable encrypted information about the properties and structure of molecules. Infrared absorption may happen when the incident photon has a matching frequency between two vibrational states and is observed in the middle and far infrared regions of the electromagnetic spectrum. Raman scattering on the other hand, couples vibrational and electronic states, and therefore needs a much higher frequency photon.

A molecule's vibrational spectrum is its unique property and can be used as a fingerprint for identification [6] [2] when compared to a reference. Whether a vibration shows up in the infrared or Raman spectrum is determined by specific selection rules. These selection rules can be derived when the symmetry of a molecule is known, but the intensity and the position of each transition is determined by molecular composition (mass and charge) and molecular potential. Furthermore, the transition in infrared absorption is seen when there is a change in the molecule's dipole moment, but the virtual transition [7] in Raman scattering is capable of changing the molecule's polarizability [8] [9].

In this chapter, a description of selection rules based on molecular symmetry and a theoretical explanation of infrared absorption and Raman scattering, on- and off-resonance, are reviewed.

1.2 Infrared Absorption

Molecular vibrations involve displacements of all the atoms inside a molecule; however, they can be explained as a linear combination of normal vibrational modes, each with an irreducible representation of the molecule's symmetry. The collective displacement of all the atoms in a particular normal mode can be thought of as a simple harmonic motion around a minimum in the potential energy surface. Therefore, the quantum mechanical description of harmonic oscillators with a normal coordinate q, which carries the symmetry of that particular vibrational mode, can be applied.

Once irradiated by electromagnetic waves, the molecule will experience a perturbing Hamiltonian [10], which in the energy basis is written as:

$$\hat{H}_{nm} = -\langle v_n|\hat{\mu}|v_m\rangle E_0 \cos(\omega t), \tag{1.1}$$

and is responsible for the coupling between the vibrational states $|v_n\rangle$ and $|v_m\rangle$.

The strength of the transition is determined by the transition dipole moment:

$$\mu_{nm} = \langle v_n|\hat{\mu}|v_m\rangle = \int_{-\infty}^{+\infty} v_n \hat{\mu} v_m dq, \tag{1.2}$$

which for a small vibration around the equilibrium can be written as:

$$\mu_{nm} = \mu_0 \int v_n v_m dq + \left(\frac{d\hat{\mu}}{dq}\right)_0 \int v_n q v_m dq = C \left(\frac{d\hat{\mu}}{dq}\right)_0 \delta_{n,m\pm1}. \tag{1.3}$$

in which the first integral vanishes due to the orthogonality of different eigenstates and C is a constant.

Assuming the molecule to be initially in the ground state of the harmonic oscillator, equation (1.3) shows that only the transition to the first excited state is allowed. In reality, anharmonicity of the potential energy curve should be considered for a more precise interpretation of infrared spectra.

For the transition dipole moment μ_{01} to be nonzero, the symmetry of dipole moment coefficients and each vibrational mode have to be considered. The ground state wavefunction will always be totally symmetric with A_1 irreducible representation, since it depends on the square of the normal coordinate q, and whatever the symmetry of q is, the square of it would be totally symmetric. The first excited state would have the same symmetry as that of q since it depends on the first power of q. Finally, the irreducible representation of the dipole moment coefficients can be read from the point group character table of the molecule.

Thus, for the integral in (1.3) to be an even function, and therefore, the vibrational mode to be infrared-active, a product of three irreducible representations is required to have a totally symmetric component. Since the ground state wavefunction is already so, the normal coordinate q needs to have the same irreducible representation as one of the dipole moment coefficients.

1.3 Raman Scattering

In the Raman effect [11], monochromatic light is scattered by a molecule in which the frequencies of the scattered photons are different from those of the probe by an amount related to the molecular vibrational frequencies. Therefore, upon examining the scattered spectrum, and along with the dominant elastic collision line referred to as Rayleigh scattering [12], pairs of new lines at frequencies $\omega_0 \pm \omega_v$, $2\omega_0 \pm \omega_v, \ldots$ will also be observed, which are associated with Raman and Hyper-Raman [13] scattering processes. Here ω_0 is the probe frequency, ω_v is a vibrational frequency of the molecule, and the positive (negative) shifts, with respect to the probe, are known as anti-Stokes (Stokes) shifts.

Unlike absorption effects, the incident light in the Raman effect does not need to match the difference between two energy states. Instead, the incident light is responsible for making the transition by perturbing the states of the molecule through the frequency-dependent transition dipole moments. However, if a laser frequency is adjusted to an electronic state, an increase in the intensity of the scattered light is observed, and it is then referred to as Resonance Raman Scattering (RRS) [14] [15]. The figure below shows a comparison of the energy levels for infrared, normal & resonance Raman and UV/vis.

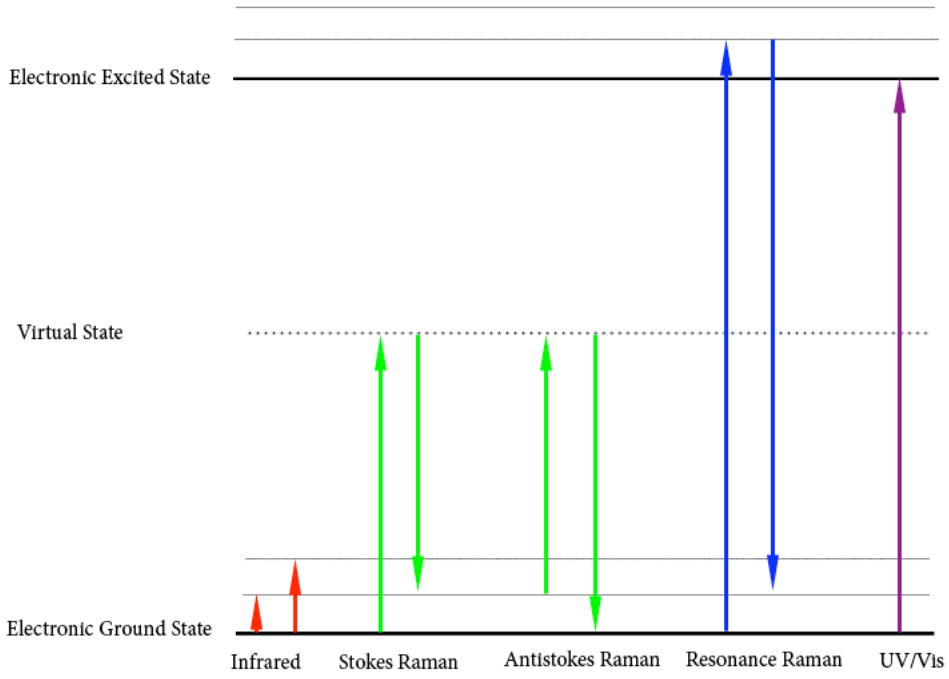

Figure 1: Comparison of the energy levels

1.3.1 Polarizability

In molecules with a nonzero polarizability, an external field changes the charge distribution within the molecule. The total induced dipole moment vector is related to the incident electric field, and its components are defined as:

$$\mu_\rho = \alpha_{\rho\sigma} E_\sigma + \beta_{\rho\sigma\tau} E_\sigma E_\tau + \dots , \tag{1.4}$$

where α and β are defined as polarizability and hyperpolarizability tensors respectively, which are molecular properties and contain information about the vibrational frequencies of the molecule. It then follows that the frequency dependence of the dipole moment (and hence the scattered photons) have contributions from both the frequency characteristics of the molecule and the probe frequency of the laser beam. In a quantum mechanical treatment of Raman scattering [16], the induced dipole moment causes a transition between two energy levels $|\psi_i'\rangle$ and $|\psi_f'\rangle$, and its strength is given by:

$$\mu_{fi} = \langle \psi_f' | \hat{\mu} | \psi_i' \rangle \, . \tag{1.5}$$

The final and the initial wavefunctions are expanded as:

$$|\psi'\rangle = |\psi^0\rangle + \epsilon\,|\psi^1\rangle + \epsilon^2\,|\psi^2\rangle \cdots . \tag{1.6}$$

The transition dipole moments in the first and second order are then written as:

$$(\mu_\rho)^1_{fi} = \langle\psi^1_f|\hat{\mu}_\rho|\psi^0_i\rangle + \langle\psi^0_f|\hat{\mu}_\rho|\psi^1_i\rangle\,, \text{ and} \tag{1.7}$$

$$(\mu_\rho)^2_{fi} = \langle\psi^2_f|\hat{\mu}_\rho|\psi^0_i\rangle + \langle\psi^0_f|\hat{\mu}_\rho|\psi^2_i\rangle + \langle\psi^1_f|\hat{\mu}_\rho|\psi^1_i\rangle\,. \tag{1.8}$$

which give the polarizability and hyper-polarizability tensors respectively, through the equation (1.4). Perturbation theory is then used to obtain the first order transition dipole moment [17] and the Kramers-Heisenberg-Dirac (KHD) equation for polarizability [18] [19] as:

$$\mu^1_{fi}(t) = \frac{e^{i\left(\omega_{fi}-\omega_0\right)t}}{2\hbar}\sum_r\left(\frac{\mu^0_{fr}\,(\mu^0_{ri}\cdot E)}{\omega_{ri}-\omega_0-i\Gamma_r} + \frac{\mu^0_{ri}\,\left(\mu^0_{fr}\cdot E\right)}{\omega_{rf}+\omega_0+i\Gamma_r}\right), \tag{1.9}$$

$$(\alpha_{\rho\sigma})_{fi} = \frac{1}{\hbar}\sum_r\left(\frac{\langle\psi^0_f|\mu_\rho|\psi^0_r\rangle\,\langle\psi^0_r|\mu_\sigma|\psi^0_i\rangle}{\omega_{ri}-\omega_0-i\Gamma_r} + \frac{\langle\psi^0_f|\mu_\sigma|\psi^0_r\rangle\,\langle\psi^0_r|\mu_\rho|\psi^0_i\rangle}{\omega_{rf}+\omega_0+i\Gamma_r}\right), \tag{1.10}$$

in which $\mu^0_{ri} = \langle\psi^0_r|\mu|\psi^0_i\rangle$ is the unperturbed dipole moment and Γ_r is the width of the level r, related to the lifetime of this level through the uncertainty principle.

It can be seen from the KHD equation that the relative magnitude of the probe frequency ω_0 and the absorption frequency ω_{ri} is indeed very important. Whenever they are close to each other, the second term in (1.10) can be ignored, while in the first term, the state r is dominant among others in the sum and the intensity is greater due to the denominator being very small (i.e. RRS). Therefore, the resonance polarizability tensor will show the characteristics of mainly one, or at most two, excited state(s). In this sense, RRS becomes an important tool for studying the properties of individual excited states [20]. Also for the numerator in (1.10) to be nonzero, the transition from the initial state to a state r, *and* the transition from the state r to the final state, should both be dipole-allowed.

1.3.2 Selection Rules

While in infrared spectroscopy, the selection rules were determined by the symmetry of a single dipole moment μ, equation (1.10) shows that in Raman spectroscopy a product of two of them has to be considered. Therefore, the polarizability tensor coefficients transform like the multiplication of two vectors, i.e. $\Gamma(\alpha_{xy}) = \Gamma(xy)$, which means that for the product

$$\Gamma\left(\psi_1\right) \otimes \Gamma\left(\alpha_{\rho\sigma}\right) \otimes \Gamma\left(\psi_0\right), \tag{1.11}$$

to have a totally symmetric component and therefore Raman-active, a vibrational mode, and hence the first excited state, has to have the same irreducible representation as one of $\rho\sigma$.

In centrosymmetric molecules, infrared active modes are ungerade because coordinate axes change direction under inversion, while Raman active modes are gerade because a product of coordinate axes remains symmetric under the inversion. In this sense, any vibration in centrosymmetric molecules is either infrared-active or Raman-active by the mutual exclusion rule [21].

1.3.3 Herzberg-Teller Coupling

The Born-Oppenheimer approximation ignores any dynamical electronic and nuclear coupling by separating the complete wavefunction as $|\psi_{Tot}\rangle = |e\rangle\,|v\rangle$, but the electronic Hamiltonian and also the electronic wavefunctions always depend, although slightly, on the motion of the nuclei. To include such interaction, the electronic Hamiltonian can be expanded in normal displacements as:

$$H_e = H_0 + \sum_k \left(\frac{\partial H_e}{\partial q_k}\right) q_k + \cdots, \tag{1.12}$$

and the first order correction to the perturbed electronic wavefunction $|e'_r\rangle$ can be obtained using the perturbation theory [22] to be:

$$|e_r\rangle^1 = \frac{1}{\hbar} \sum_{s \neq r} \sum_k \frac{\langle e_s|H'|e_r\rangle}{\omega_{rs}} q_k\,|e_s\rangle, \tag{1.13}$$

in which H' is the second term in (1.12). It can be seen from equation (1.13) that as a result of nuclear perturbation, electronic states are mixed and so are the dipole moments:

$$\langle e'_r|\mu_\sigma|e'_g\rangle = (\mu_\sigma)^0_{\sigma rg} + \frac{1}{\hbar}\sum_{s\neq r}\sum_k q_k\,(\mu_\sigma)^0_{sg}\,\frac{\langle e_s|H'|e_r\rangle}{\omega_{rs}} + \frac{1}{\hbar}\sum_{t\neq g}\sum_k q_k\,(\mu_\sigma)^0_{rt}\,\frac{\langle e_t|H'|e_r\rangle}{\omega_{gt}}, \tag{1.14}$$

where $\mu^0_{sg} = \langle e^0_s|\mu|^0_r\rangle$ is the unperturbed electronic transition dipole moment and $\omega_{rs} = \omega_r - \omega_s$. The initial and final electronic states are also assumed to be the ground electronic state. Equation (1.14) shows that the transition between the ground state to a state r, involves transitions not only between the unperturbed ground state to the state r, but also a transition from the ground state to any state s, *and* a transition from the state r to any state t, all being pure and without the perturbation. This coupling of the states under nuclear perturbation is known as the Herzberg-Teller vibronic coupling [23]. The denominator in (1.14) also implies that mainly the states close to each other in energy contribute to the coupling.

Putting the now perturbed transition dipole moments back into the equation (1.10), the polarizability tensor can be sorted into different groups, known as Albrecht terms [24][25]

$$(\alpha_{\rho\sigma})_{v_f,v_i} = A + B + C + D \tag{1.15}$$

which for Normal Raman Scattering (NRS) follows as:

$$A = \frac{1}{\hbar}\sum_{r\neq g}\frac{2\omega_{rg}}{\omega^2_{rg}-\omega^2_0}\left\{(\mu_\rho)^0_{gr}\,(\mu_\sigma)^0_{rg}\right\}\langle v_f|v_i\rangle\,, \tag{1.16}$$

$$B + C = \frac{1}{\hbar}\sum_{r\neq g}\sum_k\left(\frac{2\omega_{rg}}{\omega^2_{rg}-\omega^2_0}\right)\left\{\left(\frac{\partial\mu_\rho}{\partial q_k}\right)_{gr}\left(\mu^0_\sigma\right)_{rg} + \left(\mu^0_\rho\right)_{gr}\left(\frac{\partial\mu_\sigma}{\partial q_k}\right)_{rg}\right\}\langle v_f|q_k|v_i\rangle\,, \tag{1.17}$$

$$D = \frac{1}{\hbar}\sum_{r\neq g}\sum_{kk'}\left(\frac{2\omega_{rg}}{\omega^2_{rg}-\omega^2_0}\right)\left\{\left(\frac{\partial\mu_\rho}{\partial q_k}\right)_{gr}\left(\frac{\partial\mu_\sigma}{\partial q_{k'}}\right)_{rg}\right\}\langle v_f|q_kq_{k'}|v_i\rangle\,, \tag{1.18}$$

It should be noted that a multiplication of two unperturbed electronic transition dipole moments contributes to the A term, while in the B and C terms a multiplication of one unperturbed and one coming from the electronic nuclear coupling is involved. Also in the D term, two perturbed dipole moments are present. These couplings show that basically many electronic excited states are involved in NRS. The damping factors in the KHD equations are also absent due to the significant difference between the probe frequency and the absorption frequencies.

1.4 Cross Section

The intensity I of a radiation depends on the polarization of both the incident and the scattered light and the angle between them. The intensity of scattering from a molecule modelled as a classical dipole with dipole moment μ is given [26] as:

$$I = \frac{\omega^4 \mu^2 \sin^2 \theta}{32\pi^2 \epsilon_0 c^3}, \tag{1.19}$$

in which ω is the frequency of radiation and θ is the angle between the incident and scattered light. The scattering cross section $\sigma(\theta)$ and the total cross section σ_T are then defined as:

$$\sigma(\theta) = \frac{I}{\frac{1}{2} c \epsilon_0 E^2}, \tag{1.20}$$

$$\sigma_T = \int \sigma d\Omega. \tag{1.21}$$

The total cross section is an inherent property of a molecule; it is independent of the incident irradiance, but dependent on its polarization and frequency. Its unit, i.e. m^2 molecule^{-1}, implies that the total scattered radiation by a molecule with a σ cross section, corresponds to the effective area that the molecule presents to the incindent light.

Assuming a molecule sitting at the origin of the coordinate system is irradiated with an incident light from the z direction, which is linearly polarized in, say y direction, and looking for a 90° scattering in x direction being polarized in the y direction, the only components the polarizability tensor involved would be α_{yy}, which relates the y components of the polarization of the incident and scattered light through the equation

$\mu_y = \alpha_{yy} E_y$. Therefore, the scattered intensity for an incident polarizaiton y^i and a scattered polarizations y^s at 90 degree will be:

$$I\left(90^\circ,\, y^s,\, y^i\right) = \frac{\omega^4 \alpha_{yy}^2}{32\pi^2 \epsilon_0 c^3} E_y^2 = \frac{\omega^4}{16\epsilon_0^2 c^4 \pi^2} \left(\frac{45a^2 + 4\gamma^2}{45}\right) \left(\frac{1}{2} c\epsilon_0 E^2\right), \tag{1.22}$$

in which a and γ are the mean and anisotropy polarizability tensors, respectively. Assuming now that the same incident light is scattered with the same angle but with polarization in the z direction, the α_{yz} component of the polarizability tensor will be involved and the intensity of the scattering would be:

$$I\left(90^\circ,\, z^s,\, y^i\right) = \frac{\omega^4 \alpha_{yz}^2}{32\pi^2 \epsilon_0 c^3} E_y^2 = \frac{\omega^4}{16\epsilon_0^2 c^4 \pi^2} \left(\frac{\gamma^2}{15}\right) \left(\frac{1}{2} c\epsilon_0 E^2\right), \tag{1.23}$$

Supposing the intensity of scattering from N molecules to be N times the intensity from one molecule, the above equations have to be multiplied by the population of molecules in the initial state v_i, which is given by the Maxwell-Boltzmann distribution.

The depolarization ratio is:

$$\rho\left(90^\circ,\, y^i\right) = \frac{I\left(90^\circ,\, z^s,\, y^i\right)}{I\left(90^\circ,\, y^s,\, y^i\right)} = \frac{3\gamma^2}{45a^2 + 4\gamma^2}, \tag{1.24}$$

For linearly polarized light at 90°, depolarization ratio is always positive and less than $\frac{3}{4}$. For symmetric vibrations in symmetric molecules, anisotropy approaches zero and the depolarization ratio is close to zero.

1.5 Resonance Raman Scattering

When the probe frequency approaches that of one of the absorption bands, the electronic excited state involved in the absorption becomes dominant among others in the sum, and a Raman scattering enhancement of up to 10^6 may be observed. This is known as Resonance Raman Scattering (RRS). In this sense, RRS works as a combination of selection and enhancement, and this is unlike the case in electronic absorption in which only the selection is achieved. In both electronic absorption and RRS, an excitation from the ground state to an upper state occurs. In absorption, the electron stays in the excited state long enough for the nuclei to reach a new equilibrium and then decays, while in scattering it de-excites very fast, on a timescale of 10^{-14} s, that nuclei hardly

move. The excess energy in case of absorption is either dissipated as heat, or emitted as fluorescence [27] in which a radiationless relaxation to the lowest vibrational state in the excited state precedes the emission to the electronic ground state. It should also be noted that since water Raman-active vibrations have a very small cross section, albeit being strongly IR-active, RRS has become an important probe in studying bio-molecules in an aqueous environment [28].

According to the Albrecht's terms, all the vibrational states in the ground state as well as one of the excited states have to be considered. Also, the damping factors are now important and must be taken into account because they are comparable to the difference between the probe and the absorption frequency. Assuming again that the initial and final electronic states are the ground state, the A and B terms will be [29]:

$$A = \frac{1}{\hbar} \left(\mu_\rho^0\right)_{gr} \left(\mu_\sigma^0\right)_{rg} \sum_{v_r} \left(\frac{\langle v_f | v_r \rangle \langle v_r | v_i \rangle}{\omega_{rg} - \omega_0 - i\Gamma_r} \right), \tag{1.25}$$

$$\begin{aligned} B = &\frac{1}{\hbar^2} \left(\mu_\rho^0\right)_{gs} \frac{\langle e_s | H' | e_r \rangle}{\omega_{rs}} \left(\mu_\sigma^0\right)_{rg} \sum_{v_r} \left(\frac{\langle v_f | q_k | v_r \rangle \langle v_r | v_i \rangle}{\omega_{rg} - \omega_0 - i\Gamma_r} \right), \\ &+ \frac{1}{\hbar^2} \left(\mu_\rho^0\right)_{gr} \frac{\langle e_r | H' | e_s \rangle}{\omega_{rs}} \left(\mu_\sigma^0\right)_{sg} \sum_{v_k^r} \left(\frac{\langle v_i | v_r \rangle \langle v_r | q_k | v_i \rangle}{\omega_{rg} - \omega_0 - i\Gamma_r} \right). \end{aligned} \tag{1.26}$$

The C and D terms in RRS are negligible since they contribute to overtones and binary combinations. For the A term, known as the Franck-Condon term [30] to be nonzero, the transition from the ground state to the excited state r should be allowed. Moreover, orthogonality of the vibrational wavefunctions implies that for the numerator in equation (1.25) to be nonzero, the vibrational quantum numbers should be the same, i.e. $v_f = v_r$, which contributes only to Rayleigh scattering. Nonorthogonality, and so Raman scattering, arises when either the shape of the potential energy curve in the ground and excited states are different, or there is a displacement in their minima. Thus, the A term contribution to scattering is significant when there is a large overlap between the ground and excited vibrational state, as a function of the normal coordinate displacement.

In the B term, known as Herzberg-Teller term, the transition from the ground state to the electronic excited states r and s should be allowed, and the electronic excited states r and s should themselves be coupled by the perturbed Hamiltonian. Their energies should also be close to each other due to the frequency denominator, and this is usually the case in $\pi \to \pi^*$ transitions in amides [31]. This implies that in the B term only one

excited state $|e_s\rangle$, other than the absorption state $|e_r\rangle$, should be considered.

For the numerator in equation (1.26) to be nonzero, we should have $v_f = v_i \pm 1$. Assuming the electrons to be initially in the lowest energy, it follows that the scattering transition proceeds as $|e_g\rangle|v_0\rangle \rightarrow |e_r\rangle|v_0\rangle \rightarrow |e_g\rangle|v_1\rangle$ which is known as the $0-0$ resonance. The scattering involved in the second term in equation (1.26) is known as $0-1$ resonance and proceeds as $|e_g\rangle|v_0\rangle \rightarrow |e_r\rangle|v_1\rangle \rightarrow |e_g\rangle|v_0\rangle$. The B term is therefore, restricted to the transition between the ground and the first vibrational state, while there is no such restriction in the A term scattering.

1.6 In This Thesis

Although the establishment of the resonance Raman theory dates back half a century with the work of Albrecht and his colleagues [24] [32] [33], and the first experimental observation of it goes back even earlier [34], the computational analysis of resonance Raman spectra is very complicated and has been tried only very recent [35] [36] [37] [38].

In this thesis, a combination of infrared, UV/vis, normal and resonance Raman spectra of a family of perylene tetracarboxylic di-imides (PTCD) derivatives are studied to provide complementary information about the chemical composition and optoelectronic properties of the them, and quantative comparisons with experimental results are also made. This class of π-conjugated organic molecules are chosen because of their thermal stability, high electronic mobility and high quality of deposited films on different substrates which has made them interesting in applications such as in organic light emitting diodes and flat panel displays.

2 Quantum Chemistry Calculation

2.1 Introduction

Paul Dirac remarked in his famous paper [39] in 1929 that: "The general theory of quantum mechanics is now almost complete... The underlying physical laws necessary for the mathematical theory of a large part of physics and the whole of chemistry are completely known, and the difficulty is only that the exact application of these laws leads to equations much too complicated to be soluble. It therefore becomes desirable that approximate practical methods of quantum mechanics should be developed, which can lead to an explanation of the main features of the complex atomic systems without too much computation."

Since then, different methods have been developed to increase the quality of the approximations and at the same time reduce the cost of computations, and new developments are reported as part of the quantum chemistry research. In this chapter, a review of some of the popular ones, especially the Hartree-Fock method and the density functional theory is presented.

2.2 Electronic Structure

The starting point for the calculation of the properties of electronic systems is the Schrödinger equation. For an isolated molecule including N nuclei and n electrons, the Hamiltonian in atomic units is given as:

$$\hat{H} = \sum_{i=1}^{n} \frac{-\nabla_i^2}{2} + \sum_{\alpha=1}^{N} \frac{-\nabla_\alpha^2}{2M_\alpha} + \sum_{i,j>i}^{n} \frac{1}{r_{ij}} + \sum_{i,\alpha}^{n,N} \frac{-Z_\alpha}{r_{i\alpha}} + \sum_{\alpha,\beta>\alpha}^{N} \frac{Z_\alpha Z_\beta}{R_{\alpha\beta}}, \tag{2.1}$$

in which the spin interactions and relativistic effects are ignored. In this case, the wavefunction is a complex function of n electronic and N nuclear coordinates:

$$\Psi\left(R_1,\, R_2,\, \ldots R_N,\, r_1,\, r_2,\, \ldots r_n\right). \tag{2.2}$$

However, due to the large difference between the electron and nucleon mass, the Born-Oppenheimer approximation [40] simplifies the wavefunction by assuming the nuclei to be almost stationary in the timescale that electrons travel, and hence separates the electronic and nuclear degrees of freedom:

$$\Psi\left(R,\, r\right) = \Phi\left(r,\, R\right)\chi\left(R\right). \tag{2.3}$$

In this sense, the electronic wavefunction Φ depends on the nuclei positions only parametrically, so that the second term in (2.1) can be ignored and the last term is a constant. Even so, the electronic part is still complicated and further simplifications are required.

2.3 Thomas-Fermi Model

The Thomas-Fermi model, in which the Density Functional Theory (DFT) is rooted, was introduced [41] [42] soon after the Schrödinger equation, as an attempt to calculate the atomic fields using a local density approximation. The main idea in this theory is to keep away from the calculation of wavefunctions which depend on $3n$ variables, and instead focus on the 3-dimensional charge density $\rho\left(r\right)$ as the main variable. Furthermore, the model assumes that all of the electrons in the system see a uniform potential field $V\left(r\right)$ and writes the total energy of an electronic system as:

$$E\left(\rho\right) = C_k \int \rho\left(r\right)^{5/3} dr - \int \rho\left(r\right) V\left(r\right) dr + \frac{1}{2}\int \frac{\rho\left(r\right)\rho\left(r'\right)}{\left|r - r'\right|} dr dr', \tag{2.4}$$

in which the first term is the kinetic energy density of the Fermi electron gas, the second term is the potential energy due to the attraction of the nuclei, and the last term is the repulsive interaction of the electron density with itself. (The repulsion between different nuclei would add a constant to the above equation.)

The method of Lagrange multipliers is used to find the charge density that minimizes this energy, such that the number of electrons remain constant:

$$\delta\left(E - \mu \int \rho(r) dr\right) = 0. \tag{2.5}$$

This yields the Thomas-Fermi equation in integral form for the equilibrium electron density:

$$\frac{5}{3} C_k \rho\left(r\right)^{2/3} + V\left(r\right) + \int \frac{\rho\left(r\right)}{\left|r - r'\right|} dr' = \mu. \tag{2.6}$$

in which μ is the chemical potential.

The Thomas-Fermi model was later developed by Dirac [43], to take into account the exchange interaction, and by Weizsacker [44], to improve the kinetic energy approximation.

2.4 Hartree-Fock Method

Hartree ignored [45] the interaction of electrons with each other in a molecule and assumed that the molecular wavefunction is the product of single electron spin-orbitals:

$$\Psi\left(x_1,\, x_2,\, \ldots,\, x_n\right) = \phi\left(x_1\right)\phi\left(x_2\right)\ldots\phi\left(x_n\right), \tag{2.7}$$

in which x represents both the spatial and spin degrees of freedom.

Fock developed [46] the Hartree product by writing the molecular wavefunction as a linear combination of all the permutations of electrons. In this sense, it accounts for the exchange interaction and respects the antisymmetric properties of fermion wavefunctions. Finally Slater [47] represented this in the form of Slater determinant:

$$\Psi_{HF} = \frac{1}{\sqrt{n!}}\det\left|\phi_1\phi_2\ldots\phi_3\right|. \tag{2.8}$$

For the molecular Hamiltonian:

$$\hat{H} = \sum_{i=1}^{n}\left(-\frac{1}{2}\nabla_i^2 - \sum_{\alpha=1}^{N}\frac{-Z_\alpha}{r_{i\alpha}}\right) + \sum_{i,\ j>i}^{n}\frac{1}{r_{ij}} = \sum_{i=1}^{n}H_i + \sum_{i,j>i}^{n}V_{ij}, \tag{2.9}$$

consisting of one-electron operator H_i and two-electron operator V_{ij}, the Hartree-Fock (HF) energy is [48]:

$$E_{HF} = \langle\Psi|\hat{H}|\Psi\rangle = 2\sum_{i=1}^{n}H_{ii} + \sum_{i=1}^{n}\sum_{j=1}^{n}\left(2J_{ij} - K_{ij}\right), \tag{2.10}$$

in which:

$$H_{ii} = \langle\phi_i|H_i|\phi_i\rangle, \tag{2.11}$$

$$J_{ij} = \langle\phi_i(r_1)\phi_j(r_2)|\frac{1}{r_{12}}|\phi_i(r_1)\phi_j(r_2)\rangle, \tag{2.12}$$

$$K_{ij} = \langle \phi_i(r_1)\phi_j(r_2)|\frac{1}{r_{12}}|\phi_i(r_2)\phi_j(r_1)\rangle \,, \tag{2.13}$$

H_{ii} consists of two parts: one being the average kinetic energy, and the other being the attractive potential energy between electrons and nuclei. J_{ij} is called the Coulomb integral and represents the interaction of the charge density in orbital i with the one in orbital j, and leads to the mean-field characteristic of the HF theory. However, K_{ij} does not have a classical analogue and comes from the antisymmetric property of the electronic wavefunctions. It resembles the J_{ij} except that it exchanges the spin orbital ϕ_i and ϕ_j and so is referred to as the exchange energy.

The method of Lagrange multipliers is used to find the Molecular Orbitals (MO) that minimize energy but are constrained to be orthonormal, as follows:

$$\delta \left(E_{HF} - \sum_{i,\ j} \mu_{ij} \langle \phi_i | \phi_j \rangle \right) = 0, \tag{2.14}$$

which yields the HF equations:

$$\left[H_i(r) + \sum_j \left(2\hat{J}_j(r) - \hat{K}_j(r) \right) \right] \phi_i(r) = \sum_j \mu_{ij}\phi_j(r), \tag{2.15}$$

where the operators J_j and K_j are defined as:

$$\hat{J}_i(r) = \int \phi_i^*(r') \frac{1}{|r - r'|} \phi_i(r') dr', \tag{2.16}$$

$$K_i(r) = \int \phi_i^*(r') \frac{1}{|r - r'|} \phi_j(r') dr'. \tag{2.17}$$

The main source of error in the HF method is the ansatz, being only a single Slater determinant. There are some post Hartree-Fock procedures, based on either perturbation theory or variational principle, that reduces the error in HF energy, known as the correlation energy:

$$E_{corr} = E_0 - E_{HF}, \tag{2.18}$$

in which E_0 is the real energy of the system.

2.5 Configuration Interaction

The Configuration Interaction (CI) theory [49] goes beyond the HF theory by assuming the molecular wavefunction to not just be a single Slater determinant, but a linear combination of them. Each term in the linear combination corresponds to a different orbital scheme or "configuration" in which an occupied orbital is replaced by an unoccupied one.

The molecular wavefunction in this case is written as:

$$\Psi = c_0\Psi_{HF} + \sum_{i}^{occ.}\sum_{r}^{unocc.} c_i^r\Psi_i^r + \sum_{i<j}^{occ.}\sum_{r<s}^{unocc.} c_{ij}^{rs}\Psi_{ij}^{rs} + \sum_{i<j<k}^{occ.}\sum_{r<s<t}^{unocc.} c_{ijk}^{rst}\Psi_{ijk}^{rst} + \cdots, \tag{2.19}$$

in which Ψ_i^r is called a single (S) excitation Slater determinant and is the ground state HF Slater determinant, except that the occupied spin-orbital i is replaced by an upper unoccupied spin-orbital r. If all of the S determinants are considered and the expansion in (2.19) is truncated after the second term, we have the CIS method. The next terms in the expansion would correspond to the double (D), triple (T) and quadruple (Q) excitation Slater determinant, and hence CISD, CISDT, CISDTQ. It can go on until we have a Full Configuration Interaction (FCI) calculation which is indeed very accurate but time-consuming. The reference HF Slater determinant is still expected to be the dominant part in all of these molecular calculations, and the other terms contribute a small correction to the correlation energy.

The CI wavefunction is constrained to be normalized and is supposed to yield the minimum energy. The ground state eigenvalue equation can then be solved [50] by the the method of the Lagrange multipliers to be:

$$\sum_{i,r} H_{i,j}^{r,s} c_j^b = E c_j^a, \tag{2.20}$$

in which $H_{i,j}^{r,s} \equiv \langle\Psi_i^r|\hat{H}|\Psi_j^s\rangle$ is shown by the Slater-Condon rule [51] to be only nonzero if the two Slater determinants differ by zero, one, or two spin-orbitals.

In CIS, for example, this change the excitation energies to be:

$$E_{1,2} = \frac{H_{1,1}^{2,2} + H_{1,1}^{3,3}}{2} + \frac{1}{2}\sqrt{\left(H_{1,1}^{2,2} - H_{1,1}^{3,3}\right)^2 + 4\left|H_{1,1}^{2,3}\right|^2}, \tag{2.21}$$

but does not change the ground state energy:

$$E_0 = H_{1,1}^{1,1} = H_{HF}. \tag{2.22}$$

2.6 Density Functional Theory

In quantum mechanics, the traditional approach is to find the potential energy for a system, and then put it into the Schrödinger equation to solve for the wavefunctions. Once the wavefunctions are known, all the other observables correspond to the expectation value of the related operators. In this sense, the charge density would be nothing more than one among all the observables. DFT [52] [3] reverses this approach for the ground state. It promotes the charge density to be the main variable and calculates the wavefunction as a functional of density. The potential energy then would be one among other observables that can be calculated.

This may not be a major step from a theoretical point of view, but computationally, it is remarkable, since now, instead of dealing with a $3n$-spatial and n-spin coordinates in electronic wavefunction, we are dealing with a 3-dimensional charge density that has the averaged character of a detailed wavefunction. The ease with the computation becomes more obvious when considering that a wavefunction also has to be antisymmetric with the exchange of each and every pair of electrons, which makes it a complicated object to handle. Electron density, on the other hand, is much more simple. It has cusps at nuclei positions, resembling e^{-2Zr} in the vicinity of a nucleus with Z being the atomic number, and decaying smoothly like $e^{-2r\sqrt{2E_I}}$ far from the nucleus, with E_I being the ionization energy [53].

The Hohenberg-Kohn (HK) [54] and the Kohn-Sham (KS) [55] theorems established the main characters of DFT and brought Walter Kohn (and John Pople) the 1998 Nobel Prize in Chemistry.

2.6.1 Hohenberg-Kohn Theorems

The HK theorems state that the ground state wavefunction is a unique functional of the charge density ($HK-\mathrm{I}$):

$$\Psi_0\left(r_1,\, r_2,\, \ldots,\, r_n\right) = \Psi\left[\rho_0\left(r\right)\right], \tag{2.23}$$

and so are all other observables, including potential energy and consequently the Hamiltonian. The ground state density, furthermore, is the one that minimizes the energy functional ($HK-\mathrm{II}$):

$$E\left[\rho_0\right] \leq E\left[\rho'\right], \tag{2.24}$$

Therefore, the ground state density contains all the information needed and determines all the properties of the ground state electronic system. The total particle number is the integral over density; the nuclear locations are the density cusps, and a derivative of the density gives the atomic number [56]:

$$Z_i = \frac{a_0}{2\rho(r)} \frac{d\rho\left(r\right)}{dr}|_{r\to R_i}, \tag{2.25}$$

in which R_i is the position of the a nucleus, a_0 is the Bohr radius and Z_i is the atomic number. Thus, if we know the number of electrons as well as the positions of each nucleus and its atomic numbers in a molecule, we can write the Hamiltonian and solve the Schrödinger equation.

The Hamiltonian for the electronic system is composed of a universal part F, which remains the same for all systems and is due to the kinetic energy of electrons and the repulsive interactions between them. It also has a system-dependent term V_{ext} which basically distinguishes atoms, molecules and solids:

$$H = \sum_{i=1}^{n}\left(-\frac{1}{2}\nabla_i^2 + \sum_{j>i}^{n}\frac{1}{|r-r'|}\right) + \sum_{\alpha=1}^{N}\frac{Z_\alpha}{|r-r'|} = F + V_{ext}. \tag{2.26}$$

The ground state energy then would be:

$$E\left[\rho\right] = F\left[\rho\right] + \int V_{ext}(r)\rho(r)dr. \tag{2.27}$$

The HK theorems emphasizes that there actually exists a ground state density functional, which contains the properties of a system; however it does not offer a practical way of obtaining it, since the actual dependence of the universal part of functional is not known. For this purpose, the Kohn-Sham equations are needed.

2.6.2 Kohn-Sham Equations

The KS theorem replaces the interacting electrons in an external potential with noninteracting ones (i.e. $V_{ee} = 0$) in an effective local potential, known as the KS potential. It then proves that if the density of these two systems is the same, the effective potential is unique.

The Schrödinger equation for such a noninteracting system is then the KS equation:

$$\left(-\frac{1}{2}\nabla^2 + V_{eff}(r)\right)|\psi_i\rangle = \epsilon_i |\psi_i\rangle , \tag{2.28}$$

with the charge density and kinetic energy of this noninteracting system defined as:

$$\rho = \sum_{i=1}^{n} |\psi_i(r)|^2, \qquad T(\rho) = \sum_{i=1}^{n} \langle\psi_i| - \frac{\nabla^2}{2}|\psi_i\rangle . \tag{2.29}$$

To obtain the effective potential of this noninteracting system, the ground state energy of the original interacting system is written as:

$$E[\rho] = -\frac{1}{2}\sum_{i=1}^{n}\int \psi_i^*(r)\nabla^2\psi_i(r)dr + E_{XC}[\rho] + \frac{1}{2}\int \frac{\rho(r)\,\rho(r')}{|r-r'|}drdr' + \int V_{ext}(r)\rho(r)dr. \tag{2.30}$$

In this equation, the first term represents the kinetic energy of the noninteracting system, and the second term, known as the exchange-correlation energy, is the remainder of the kinetic energy for the interacting system; it is added to compensate for the simplification made in going from the interacting system to the noninteracting one. It is the only unknown variable in DFT and determines the quality of the results.

Using the Lagrange multiplier method, the energy functional in equation (2.30) is minimized by varying $\rho(r)$ over all densities constrained to be normalized to n electrons:

$$\delta\left(E[\rho] - \mu\int \rho(r)dr\right) = 0, \tag{2.31}$$

which yields the effective potential to be:

$$V_{eff}(r) = V_{ext}(r) + \int \frac{\rho(r')}{|r-r'|}dr' + V_{XC}, \tag{2.32}$$

where V_{XC} is called the exchange-correlation potential defined as: $V_{XC} = \frac{\delta E_{XC}[\rho(r)]}{\delta \rho(r)}$.

This equation has to be calculated iteratively in a self-consistent method becuase the effective potential depends on the density; yet the density itself is determined by the orbitals which are used to construct the density. This goes on iteratively until the charge density converges.

Therefore, the KS theorem states that, as far as the density is concerned, interacting electrons are the same as noninteracting ones, for which the kinetic energy form is known, but in a local Exchange-Correlation (XC) potential. In this sense, it offers a practical approach to calculate the density. There are many XC potentials available in the literature [57]. The Local Density Approximation (LDA), first introduced by Kohn and Sham in their original paper, and the Generalized Gradient Approximations (GGA) [58], are among the famous XC potentials.

2.6.3 Local Density Approximation

The basic assumption in LDA is that the electron density is spatially varying so slowly in the electronic system that the XC energy can be written solely in terms of the density at that point, and is independent of the gradient of the density:

$$E_{XC}^{LDA}[\rho] = \int \rho(r)\epsilon_{XC}(r)dr. \tag{2.33}$$

In this equation, ϵ_{XC} is the exchange-correlation energy per particle in the system, which is weighted by the probability of finding an electron at each point, to give the XC energy of the whole system.

The idea in LDA is borrowed from the uniform electron gas model [59] in metals, such as sodium, in which electrons travel freely in an embedded background of positive charges. This idealized model is the only one for which the form of XC functional is known to be almost correct, and is written as:

$$\epsilon_X^{LDA}(r) = -\frac{3}{4}\left(\frac{3}{\pi}\rho(r)\right)^{1/3} \tag{2.34}$$

In open-shell systems, where the α and β spin densities are different, a Local Spin Density Approximation (LSDA) is needed [60]; however, it is not pursued further here due to the closed-shell molecules studied in this thesis.

LDA has provided satisfactory results for molecules that behave like the uniform electron gas, as in metallic solids with delocalised electrons. However, it lacks the necessary precision in the calculation of binding energies and bond distances of molecules which do not resemble metalic solids [61]. The precision in binding energies and bond distances, however, has been improved significantly by the introduction of GGA functionals.

2.6.4 Generalized Gradient Approximation

In most molecules, the electron density is far from uniform. By assuming the XC energy to be also dependent on the gradient of the electron density, GGA functionals improve the quality of calculations significantly, especially in bonding areas in which the electron density changes greatly. They usually have LDA as their core, but, in addition, they include further components and can be written as:

$$E_{XC}\left[\rho\right] = \int \rho(r)\epsilon_{XC}\left(\rho,\, \nabla\rho\right) dr = E_{Xc}^{LDA}\left[\rho(r)\right] + \Delta\epsilon_{XC}\left[\nabla\rho\right], \tag{2.35}$$

In this way, the LDA can be interpreted as the first term in a Taylor expansion of the electron density, and there is a chance of considerable improvement by the introduction of the GGAs.

For most of the calculations in this thesis, the Becke-Perdew (GGA-BP) [62] [63] functional is implemented:

$$\Delta\epsilon = \beta\rho^{1/3}\frac{x^2}{1 + 6\beta x \sinh^{-1} x} \qquad\qquad x = \frac{|\nabla\rho|}{\rho^{4/3}}. \tag{2.36}$$

This functional is famous for its correct asymptotic behavior at long distance. The β parameter, furthermore, is an empirical coefficient (0.0042) determined by fitting the calculated results to the known values of some noble gases. The dimensionless parameter, x, is also called the reduced density gradient.

2.7 Time-Dependent DFT

DFT is limited to the treatment of electronic systems only in their ground states, while many of the properties of molecules that scientists are interested in have to do with either excited states or time-dependent external fields. For this purpose, a time-dependent DFT [64] [65] is needed. The time-dependent Schrodinger equation calculates the wavefunctions and charge density of a time-dependent potential, as follows:

$$i\frac{\partial}{\partial t}\Psi(t) = \hat{H}(t)\Psi(t) \qquad \rho(r,\,t) = \langle\Psi(t)|\rho(r)|\Psi(t)\rangle\,, \tag{2.37}$$

and therefore makes a map from the the potential to the density. A time-dependent analogue of HK and KS equations were first developed by Runge and Gross [66], which proves that for an arbitrary time-dependent system, the above map is bijective up to a purely time-dependent function $c(t)$. Thus, it determines the time-dependent wave-function as a unique functional of the electron density, up to a purely time-dependent phase factor (which cancels in expectation values):

$$\Psi(t) = e^{-i\alpha(t)}\Psi\left[\rho\right](t). \tag{2.38}$$

Furthermore, it replaces the interacting system with a noninteracting one, but in a local time-dependent KS potential $v_s\,(r,\,t)$ which yields the same electron density. The time dependent KS equation would then be:

$$i\frac{\partial}{\partial t}\psi_i\,(r,\,t) = \left(-\frac{\nabla^2}{2} + v_s\,(r,\,t)\right)\psi_i\,(r,\,t)\,, \tag{2.39}$$

in which the local potential has, again, the exchange correlation energy $v_{XC}\left[\rho\right](r,\,t)$ as a part, which has to approximated.

3 Calculations

3.1 Introduction

For the calculations in this thesis, the Amsterdam Density Functional (ADF) program package [67] is used. ADF is a FORTRAN-based software developed by two research groups in Amsterdam and Calgary that uses TD-DFT as the basis for its calculations, and has been shown [68] to be useful for a variety of computational chemistry calculations.

The molecules used for the calculations in this thesis are 3,4,9,10-perylene tetracarboxylic dianhydride $C_{24}H_8O_6$ (PTCDA) [69][70][71], bis-benzylimido perylene $C_{38}H_{22}N_2O_4$ (BBIP-PTCD) [72], and N,N′-dimethyl-3,4,9,10-perylene tetracarboxylic acid di-imide $C_{26}H_{14}N_2O_4$ (PTCDMe) [73]. They are all derivatives of perylene tetracarboxylic di-imides (PTCD), which is a prototype organic semiconductor dye. The resonance Raman calculations have been done at two excitation frequencies: 244 nm and 514.5 nm, both of which overlap with the absorption bands of all the family of PTCD. In this chapter, the results of the calculations for PTCDA are presented and discussed. Detailed information about the other molecules is presented in Appendix *C*.

3.2 Applications

PTCDA and other derivatives of perylene are all organic semiconductor dyes [74]. They have been used as high-grade paints in the automotive industry as a result of their distinctive thermal and solvent stability, and resistance to chemical reactions, light and weather conditions[75].

The energy difference between the highest occupied molecular orbital (HOMO) and the lowest unoccupied molecular orbital (LUMO) of these molecules are in the range of the typical band-gap of semiconductors. Therefore, they have been utilized in the fabrication of $n-$channel transistors [76]. They also have found many applications in light-based industries due to their photophysical properties [1], such as significant absorption in the visible range. For instance, the photovoltaic properties of some derivatives of perylene tetracarboxylic acid has been employed in constructing organic solar cells [77]. Moreover, they have been used as sensitizers of tin oxides [78][79], in which the dye gets excited to an upper level by absorbing light, but de-excites to the ground state by transferring an electron to the conduction band of tin oxides.

3.3 Calculation Settings

Each of the calculations in ADF has, among others, three important parameters that need to be understood and assigned: basis sets, exchange-correlation potential and core electrons. A brief discussion of these settings is as follows.

3.3.1 Basis Sets

Basis sets [80] are mathematical functions, usually in the form of Atomic Orbitals (AO) centered on atomic nuclei, such that by a linear combination of them, molecular wavefunctions are described.

ADF, unlike Gaussian that uses Gaussian-Type Orbitals (GTO) [81], is using Slater-Type Orbitals (STOs) [82]:

$$\Psi_{STO} = (2\zeta)^n \sqrt{\frac{2\zeta}{(2n)!}} r^{n-1} \exp(-\zeta r) Y_{lm}, \tag{3.1}$$

in which n is a principal quantum number, Y_{lm} is a spherical harmonic, and ζ is defined by Slater as $\left(\frac{Z-s}{n}\right)$, where s is a shielding constant. STOs are centered on atomic nuclei and imitate Shrödinger's solution to the hydrogen atom. They show, as they should, cusps on nuclear positions, and have proper asymptotic behaviour as compared to GTOs [83].

Basis sets in ADF include SZ ,DZ ,DZP ,TZP ,$TZ2P$ and $QZ4P$, in which S stands for "Single", D for "Double", T for "Triple", Q for "Quadruple", Z for "Zeta" (ζ), and P for "Polarization".

A single zeta basis set, for example, assigns one single STO to the s orbital of a hydrogen atom. For carbon, it becomes one STO to the s orbital, and a set of three STOs to the p orbitals. Larger basis sets essentially indicate more accurate results. Thus, it is expected that the DZ basis sets, which assigns two STOs with two different zeta functions to the s orbital of hydrogen, and two sets of three STOs to the p orbitals of carbon, to give more accurate results than the SZ calculations. However, it would be beneficial in some calculations not to add more zeta functions, but to use basis sets with "Polarization" , which add STOs with higher angular momentum. Therefore, the $TZ2P$ basis set that has been used for the polarizability and hyperpolarizability calculations below, assigns three STOs with three different zeta functions to the s orbital of carbon,

three sets of three STOs to the p orbitals, as well as one set of five STOs to the f orbitals, and one set of seven STOs to the d orbitals. The last two STOs correspond to the "Polarization" basis sets. It concludes that 24 different STOs are implemented for describing a single carbon in the $TZ2P$ level of theory. For hydrogen atoms, it would be 11. oxygen and nitrogen, on the other hand, need the same number of STOs as carbon, since they are all in the same row of the Periodic Table.

BBIP-PTCD, for example, has 22 hydrogens and 44 carbons, oxygens and nitrogens altogether. As a result, a molecular calculation of BBIP-PTCD with the $TZ2P$ basis sets, needs $22 \times 11 + 44 \times 24 = 1298$ different STOs assigned to the valence electrons, and a combination of all these would specify the molecular orbitals, and hence the molecular properties.

There is also a flexibility in using different basis sets for different fragments in molecules; however, this was not tried in the calculations in this thesis since all the atoms in these molecules are in the same row of the Periodic Table, and so their valence electrons behave quite similarly. Moreover, no relativistic basis sets were implemented in the calculations since no heavy atom is present. In this thesis, the TZP basis sets have been used for all the calculations, except polarizability and excitation energy calculations, in which the $TZ2P$ basis sets is used, and RRS calculations, in which the DZP basis sets is used.

3.3.2 Exchange-Correlation Potential

As explained in Chapter 2, the only unknown variable in DFT is the Exchange-Correlation (XC) function, which is responsible for the interaction of electrons in a molecular system. Many XC potentials based on different approximations are available in the literature, each with some strengths and deficiencies, and it is of paramount importance to choose the proper XC functional for a particular calculation.

In ADF, the XC functionals are sorted in different groups. In the Local Density Approximation (LDA) functionals, the energy of a molecule is assumed to be related to just the local electron density. However, in the Generalized Gradient Approximation (GGA) functionals, the energy depends also on the first derivative of the electron density. Meta-GGA functionals have, in addition to the GGA part, a dependence on the second derivative of the electron density (i.e. the kinetic energy density). The hybrid functionals depend on a combination of a GGA functional and the Hartree-Fock potential, and finally, the meta-hybrid functionals have a part related to the electron kinetic

energy density, in addition to the hybrid functional.

In this thesis, the GGA-BP86 functional has been implemented for the geometry optimization, infrared and Raman calculations, because this functional has shown to give frequencies in a good agreement with experimental results, without the need to use scaling factors[85]. For the calculations of the excitation energies and UV/vis spectra, the BP98, B3LYP [86], and SAOP [87] functionals have been tried, but only the results from B3LYP are presented here, since they show very close agreement to the experimentally observed values for the molecules studied in this thesis. For (hyper) polarizability calculations, the BP86, SAOP, and LB94 [88] functional have been tried and the results from the LB94 are presented here since it has shown to have correct asymptotic behaviour [89].

3.3.3 Core Electrons

Core electrons do not engage in chemical reactions as much as the valence electrons do. In ADF, core electrons can either be frozen in the inner atomic orbitals, and therefore be left out of the calculations, or they can be described by small basis sets, which result in more accurate but more costly calculations. In ADF, the participation of frozen core electrons in calculations decreases from the "Small" to the "Medium" and to the "Large" core. The exact meaning of them varies for different atoms. For transition metals, for instance, "Small" means that the electrons up to the second layer i.e. 1s2s2p are frozen, while for "Medium" the electrons in the s and p orbitals of the third layer is also frozen. In all the calculations presented in this thesis, no core electron is frozen for more accurate results.

3.4 Geometry Optimization

A molecule is not just a pile of atoms but a collection with particular length and angle between each and any of them in particular positions in space. In other words, all the properties of a molecule depend strongly not only on the type and the number of its fragments, but also on the particular position of them with respect to each other. Therefore, the first step, and the most important step, in any molecular calculation should be the determination of the molecule's structure, ı.e. the geometry optimization [90].

The energy of a molecule as a function of its nuclear positions defines the $(3N-6)$ dimensional Potential Energy Surface (PES), and the main task of geometry optimiza-

tion is to find the minima (optimal structures) and saddle points (transition states) of PES. The program starts with the initial geometry given by the user, and by iterative calculations of the first derivative of energy with respect to the nuclear movements, it finds the configuration in which the obtained gradient is closer to zero than a pre-assigned criterion. The second derivative of energy (Hessian matrix) should also be calculated to distinguish a minimum from a saddle point, and hence the frequency calculation. Frequencies are the square root of the eigenvalues of Hessian matrix. Positive frequencies indicate a minimum, while a single imaginary frequency means a transition state, which is a minimum in energy in all direction except the one from reactants to products. Higher order saddle points have more than one imaginary frequency and are uninteresting points on PES.

The geometry optimization of PTCDA has been carried on without imposing any constraints on the angles and bond lengths of the constituent atoms, or the symmetry of the molecule. A 0.0001 value has been chosen for the gradient convergence of the geometry optimization, which is 10 times more strict than the default value in ADF.

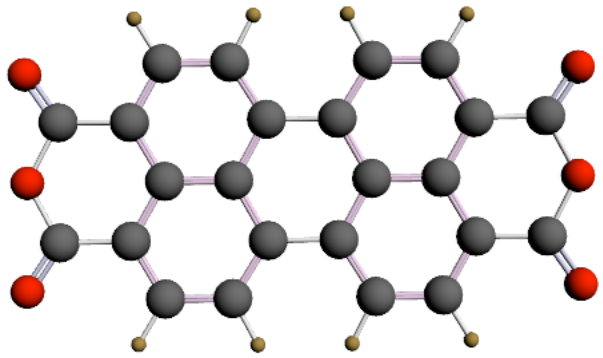

Figure 2: PTCDA

PTCDA is an aromatic structure with the Benzene ring as the structural building block. It has 38 atoms connected by covalent bonds, and also a conjugated π-system on the chromophore. This molecule is calculated to be a planar rectangular one (11.4×6.7 A), with 108 vibrational modes and 140 valence electrons. Moreover, it is calculated to be possessing a 6.81 eV zero-point energy, and a -283.03 eV bond energy in the minimum configuration.

The carbon bond length within each naphthalene in PTCDA is calculated to be varying between 1.38 A and 1.43 A, which is smaller than the peri-bonds connecting the two naphthalenes (1.46 A), and the bonds between the naphthalene and the carboxylic

groups (1.47 A). The carbonyl bond length is also calculated to be 1.21 A and the single bonded C–O is found to be 1.40 A.

PTCDA is also calculated to be a centrosymmetric molecule with D_{2h} point group symmetry. Three C_2 axes of proper rotation, three planes of reflection, and an inversion center transform this molecule to itself. The rule of mutual exclusion is therefore applicable to this molecule, and the Raman and infrared spectra can be studied separately. The irreducible representation is also found to be:

$$\Gamma = 19A_g + 18B_{1g} + 7B_{2g} + 10B_{3g} + 8A_u + 10B_{1u} + 18B_{2u} + 18B_{3u}. \tag{3.2}$$

An analytical derivation of the irreducible representation of PTCDA can be found in [98]. In Appendix A, the irreducible representation of BBIP-PTCD is derived, which verifies the one computed by ADF.

PTCDMe and BBIP-PTCD are not planar molecules due to the presence of methyl groups and benzene rings at both ends of the perylene plane, respectively. These functional groups, which are bound to the main plane by sp^2-hybridized nitrogen atoms, make calculations substantially costly. Especially, optimized geometries are much harder to reach, as a result of the movement of the out-of-plane structures.

In PTCDMe, the two possible arrangements of the methyl group at both ends, i.e. the eclipsed or staggered conformations, result in two different symmetries: C_{2v} and C_{2h}. Even though the vibrational spectra and the electronic energies of these two configurations are found not to being affected by this geometry difference, the C_{2v} configuration is found to be the more probable geometry, because of the presence of imaginary frequencies in the vibrational spectrum of the C_{2h} configuration.

3.5 Infrared Spectrum

All of the vibrational frequencies for PTCDA are calculated to be positive, which attests to the fact that a minimum has been attained in the geometry optimization calculation. The smallest frequency is $3\,\mathrm{cm}^{-1}$ and the highest occurs at $3133\,\mathrm{cm}^{-1}$. None of the gerade vibrations can change the dipole moment in centrosymmetric molecules, since they are symmetric with respect to the center of inversion. In other words, the change in the dipole moment due to each stretching or bending in one side of the molecule, is cancelled with the same stretching or bending on the other half. The net change in the dipole moment would then be zero, and the vibration will be absent in the infrared

spectrum. In PTCDA, the A_u vibrations are also silent since they are symmetric with respect to the rotation around the principal axis of the molecule, and the change in the dipole moment would be again zero.

Thus, the infrared spectrum of PTCDA consists of 46 vibrations:

$$\Gamma_{IR} = 10B_{1u} + 18B_{2u} + 18B_{3u}. \tag{3.3}$$

The B_{1u} vibrations all occur below $1000\,\mathrm{cm}^{-1}$. All of them are found to be out-of-plane vibrations with weaker intensities compared to the other two groups, that are all in-plane and are able to occur beyond $3000\,\mathrm{cm}^{-1}$.

The higher the strength of a covalent bond between two atoms, the higher is the frequency needed to excite it. The bond length of C–H and C=O are calculated at the optimized geometry to be as small as $1.089\,\mathrm{A}^\circ$ and $1.210\,\mathrm{A}^\circ$, respectively. Furthermore, the lighter the atoms involved in a vibrational mode, the higher will be the vibrational frequency. These facts explain the occurrence of the C–H stretching vibration at a high frequency around $3100\,\mathrm{cm}^{-1}$, and the double-bonded C=O stretching mode at around $1700\,\mathrm{cm}^{-1}$.

The highest infrared intensities in PTCDA correspond to the C=O symmetric and antisymmetric stretching, at $1745\,\mathrm{cm}^{-1}$ and $1714\,\mathrm{cm}^{-1}$, respectively, with the change in the dipole moment being almost 1.3 times larger in the symmetric stretching than in the antisymmetric one. The aromatic C–C stretching, the deformation in the chromophore, and the anhydride symmetric and antisymmetric vibrations are the next high intensities at 1580, 1268 and $971\,\mathrm{cm}^{-1}$.

Moreover, a solvent effect is investigated by optimizing and analysing the vibrational frequencies of PTCDA in chloroform. While the overall profile of the infrared spectra are found to remain almost unchanged, the infrared intensities are found to be more than two times larger in chloroform than in the gas state.

Detailed information about the dipole moment and the infrared intensity of all vibrations of PTCDA in the gas state and chloroform are presented in Appendix C. The calculated infrared spectra, broadened with a Lorentzian having a width of $9\,\mathrm{cm}^{-1}$, as well as the experimental spectrum and a number of characteristic regions with high infrared intensity are as follows:

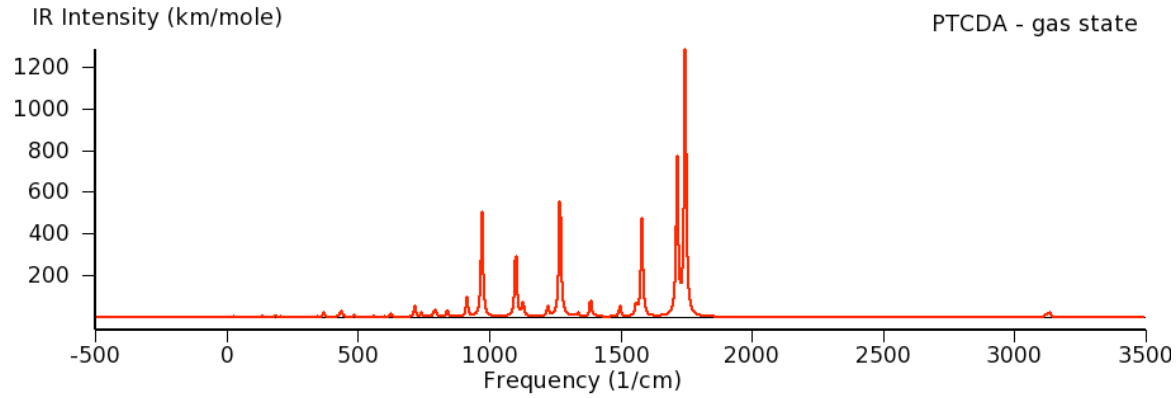

(a) Calculated infrared spectrum in the gas state

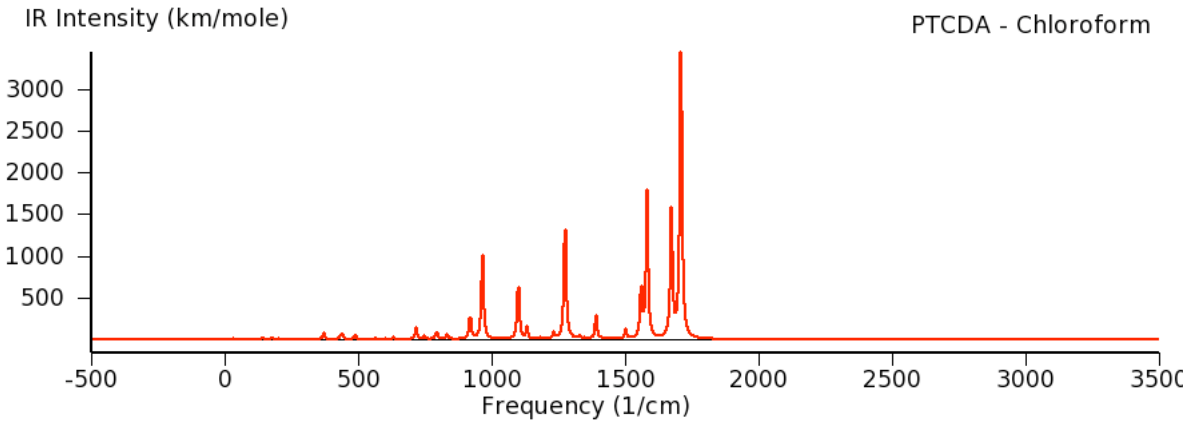

(b) Calculated infrared spectrum in chloroform

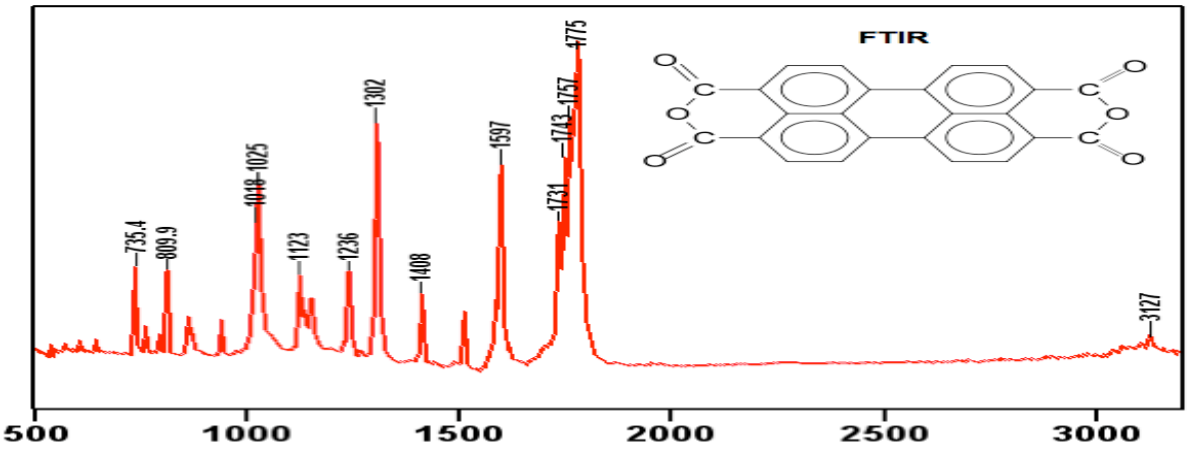

(c) Experimental infrared spectrum

Figure 3: Infrared spectrum, PTCDA

3133: C–H stretching

1745: C=O symmetric stretching, C–O–C scissoring, the Benzene groups at both ends expanding and contracting, chromophore hardly moving

1714: C=O antisymmetric stretching, C–O–C rocking, the Benzene groups at both ends deforming, chromophore hardly moving

1580: chromophore stretching, C–H scissoring

1384: chromophore deformation, C–H scissoring

1268: C–O–C symmetric stretching, C–C stretching, C–H rocking

1100: C–O–C symmetric stretching, chromophore deforming, C–H scissoring

971: chromophore deformation, C–O–C antisymmetric stretching, C–H in the chromophore scissoring

3.6 UV/Vis Spectrum and Excitation Energies

The first twenty-five lowest energy singlet transitions of PTCDA have been calculated with a B3LYP XC-potential and at the TZ2P level of theory. The most intense transition, with an oscillator strength of 0.58, appears at 516.1 nm. It has a 98.1% contribution from the HOMO to the LUMO, and should be attributed to the $\pi \rightarrow \pi^*$ transition. Considering the fact that DFT is mostly successful for the ground state calculations, and also that TD-DFT has not been as rewarding as DFT is, this calculated transition shows a surprisingly good agreement with the experimentally observed value at 520 nm. It should also be noted that the excitation energy calculation was repeated with BP86, SAOP and LB94 functionals, but all of them are found to underestimate this transition, and are not followed further.

HOMO (-6.28 eV) is calculated to have A_u symmetry, while LUMO (-3.88 eV) has B_{2g} symmetry, and the energy difference between them (2.4 eV) is in the range of semiconductor band gaps. The symmetry of the transition dipole moment can also be found by the direct product of the symmetry of the HOMO and LUMO: $A_u \otimes B_{2g} = B_{2u}$, which verifies the one calculated by ADF.

It is interesting to note that the $S_0 \rightarrow S_1$ transition in all the perylene derivatives are found to be separated quite significantly from the other transitions in the UV/vis spectrum; this is due to a large gap between the HOMO and (HOMO $-$ 1) on one hand, and another large gap between the LUMO and (LUMO + 1) on the other hand.

The next highest intensity transition in PTCDA is found at 241 nm, with an oscillator strength of 0.56, which should be attributed to the HOMO $\longrightarrow$ (LUMO + 4) transition, and corresponds to the UV transition in this molecule. It again shows a very good agreement with the experimentally observed value in this spectral region.

It is also found that the HOMO and LUMO of all the perylene derivatives mainly consist of the conjugated π-electron p orbitals in the perylene plane. The π-electrons of the functional groups at both ends of the main plane, as well as the hydrogen AOs, do not contribute to the HOMO and LUMO, since they are not in the same plane as those in the middle, and as such, the overlap between the ends and the middle is not significant. Localization of the HOMO and LUMO on the chromophore also indicates that for the most part, the vibration that involve in the chromophore are expected to be strongly enhanced in RRS by the transition to the S_1 state.

A solvent effect is also investigated by analyzing the excitation energies in chloroform. The band gap is found to be smaller by a negligible amount of 0.0015 eV, and the

oscillator strength of the $S_0 \rightarrow S_1$ transition is calculated to be larger by an amount of 0.03 in chloroform. The UV/vis spectra in the gas state and chloroform, and also the energy levels of PTCDA are as follows:

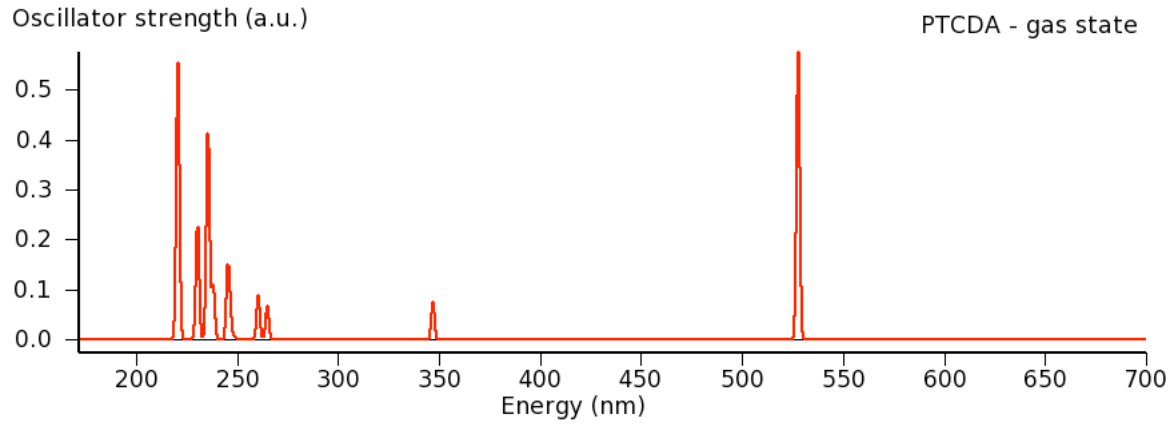

(a) In gas state

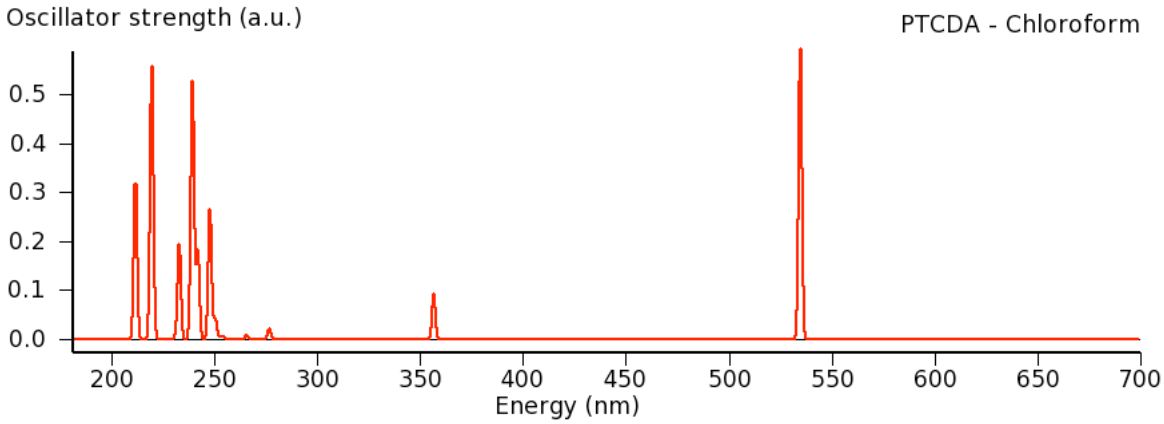

(b) In chloroform

Figure 4: Calculated UV/vis spectrum, PTCDA

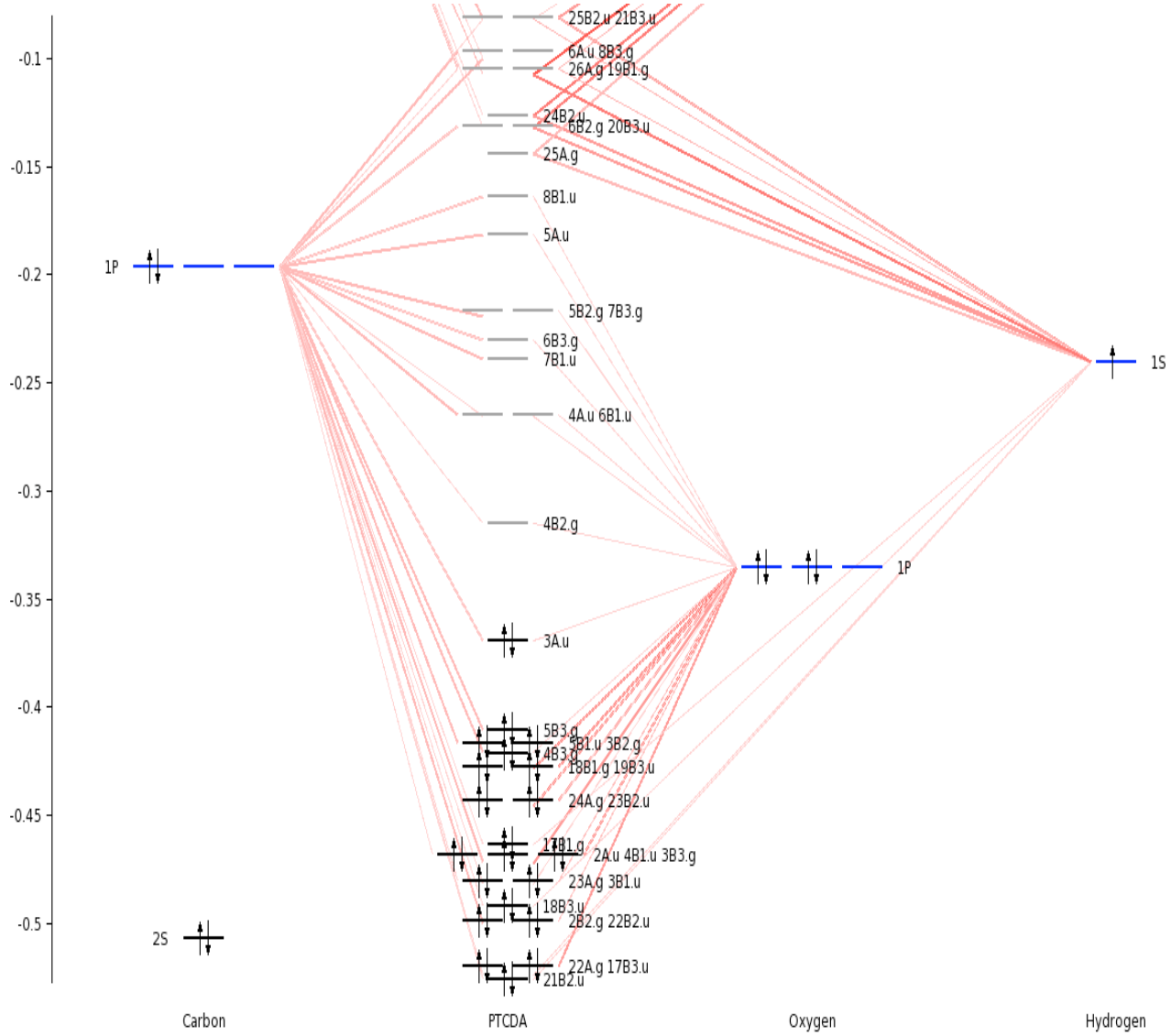

Figure 5: Energy levels, PTCDA

3.7 Normal Raman Spectrum

The polarizability tensor is usually illustrated by the idea of the polarizability ellipsoid, which is defined as:

$$\sum_{i=1}^{3}\alpha_{ii}X_i^2 + 2\sum_{i\neq j}\alpha_{ij}X_iX_j = 1, \tag{3.4}$$

in which the second term would be zero, if the polarizability tensor is written in terms of its principal axes. Moreover, the distance from any point on the ellipsoid surface to the origin is equal to $\frac{1}{2}\alpha_E$, where α_E is the polarizability in that direction. In this sense, the molecule behaves as if it is a 3-dimensional ellipsoid, and the change of the polarizability, and hence Raman-activity, can be explained in terms of the changes in the ellipsoid volume.

In interpreting Raman spectra, it should also be considered that in the case of NRS, unlike RRS, as long as the frequency of the incident light stays far from any absorption band, the position and the intensity of each vibration is almost independent of the frequency of the incident laser beam.

In PTCDA, none of the the ungerade vibrations changes the ellipsoid volume, and the Raman intensity of them is calculated to be exactly zero. This is due to the fact that in ungerade vibrations, any stretching or bending on one side of the molecule, is followed in the same direction by exactly the same stretching or bending on the other side of the molecule, which causes the changes in the volume of the ellipsoid to be exactly zero. Thus, the Raman spectrum of PTCDA consists of only 54 gerade vibrations:

$$\Gamma_R = 19A_g + 18B_{1g} + 7B_{2g} + 10B_{3g}. \tag{3.5}$$

Among these vibrations, the B_{2g} and B_{3g} ones that are all out-of-plane vibrations and occur in less than $1000\,\mathrm{cm}^{-1}$, do not change the ellipsoid volume very much. These vibrations are all antisymmetric with respect to both the rotation about the principal axis, and the reflection about a plane of symmetry. However, the B_{1g} vibrations have higher Raman intensities, since they are at least symmetric with respect to the reflection about a plane of symmetry, and this helps the ellipsoid volume to change a little, even though they are still antisymmetric with respect to the rotation around the principal axis. Finally, the most intense Raman vibrations are the A_g vibrations, which are totally symmetric and correspond to the largest change in the ellipsoid volume.

The first seven most intense Raman vibrations all have A_g symmetry and occur in the range of 1250-1750 cm^{-1}. The maximum peak in the normal Raman spectra is assigned to the symmetric stretching of chloroform and symmetric in-plane bending of C–H at 1552 cm^{-1}. The figure below shows for this vibration, an intense variation of the H–C–C bending angle, $(110.6° - 129.9°)$, and the related C=C stretching bond length, $(1.33 - 1.46\,\mathrm{A})$. It can also be seen that for this vibration, the maximum bending happens at the minimum stretching.

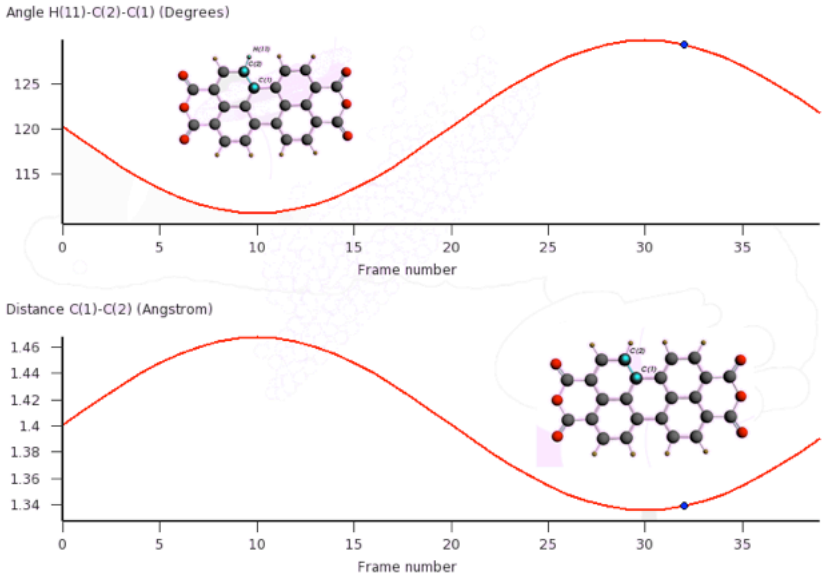

Figure 6: 1552 cm^{-1} vibration, PTCDA

This vibration is followed immediately by another high-intensity vibration at 1566 cm^{-1}, mainly a ring stretching mode, which has much less contribution from the C–H bending in the middle (2.2°), but a much larger contribution from the C–H bending on both sides (34.0°). The next intense vibration, comparable to the first two, occurs at 1288 cm^{-1}. This vibration should be assigned to the symmetrical in-plane expansion and contraction of the central benzene in the perylene plane, with the middle C–H bending, and the other C–H at both ends almost stationary. A maximum bending of 17.7° for the C–H in the middle, and a maximum stretching of 0.13 A for the related C=C is found for this vibration. The figure below shows that in this vibration, unlike the 1552 cm^{-1} vibration, the maximum bending happens at the maximum stretching, which corresponds to the expansion and contraction of the central benzene ring.

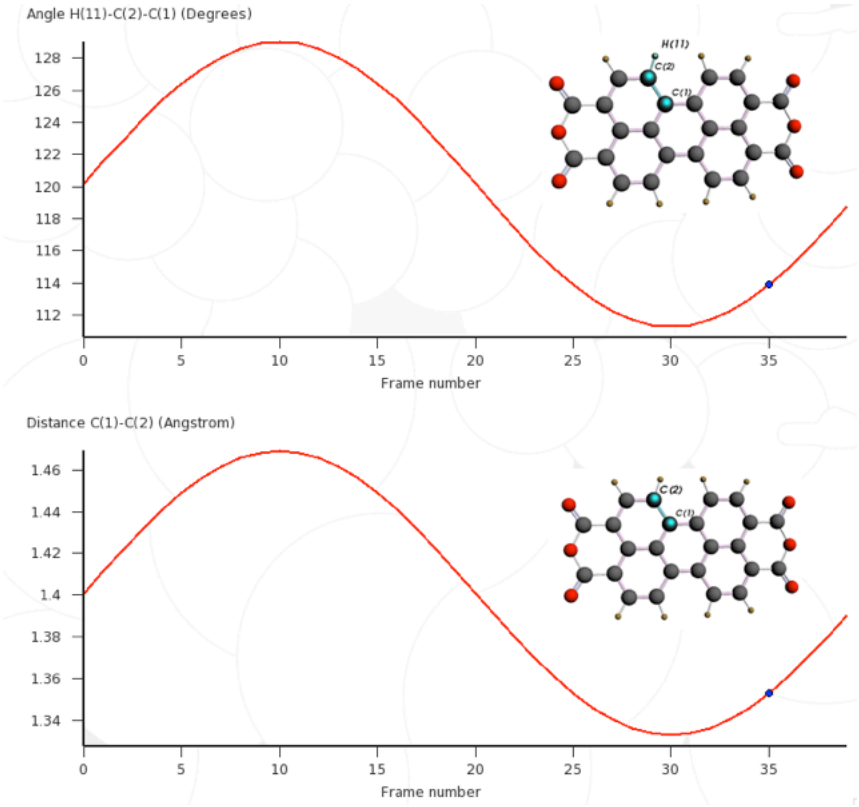

Figure 7: 1288cm^{-1} vibration, PTCDA

Two B_{1g} vibrations, with Raman intensities comparable to some of the weak A_g vibrations, are also found at 1593 cm^{-1} and 1713 cm^{-1}, which corresponds to the chromophore deformations and antisymmetric stretching of the carboxyl groups.

In addition, the normal Raman spectrum of PTCDA is investigated in chloroform and the overall normal Raman profile is found to be almost unchanged in chloroform. The first three high intensity vibrations show small blue-shift by the amount of 5, 5 and 3 cm^{-1}, respectively, while the intensities are approximately 1.1 to 1.5 times larger in chloroform.

Depolarization ratios are also calculated for PTCDA, and as explained in Chapter 1, the symmetric vibrations are found to have the lowest values. While the depolarization ratios for the B_{1g}, B_{2g} and B_{3g} vibrations are calculated to be in the range of $0.5-0.75$, the depolarization ratios of the A_g vibrations are found to be in the range of $0.1-0.4$. This provides an easy tool for the assignment of symmetric peaks in a Raman spectrum.

Detailed information about the normal Raman intensity and the depolarization ratio of each vibration is presented in Appendix C. The normal Raman spectrum of PTCDA

in the gas state and chloroform, and a number of characteristic scattering bands are as follows:

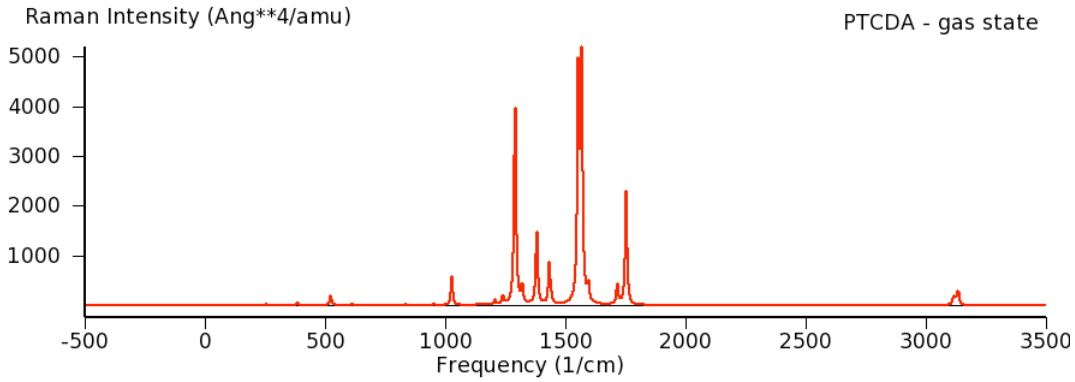

(a) Gas state

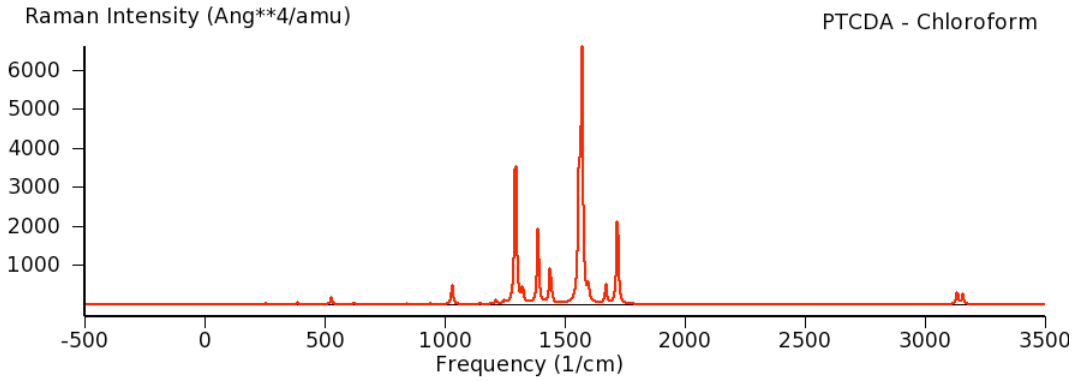

(b) Chloroform

Figure 8: Calculated normal Raman spectrum, PTCDA

1288: the central benzene expanding and contracting with each C–H on each corner of the ring scissoring, other benzene groups and other C–Hs hardly moving

1378: chromophore symmetrically expanding and contracting, C–H scissoring, C=O hardly moving

1552: chromophore stretching, C–H scissoring vigorously, C=O hardly moving

1566: central Benzene slightly expanding and contracting , C–C stretching slightly, C–H rocking

1593: chromophore stretching, C–H rocking, B_{1g} vibration

1713: C=O antisymmetric stretching, C–C stretching, chromophore hardly moving

1750: C=O symmetric stretching, C–O–C scissoring, the benzene groups at both ends expanding and contracting symmetrically, C–H and central rings hardly moving

3132: C–H stretching symmetrically, chromophore and carbonyl groups hardly moving

3.8 Resonance Raman Spectrum

Analysing the resonance Raman spectrum of a large molecule is a demanding task and for this purpose, the two different mechanisms contributing to the intensity enhancement, i.e. the Franck-Condon (A) and the Herzberg-Teller (B), should be taken into account. The A-enhancement scales with the second power of the electronic transition dipole moment, while in the B-enhancement, its derivative with respect to a normal mode is involved. Therefore, an electronic transition with a small oscillator strength is very unlikely to be enhanced by the A-mechanism, while the B-enhancement can arise from weak oscillator strengths or even forbidden electronic transitions.

The absorption band of PTCDA in the visible region is calculated to be possessing a significant oscillator strength of 0.58, which is attributed to the $\pi \rightarrow \pi^*$ transition of the conjugated system in the perylene plane. De-population of the bonding MO and the consequent population of the antibonding MO in this electronic transition, results to the lowering of the bond order in the conjugated system, implying the elongation of the C–C bonds in the chromophore. Thus, the molecular symmetry in this excited state remains the same as in the ground state, and only bond lengths and bond angles that do not change the molecule's symmetry are involved.

The elongation of the C–C bonds in the excited state displaces the potential energy minimum with respect to the ground state, and this becomes a source of nonorthogonality in the Franck-Condon factors. In addition, these changes in the geometry which are limited to those along totally symmetric coordinates will essentially couple only to the displacements along totally symmetric normal coordinates. In conclusion, the A-enhancement requires intense absorption bands and can only be observed for totally symmetric vibrational modes.

As in the case of NRS, the ungerade vibrations in PTCDA are calculated to have exactly zero Raman intensity in RRS. The B_{2g} and B_{3g} vibrations are also expected to have very weak intensities, while the B_{1g} vibrations have higher intensities than B_{2g} and B_{3g}, but still much weaker than the totally symmetric A_g vibrations.

The first eleven high intensity vibrational modes of the resonance Raman spectrum of PTCDA at 514.5 nm are all found to have A_g symmetry. The spectrum shows two close peaks at 1549 cm^{-1} and 1562 cm^{-1}. These two vibrations, which in the case of NRS happen to be at 1552 cm^{-1} and 1566 cm^{-1}, are assigned to the symmetric stretching of the chromophore, and intensity enhancements of 90.8 and 112.3 are found for these two vibrations, respectively. The difference in the calculated frequncies of NRS and RRS,

are due to the fact that different basis sets has been used for these calculations.

The next high intensity enhancement happens at $1290\,\mathrm{cm}^{-1}$ which, as explained in the case of NRS, should be assigned to the symmetric expansion and contraction of the central Benzene ring and the bending of the related C–H. This vibration shows an intensity enhancement of 71.8 with respect to the $1288\,\mathrm{cm}^{-1}$ in NRS. This peak is followed by another intense peak at $1318\,\mathrm{cm}^{-1}$ with an enhancement of 88.9 with respect to the NRS. All of these four high intensity peaks can be seen in the experimental spectrum of PTCDA at 1586, 1570, 1437, and $1300\,\mathrm{cm}^{-1}$, respectively, which shows a good agreement with the ones calculated by ADF.

Nontotally symmetric vibrations are also found to be enhanced in the calculated spectrum of PTCDA at 514.5 nm. Most significantly, the B_{1g} vibrations at $1590\,\mathrm{cm}^{-1}$ and $1518\,\mathrm{cm}^{-1}$ show enhancement by factors of 183 and 135, respectively. The B-term should be responsible for the enhancement of these vibrations, since nontotally symmetric fundamentals can only gain intensity via the Herzberg-Teller mechanism. Since the $\langle e_s|H'|e_r\rangle$ term in the B-enhancement mechanism couples electronic states, both totally and nontotally symmetric fundamentals can basically be enhanced in this mechanism; however, in totally symmetric vibrations, both of the coupled electronic states should carry the same symmetry, while electronic states of the same symmetry are not usually close to each other in energy. Therefore, totally symmetric fundamentals do not gain much enhancement via the B-term, since the energy difference in the denominator is large.

It should also be noted that in B-term enhancement, only the vibronic transitions in which there is exactly one vibrational unit difference between the ground and the excited states are allowed. Therefore, there would be no overtone in the B-term scattering. On the contrary, there is no normal coordinate q in the Franck-Condon factors of the A-enhancement, and whenever there is a significant displacement in the potential energy minimum, overtones can also be observed along with the fundamentals. Despite the fact that overtones are more likely to be significant in small molecules, the resonance Raman spectrum of PTCDA at 514.5 nm shows overtones for the totally symmetric modes at $3174\,\mathrm{cm}^{-1}$ and $3190\,\mathrm{cm}^{-1}$ which are enhanced by factors of 13.8 and 3.7, respectively. Since in a pure C–H stretching vibration, the bond lengths in the chromophore remain almost unchanged, the potential energy minimum does not change. Therefore, no A-enhancement is expected for this pure stretching, and the observed peak should be attributed to an overtone.

The resonance Raman spectrum of PTCDMe at 514.5 nm has also been calculated,

and it can be seen that the overall profile of the spectrum remains almost the same as that of PTCDA. The high intensity peaks for PTCDMe are found to occur at 1563, 1551, and 1294 cm^{-1}, while in PTCDA they were calculated to occur at 1562, 1549, and 1290 cm^{-1}. The fact that the resonance Raman spectra of them look very similar implies that it is indeed the chromophore in the perylene plane which is responsible for the electronic transitions as well as the vibrational modes, and the functional groups at both ends of the perylene plane do not have appreciable contribution.

Solvent effects are not considered in the RRS calculations due to the computational burden, and this is one of the possible sources of error. The calculated resonance Raman spectra of PTCDA and PTCDMe for the 514.5 nm excitation and the experimental spectrum are as follows:

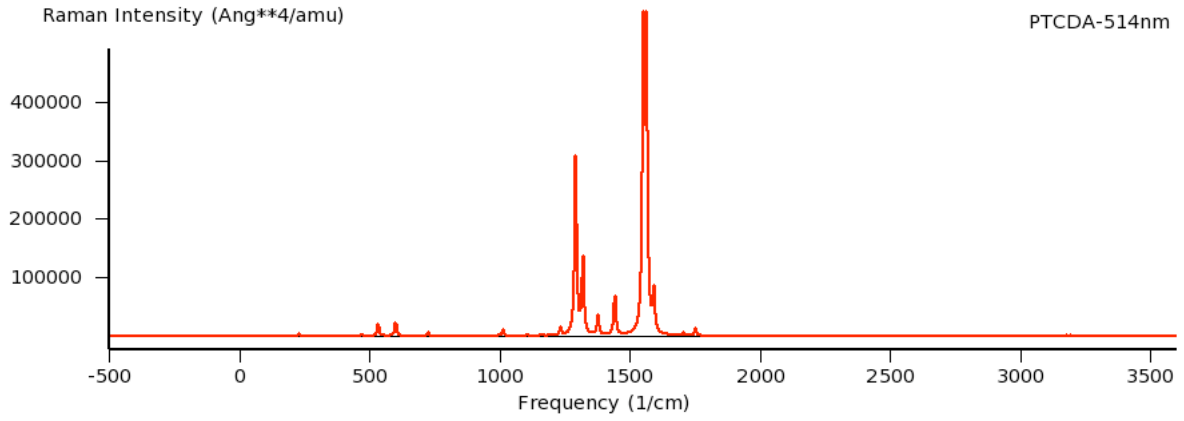

(a) PTCDA

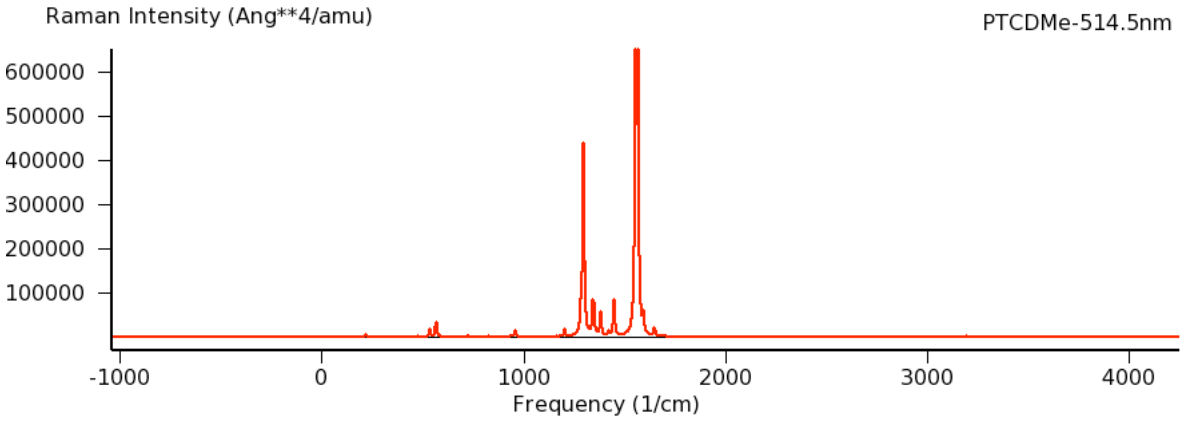

(b) PTCDMe

Figure 9: Calculated resonance Raman spectrum at 514.5 nm, broaden with a Lorentzian having a width of 9 cm^{-1}

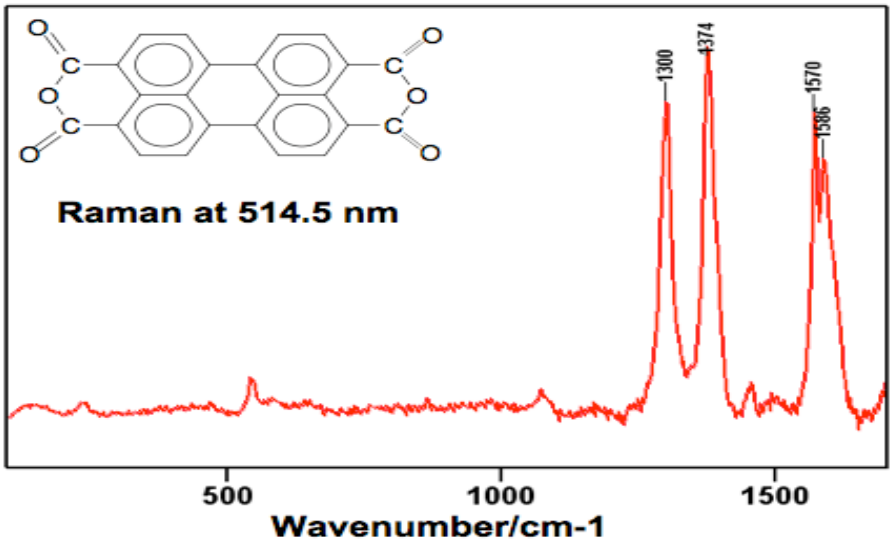

Figure 10: Experimental RR spectrum at 514.5 nm, PTCDA

PTCDA has another electronic absorption observed in the UV region, in resonance with the 244 nm laser line, and with a calculated oscillator strength of 0.56 in chloroform. Three high intensity vibrations are easily noticeable at 244 nm excitation. The maximum peaks occur at 1549 nm and 1567 nm which have A_g symmetry and enhancement factors of 945 and 1013 with respect to the NRS intensities at 1551 cm^{-1} and 1566 cm^{-1}. The next high intensity vibration occur at 1375 cm^{-1} with 730 enhancement with respect to the 1378 cm^{-1} vibration in NRS. The A-term is responsible for the enhancement in all of these vibrations since they are totally symmetric vibrations, but there is also significant enhancement from the B-term for the nontotally symmetric vibration at 1590 cm^{-1}, with an enhancement factor of 1060.

These facts show that the spectrum at 244 nm is completely dominated by the ring vibrations of the chromophore. This can be attested by the experimental spectrum of BBIP-PTCD as well, in which only one very strong band is observed around 1590 cm^{-1}.

The calculated resonance Raman spectra of PTCDA and the experimental spectra of BBIP-PTCD at 244 nm are as follows:

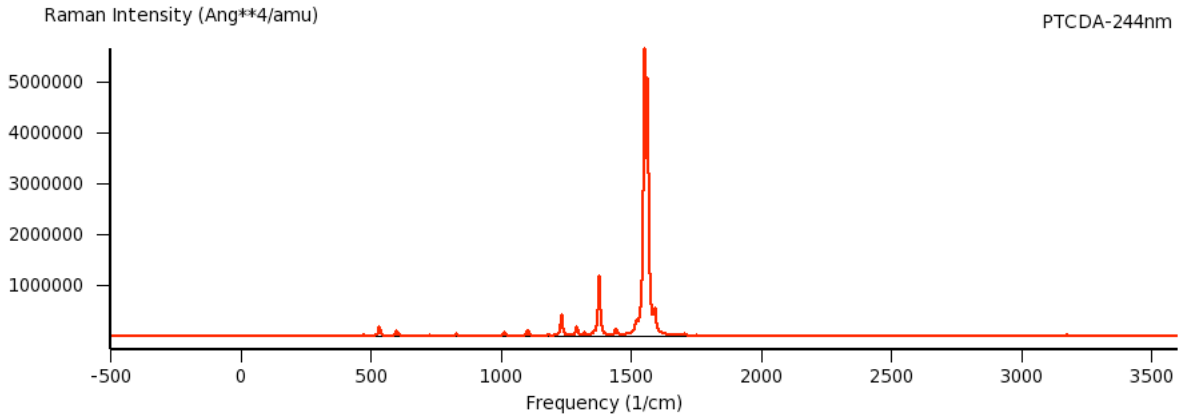

Figure 11: Calculated resonance Raman spectra at 244 nm, broaden with a Lorentzian having a width of 9cm^{-1}, PTCDA

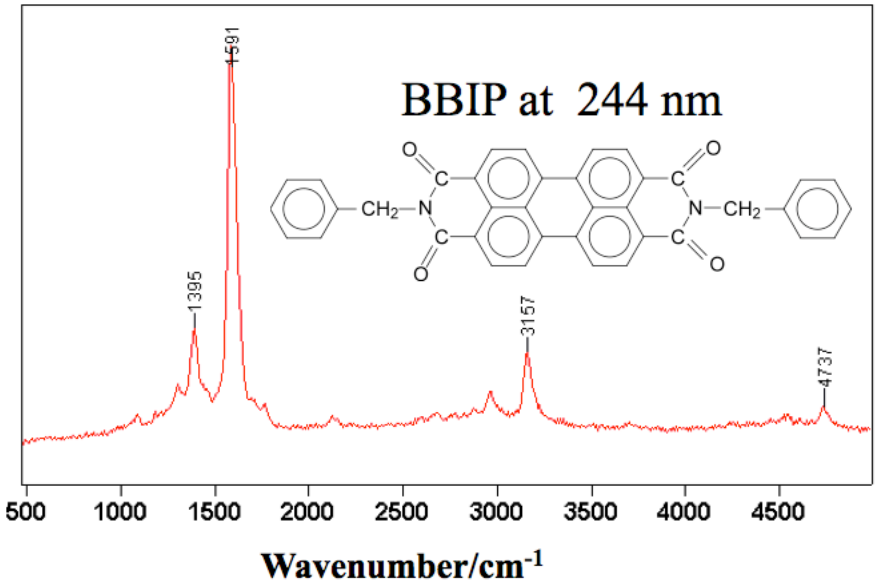

Figure 12: Experimental RRS spectrum at 244 nm, BBIP-PTCD

4 Conclusion and Future Work

In this study, the spectroscopic properties of a family of perylene derivatives are calculated. In particular, the resonance Raman spectra obtained using the time dependent density funcitonal theory are found to be in good agreement with the experimental data. Moreover, the maximum peaks in the resonance Raman spectra are assigned to the chromophore vibrations, which are the same in all the perylene derivatives, and thus, independent of the functional groups at both ends of the perylene plain. Therefore, it is seen that the computational study of the resonance Raman intensities yields a more detailed understanding of the molecules than the experimental approach, as it shows what types of vibrational modes in a molecules are responsible for an intensity enhancement upon excitation.

This research can be improved in a number of ways. During the course of this project, the 2010 version of ADF was released (Sep. 2010) with substantial improvement in spectroscopic properties. One of the interesting features of ADF2010 is the implementation of the geometry optimization and frequency analysis in excited states. This can greatly enhance our understanding of the symmetry, charge density, charge population analysis and vibrational spectra of molecules in their excited states. Moreover, ADF2010 is now capable of calculating the Franck-Condon factor for the transition between two electronic states. This information is of absolute importance in the RRS calculations. Using ADF2010, it is also possible to select the range of an excitation energy calculation and thus, it can reduce the computation costs when there is a focus on a particular region of the electronic spectra.

This research can also be extended to the calculation of Surface Enhanced Raman Scattering (SERS). This will open the doors for many interesting and yet complicated features of SERS, and help further the understanding of the chemical and electromagnetic enhancements in SERS. The TD-DFT method of ADF is, to the best knowledge of the author, the only program package that has been used for SERS computation [99][100][101].

It should also be noted that for large molecules, the RRS calculations are very involved and time-consuming. A typical RRS calculation of BBIP-PTCD, with large diffuse basis sets and hybrid functional, is expected to take more than half a year. In addition, there is no restart option at the moment in ADF to resume RRS calculations, and if for any reason, a RRS calculation is terminated, it has to be started from the beginning. Finally, solvent effects are likely to be important in RRS calculations; however, they

were not considered in the RRS calculations in this thesis, due to their computational costs. In conclusion, the RRS calculations in this thesis can be improved by allocating more run-times on more stable clusters of computers.

Appendices

A Irreducible Representation of BBIP-PTCD

In this Appendix, a derivation of the irreducible representation of BBIP-PTCD is presented. For a derivation of the irreducible representation of PTCDA, look at [98].

BBIP-PTCD is calculated to be a centrosymmetric molecule with C_{2h} point group symmety. A C_2 axis of proper rotation, an inversion center i, and a horizontal plane σ_h, perpendicular to the principal axis, transform this molecule into itself. The character table for the C_{2h} point group is shown in the table below, in which A and B representations are symmetric and antisymmetric with respect to the C_2 symmetry operation, and the subscripts g or u indicate the symmetric or antisymmetric property of the representations with respect to the inversion operation i.

C_{2h}	E	C_2	i	σ_h	
Ag	1	1	1	1	R_z
B_g	1	-1	1	-1	R_x, R_y
A_u	1	1	-1	-1	z
B_u	1	-1	-1	1	x, y

Table 1: C_{2h} character table

As we can see, the number of the irreducible representations is equal to the number of classes, such that the character table is a square matrix.

Assigning 3 degrees of freedom to each atom, the molecule will have 198 degrees of freedom, in which 6 of them are pure rotational or translational, and thus, uninteresting for vibrational spectroscopy. The remaining 192 vibrational degrees of freedom will not have the full symmetry of the molecule with all the symmetry elements, but only an irreducible representation of it. The ultimate goal of determining the irreducible representation of each vibrational mode is to find the symmetry of them, and therefore, their contribution to the infrared or the Raman spectrum.

Starting from a reducible representation and then reducing it to an irreducible one by using the reduction formulae is the usual trend in vibrational spectroscopy. For a reducible representation, three axes of coordinates are usually placed on each atoms. If the position of the axes are changed under a symmetry elements, then nothing contributes to the character of that representation. However, if the the position does not

change but the direction of the axes reverses, a character of -1, i.e. antisymmetric, and if both the position and direction remains unchanded, a character of 1, i.e. symmetric, would contribute to the character table.

Under the unity symmetry element, E, all of the coordinate axes remain the same, and therefore, the character for this element would be 198, i.e. the number of the degrees of freedom. Under the C_2 proper rotation and the inversion i, the position of all the atoms change, and thus, nothing contribute to the character of these two elements. However, under the σ_h reflection, all of the fourteen atoms on the reflection plane remain unchanged, and for each of them, two of the axes of coordinates remain unchanged, while one axis reverses direction. Thus, $14 \times (2 - 1) = 14$ would be the character for this element. The character table for this reducible representation be as follows:

C_{2h}	E	C_2	i	σ_h
Γ	198	0	0	14

Table 2: Reducible representation of BBIP-PTCD

Any reducible representation can be written as a linear combination of irreducible ones as:

$$\chi_\Gamma(c) = \sum_i n_i \chi(c). \tag{A.1}$$

Using the orthogonality property of the irreducible representations:

$$\sum_0 g_c \chi_i(c) \chi_j(c) = h \delta_{ij}, \tag{A.2}$$

in which c is a class of symmetry elements with g_c operators, and h is total number of symmetry operators, we can use the reduction formula to calculate the contribution of each irreducible representation as:

$$n_i = \frac{1}{h} \sum_c g_c \chi_i(c) \chi_\Gamma(c). \tag{A.3}$$

For BBIP-PTCD, it would be:

$$
\begin{aligned}
n_{A_g} &= \frac{1}{4}\left(194\times 1+0\times 1+0\times 1+14\times 1\right)=53,\\
n_{B_g} &= \frac{1}{4}\left(194\times 1+0\times (-1)+0\times 1+14\times (-1)\right)=46,\\
n_{A_u} &= \frac{1}{4}\left(194\times 1+0\times 1+0\times (-1)+14\times (-1)\right)=46,\\
n_{B_u} &= \frac{1}{4}\left(194\times 1+0\times (-1)+0\times (-1)+14\times 1\right)=53.
\end{aligned}
$$

In the rightmost column of character tables, the irreducible representation of pure rotation and translation can be seen. Subtracting them from the numbers above we find the irreducible representation for the vibrational frequencies of BBIP-PTCD to be:

$$\Gamma_i = 52A_g + 44B_g + 45A_u + 51B_u, \tag{A.4}$$

which is the same as calculated by ADF. It can be double-checked that the sum of numbers above produces the total number of vibrational frequencies i.e.192.

B Charge Population Analyses

One important question about molecules is how electron charges are distributed among different atoms. Being a byproduct of quantum chemistry computations, charge population analyses can help interpreting the molecule's behaviour and reactivity in terms of the individual atoms carrying excess negative or positive charges. They are not integer numbers though and should be understood as the percentage of time an electron spends in the vicinity of an atom.

Mulliken [91] and Hirshfeld [93] population analyses, and Voronoi Deformation Density [94] are among the well-known schemes for partitioning charges among atoms, which are calculated for the molecules studied in this thesis. It should also be noted that all of them are to some extent dependent on basis sets; however, a relative population of two atoms in a partitioning scheme contains useful information, since charge populations are not usually used for predicting the result, but interpreting them.

B.1 Mulliken Population Analysis

The basic idea in Mulliken Population Analysis (MPA), is to partition an electron in a MO among different atoms, each with a share proportional to the contribution of its AO in that MO. An atom charge would then be the sum of the contributions from all MOs. In this respect, a MO is expanded in terms of the basis functions:

$$\phi_i = \sum_{\alpha} c_{i\alpha}\chi_{\alpha}, \tag{B.1}$$

in which χ_a are normalized but nonorthogonal basis functions. The total number of electrons then would be the sum over all occupied MOs:

$$N = \sum_{i}^{occ} \int \phi_i^2 dr = \sum_{i} \sum_{\alpha\beta} c_{\alpha i} c_{\beta i} \int dr \chi_{\alpha}\chi_{\beta} = \sum_{i} \left(\sum_{\alpha} c_{\alpha i}^2 + \sum_{\alpha \neq \beta} c_{\alpha i} c_{\beta i} S_{\alpha\beta} \right), \tag{B.2}$$

where $S_{\alpha\beta}$ is the overlap integral. It can be seen that the total number of electrons is composed of either the square of a basis function of an AO, which should be interpreted as the charge belonging to that atom, or an overlap of different AOs, which Mulliken assumed to be shared equally between them.

The charge owned by an atom is determined in MPA to be the contribution from all basis functions describing the atomic orbital of the atom:

$$\rho_A = \sum_{\alpha_A} \sum_{\beta} c_{\alpha i} c_{\beta i} S_{\beta\alpha}, \tag{B.3}$$

and the net charge of an atom A is then defined to be the sum of nuclear and electronic part:

$$Q_{m_A} = Z_A - \rho_A. \tag{B.4}$$

B.2 Hirshfeld Population Analysis

Unlike MPA, which uses wavefunctions for partitioning, the Hirshfeld Population Analysis (HPA), also known as stockholder, uses electron density for distributing charges among atoms. A weighting factor is defined in HPA as the ratio of an electron density

of an atom to the sum of the density of all the atoms present in the molecule, known as promolecular density:

$$w_A = \frac{\rho_A}{\sum_B \rho_B}, \tag{B.5}$$

the Hirshfeld charge of an atom A is then assigned as the difference between the nuclear charge and the weighted electron density:

$$Q_{h_A} = Z_A - \int \rho(r) w_A dr. \tag{B.6}$$

In this sense, HPA distribute the molecular charge density among the constituents, each with a share proportional to its contribution to the promolecular density, and since in HPA the building blocks are the atomic densities, more information about atoms are protected, and it is usually considered in literature to be more reliable [95] [96][97].

B.3 Voronoi Deformation Density

Voronoi Deformation Density (VDD), differs from the other partitioning methods in that it distributes the charge among atoms, each with a share proportional to the space which is closest to that atom than any other one, known the Voronoi cell and also known as the Wigner-Seitz cell in solid state physics. The electron charge for each atom, is then defined as the integrated charge in Voronoi cell.

Within the Voronoi cell, the subintegrals over the atomic sphere and the remaining part are evaluated separately to give the numbers of electrons (negative charge) in these regions. The net total charge in the cell (including the nuclear charge) is also given. In this sense, the change in the charge of any atom in a molecule, relative to the neutral one, shows the flow of charge when a chemical bond is formed.

The VDD charge of an atom A is then defined as the integral of deformation density associated with the formation of the molecule from its constituent fragments in the Voronoi cell:

$$Q_{d_A} = \int_V \left(\rho(r) - \sum_B \rho_B(r) \right) dr. \tag{B.7}$$

Here, $\sum_B \rho_B(r)$ is the superposition of atomic densities in neutral situation. VDD has also been shown to be less sensitive to the choice of basis set.

C Detailed Information of the Calculations

In this Appendix, detailed information of the calculations done for the molecules studied in this thesis are presented. The following units are used for the values:

Frequency: cm^{-1}

Distance: $Angstrom$

Orbital Energies: eV

Dipole Moment: $esu^2cm^2 10^{-40}$

Infrared Intensity: $km/mole$

Raman Intensity: Ang^4/amu

C.1 PTCDA

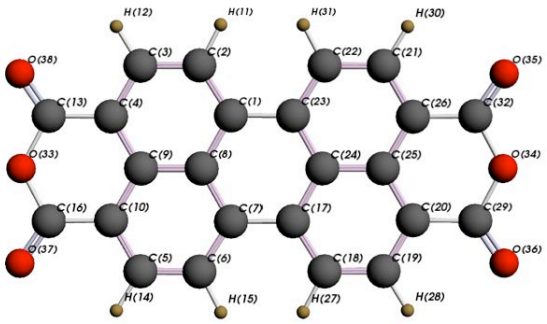

Figure 13: PTCDA structure

C.1.1 Optimized Geometry

Atom	X	Y	Z	Atom	X	Y	Z
1 C	-1.250169	-0.732541	0.000000	20 C	1.225130	3.568850	0.000000
2 C	-2.435794	-1.479026	0.000000	21 C	-2.428190	2.875458	0.000000
3 C	-2.428190	-2.875458	0.000000	22 C	-2.435794	1.479026	0.000000
4 C	-1.225130	-3.568850	0.000000	23 C	-1.250169	0.732541	0.000000
5 C	2.428190	-2.875458	0.000000	24 C	0.000000	1.427708	0.000000
6 C	2.435794	-1.479026	0.000000	25 C	0.000000	2.858425	0.000000
7 C	1.250169	-0.732541	0.000000	26 C	-1.225130	3.568850	0.000000
8 C	0.000000	-1.427708	0.000000	27 H	3.398820	0.974992	0.000000
9 C	0.000000	-2.858425	0.000000	28 H	3.357567	3.443086	0.000000
10 C	1.225130	-3.568850	0.000000	29 C	1.239944	5.044197	0.000000
11 H	-3.398820	-0.974992	0.000000	30 H	-3.357567	3.443086	0.000000
12 H	-3.357567	-3.443086	0.000000	31 H	-3.398820	0.974992	0.000000
13 C	-1.239944	-5.044197	0.000000	32 C	-1.239944	5.044197	0.000000
14 H	3.357567	-3.443086	0.000000	33 O	0.000000	-5.698279	0.000000
15 H	3.398820	-0.974992	0.000000	34 O	0.000000	5.698279	0.000000
16 C	1.239944	-5.044197	0.000000	35 O	-2.239214	5.727975	0.000000
17 C	1.250169	0.732541	0.000000	36 O	2.239214	5.727975	0.000000
18 C	2.435794	1.479026	0.000000	37 O	2.239214	-5.727975	0.000000
19 C	2.428190	2.875458	0.000000	38 O	-2.239214	-5.727975	0.000000

Table 3: Optimized geometry, PTCDA

C.1.2 Orbital Energies

	Energy		
1	-522.78	13	-23.98
2	-521.08	14	-22.12
3	-281.66	15	-19.66
4	-279.16	16	-18.99
5	-279.05	17	-15.92
6	-279.02	18	-15.47
7	-278.79	19	-14.24
8	-278.63	20	-13.41
9	-278.59	21	-12.83
10	-31.20	22	-11.48
11	-28.39	23	-10.59
12	-26.10	24	-9.01

(a) Ag

	Energy		
1	-521.08	10	-19.25
2	-281.66	11	-18.17
3	-279.15	12	-16.09
4	-278.79	13	-14.86
5	-278.63	14	-13.04
6	-278.59	15	-12.78
7	-29.63	16	-12.22
8	-23.93	17	-10.40
9	-21.15	18	-8.39

(b) B1g

	Energy
1	-11.99
2	-10.97
3	-8.45

(c) B2g

	Energy
1	-13.84
2	-11.82
3	-9.47
4	-8.54
5	-8.28

(d) B3g

	Energy
1	-11.96
2	-10.09
3	-6.81

(e) Au

	Energy
1	-13.88
2	-12.77
3	-10.25
4	-9.39
5	-8.46

(f) B1u

	Energy		
1	-522.78	12	-25.43
2	-521.08	13	-22.44
3	-281.66	14	-21.77
4	-279.15	15	-18.05
5	-279.05	16	-17.92
6	-279.02	17	-15.10
7	-278.79	18	-13.90
8	-278.63	19	-13.17
9	-278.59	20	-12.87
10	-31.20	21	-12.08
11	-28.39	22	-10.82

(g) B2u

	Energy		
1	-521.08	11	-18.73
2	-281.66	12	-16.80
3	-279.16	13	-16.06
4	-278.79	14	-14.25
5	-278.63	15	-13.53
6	-278.59	16	-12.77
7	-29.63	17	-12.12
8	-24.51	18	-11.17
9	-22.41	19	-8.39
10	-20.05	20	

(h) B3u

Table 4: Orbital energies, PTCDA

C.1.3 Infrared Intensities

Gas state

	Freq.	Dipole	IR Int.
1	368.26	290.62	26.83
2	437.65	231.34	25.38
3	485.13	75.24	9.15
4	624.46	101.00	15.81
5	701.20	3.55	0.62
6	787.40	88.31	17.43
7	918.91	0.58	0.13
8	1099.66	1306.38	360.08
9	1127.03	127.48	36.01
10	1268.00	2084.10	662.39
11	1337.49	55.55	18.62
12	1384.43	266.82	92.59
13	1404.78	25.36	8.93
14	1557.19	149.81	58.47
15	1579.88	1146.44	454.00
16	1744.66	3038.20	1328.64
17	3110.72	0.63	0.49
18	3123.08	17.31	13.55

(a) B2u

	Freq.	Dipole	IR Int.
1	26.74	704.27	4.72
2	123.76	47.83	1.48
3	183.08	195.04	8.95
4	204.65	75.24	3.86
5	461.61	0.66	0.08
6	560.01	38.67	5.43
7	715.32	296.19	53.11
8	794.77	155.18	30.91
9	838.53	175.70	36.93
10	967.54	10.35	2.51

(b) B1u

	Freq.	Dipole	IR Int.
1	136.41	191.97	6.56
2	342.88	27.69	2.38
3	431.51	163.40	17.67
4	598.78	17.21	2.58
5	740.54	102.85	19.09
6	913.53	412.11	94.37
7	971.05	2096.38	510.26
8	1128.10	127.16	35.96
9	1178.85	15.48	4.57
10	1221.69	160.34	49.10
11	1287.61	20.00	6.45
12	1316.87	18.26	6.03
13	1460.55	0.56	0.20
14	1496.00	147.74	55.40
15	1576.45	58.19	22.99
16	1713.99	1782.41	765.76
17	3116.08	10.22	7.98
18	3132.58	26.78	21.03

(c) B3u

	Freq.	Dipole	IR Int.
1	368.8	971.8	89.8
2	439.9	457.1	50.4
3	487.7	474.9	58.0
4	630.8	153.3	24.2
5	704.1	17.0	3.0
6	787.1	162.5	32.1
7	926.3	1.2	0.3
8	1097.7	2824.3	777.1
9	1131.3	216.9	61.5
10	1272.9	5035.2	1606.5
11	1345.6	43.0	14.5
12	1388.7	885.6	308.3
13	1411.0	46.3	16.4
14	1557.8	1744.2	681.1
15	1580.1	4292.4	1700.1
16	1706.9	9373.0	4010.2
17	3135.5	2.8	2.2
18	3146.9	0.3	0.2

(d) B2u

	Freq.	Dipole	IR Int.
1	29.8	1882.4	14.1
2	133.7	89.4	3.0
3	174.6	500.1	21.9
4	201.9	168.3	8.5
5	456.6	0.0	0.0
6	561.3	84.6	11.9
7	714.8	763.8	136.8
8	793.2	392.9	78.1
9	831.2	294.3	61.3
10	960.6	4.5	1.1

(e) B1u

	Freq.	Dipole	IR Int.
1	140.7	548.1	19.3
2	344.6	36.3	3.1
3	432.5	476.7	51.7
4	600.2	50.2	7.6
5	745.1	192.5	35.9
6	917.4	1372.0	315.5
7	963.5	4630.1	1118.2
8	1130.0	276.3	78.3
9	1181.1	67.3	19.9
10	1231.1	249.5	77.0
11	1295.4	59.5	19.3
12	1328.3	109.3	36.4
13	1466.4	8.3	3.1
14	1500.5	287.2	108.0
15	1580.7	141.4	56.0
16	1671.3	3921.1	1642.6
17	3137.5	2.3	1.8
18	3151.0	3.2	2.5

(f) B3u

Chloroform

Table 5: Dipole strength & infrared intensities , PTCDA

C.1.4 Vibrational Frequencies

	Freq.		
1	226.64	11	1288.05
2	387.56	12	1317.93
3	456.97	13	1378.48
4	521.41	14	1431.01
5	612.05	15	1551.83
6	708.16	16	1565.72
7	812.29	17	1750.45
8	1024.94	18	3115.74
9	1124.73	19	3132.24
10	1237.23		

(a) Ag

	Freq.		
1	250.55	10	1171.30
2	382.19	11	1203.57
3	421.84	12	1353.54
4	560.78	13	1439.53
5	665.68	14	1512.89
6	831.90	15	1593.27
7	948.24	16	1713.48
8	1030.10	17	3111.05
9	1143.33	18	3123.33

(b) B1g

	Freq.
1	59.28
2	253.40
3	423.64
4	615.50
5	728.60
6	835.19
7	966.24

(c) B2g

	Freq.
1	86.02
2	123.29
3	176.87
4	337.14
5	447.66
6	631.83
7	726.70
8	810.68
9	844.27
10	958.18

(d) B3g

	Freq.
1	3.06
2	74.62
3	289.39
4	511.99
5	643.59
6	740.83
8	957.67

(e) Au

	Freq.
1	26.74
2	123.76
3	183.08
4	204.65
5	461.61
6	560.01
7	715.32
8	794.77
10	967.54

(f) B1u

	Freq.		
1	368.26	10	1268.00
2	437.65	11	1337.49
3	485.13	12	1384.43
4	624.46	13	1404.78
5	701.20	14	1557.19
6	787.40	15	1579.88
7	918.91	16	1744.66
8	1099.66	17	3110.72
9	1127.03	18	3123.08

(g) B2u

	Freq.		
1	136.41	10	1221.69
2	342.88	11	1287.61
3	431.51	12	1316.87
4	598.78	13	1460.55
5	740.54	14	1496.00
6	913.53	15	1576.45
7	971.05	16	1713.99
8	1128.10	17	3116.08
9	1178.85	19	3132.58

(h) B3u

Table 6: Vibrational frequencies, PTCDA

C.1.5 Normal Raman Intensities and Depolarization Ratio

Gas state

	Freq.	Int.	Ratio
1	226.6	1.5	0.25
2	387.5	6.9	0.37
3	457.0	1.1	0.22
4	521.4	199.5	0.12
5	612.0	41.8	0.18
6	708.2	4.6	0.64
7	812.2	2.8	0.26
8	1024.8	578.6	0.27
9	1124.7	7.0	0.53
10	1237.2	198.4	0.21
11	1288.2	4546.2	0.26
12	1317.9	411.4	0.18
13	1378.4	1621.0	0.30
14	1430.9	844.9	0.27
15	1551.8	5423.1	0.40
16	1565.5	4689.9	0.37
17	1750.4	2318.4	0.27
18	3115.8	95.1	0.16
19	3132.3	318.6	0.26

(a) Ag

	Freq.	Int.	Ratio
1	250.5	26.3	0.75
2	382.2	45.8	0.75
3	421.8	2.5	0.75
4	560.7	8.1	0.75
5	665.6	0.5	0.69
6	831.9	13.4	0.74
7	948.2	22.0	0.75
8	1030.0	0.2	0.31
9	1143.3	29.8	0.72
10	1171.5	0.1	0.49
11	1203.5	104.5	0.75
12	1353.5	13.1	0.74
13	1439.5	102.6	0.75
14	1512.8	3.6	0.75
15	1593.2	388.7	0.75
16	1713.5	429.1	0.75
17	3111.2	102.8	0.75
18	3123.4	91.7	0.75

(b) B1g

	Freq.	Int.	Ratio
1	59.2	0.8	0.72
2	253.5	0.8	0.75
3	423.9	7.2	0.75
4	615.6	0.5	0.70
5	728.8	1.6	0.73
6	835.5	0.7	0.53
7	967.0	0.2	0.75

(c) B2g

	Freq.	Int.	Ratio
1	85.9	0.8	0.71
2	123.1	0.7	0.73
3	176.8	0.2	0.51
4	337.4	3.1	0.74
5	447.9	0.2	0.72
6	631.9	0.4	0.13
7	726.9	0.7	0.75
8	811.0	1.1	0.55
9	844.4	3.4	0.75
10	959.1	3.4	0.75

(d) B3g

	Freq.	Int.	Ratio
1	228.8	1.1	0.28
2	386.2	10.8	0.42
3	460.6	2.1	0.15
4	525.7	194.9	0.12
5	619.8	44.8	0.21
6	712.4	12.4	0.49
7	813.1	8.9	0.29
8	1028.9	524.7	0.26
9	1125.5	6.5	0.75
10	1246.0	66.0	0.23
11	1292.5	4565.1	0.27
12	1322.2	418.5	0.19
13	1386.1	1997.7	0.28
14	1436.6	989.3	0.27
15	1557.0	3482.7	0.41
16	1568.9	6559.8	0.37
17	1717.1	2524.9	0.27
18	3132.3	213.9	0.14
19	3155.4	252.4	0.28

(e) Ag

	Freq.	Int.	Ratio
1	252.0	23.9	0.75
2	383.7	44.5	0.75
3	422.9	3.8	0.68
4	561.8	6.3	0.74
5	669.4	1.1	0.75
6	838.3	11.8	0.75
7	937.7	39.8	0.75
8	1036.6	0.1	0.29
9	1146.0	21.1	0.75
10	1176.0	0.3	0.68
11	1211.5	119.3	0.75
12	1364.4	5.9	0.72
13	1445.6	94.5	0.75
14	1517.4	3.6	0.75
15	1596.4	378.3	0.75
16	1669.1	492.1	0.75
17	3131.9	162.3	0.75
18	3145.4	20.0	0.75

(f) B1g

	Freq.	Int.	Ratio
1	59.8	0.2	0.73
2	248.0	0.1	0.75
3	420.1	2.1	0.75
4	612.1	0.0	0.19
5	723.8	0.4	0.69
6	825.1	1.3	0.75
7	958.7	0.0	0.75

(g) B2g

	Freq.	Int.	Ratio
1	85.0	0.3	0.74
2	133.0	1.5	0.58
3	171.1	0.6	0.52
4	331.7	2.1	0.75
5	446.4	1.1	0.50
6	634.5	0.2	0.43
7	723.6	1.4	0.51
8	811.6	0.9	0.57
9	842.9	4.6	0.60
10	951.9	2.0	0.75

(h) B3g

Chloroform

Table 7: Raman intensities & depolarization ratio, PTCDA

C.1.6 Resonance Raman Intensities

	Freq.	514.5	244
1	226.11	4821.00	9165.4
2	360.10	391.80	1979.5
3	469.18	2803.58	24834.2
4	532.01	23063.10	201027.0
5	599.04	27618.80	117785.0
6	723.46	6477.90	16252.3
7	827.02	966.20	51006.1
8	1010.64	12679.30	94278.8
9	1101.69	2736.35	137048.0
10	1231.25	13830.20	441754.0
11	1289.86	326321.00	196835.0
12	1317.80	144148.00	60502.6
13	1375.78	34473.30	1184360.0
14	1440.27	78614.20	140066.0
15	1549.43	492775.00	5128230.0
16	1561.67	527007.00	4754400.0
17	1749.95	13968.90	12111.5
18	3173.98	1311.80	30391.3
19	3189.83	1186.19	1392.4

(a) Ag

	Freq.	514.5	244
1	238.74	270.27	1.7
2	384.62	736.91	5543.5
3	426.83	0.03	211.4
4	579.34	246.26	1859.7
5	679.41	12.31	3125.0
6	843.04	433.76	443.1
7	994.29	523.86	1777.4
8	1043.31	1.07	689.1
9	1158.46	2308.47	6352.2
10	1181.32	39.90	24141.0
11	1207.66	798.81	958.0
12	1355.16	7.63	39172.1
13	1443.58	1792.26	2719.6
14	1517.56	491.63	183163.0
15	1590.07	71241.80	411463.0
16	1702.45	5401.86	32525.3
17	3169.22	256.13	203.0
18	3180.61	262.02	10.0

(b) B1g

	Freq.	514.5	244
1	61.76	1.14	12.4
2	101.63	27.70	38.5
3	180.76	1.55	4.6
4	346.22	1.28	20.1
5	449.06	66.95	62.0
6	630.32	22.36	164.5
7	720.65	44.52	14.3
8	822.20	2.09	110.2
9	861.76	112.64	78.6
10	942.42	326.21	268.2

(c) B3g

	Freq.	514.5	244
1	35.52	1.08	1.4
2	259.76	0.05	13.0
3	428.16	6.97	1.7
4	616.55	0.01	0.3
5	713.48	0.45	8.8
6	829.96	2.06	5.3
7	951.13	0.03	15.9

(d) B2g

Table 8: Resonance Raman intensities at 244 & 514.5 nm, PTCDA

C.1.7 Mulliken & Hirshfeld Charge

Atom	Charge	Atom	Charge
1 C	0.0477	20 C	-0.0665
2 C	0.2050	21 C	0.1731
3 C	0.1731	22 C	0.2050
4 C	-0.0665	23 C	0.0477
5 C	0.1731	24 C	0.0093
6 C	0.2050	25 C	0.0873
7 C	0.0477	26 C	-0.0665
8 C	0.0093	27 H	-0.2001
9 C	0.0873	28 H	-0.1286
10 C	-0.0665	29 C	0.7114
11 H	-0.2001	30 H	-0.1286
12 H	-0.1286	31 H	-0.2001
13 C	0.7114	32 C	0.7114
14 H	-0.1286	33 O	-0.5068
15 H	-0.2001	34 O	-0.5068
16 C	0.7114	35 O	-0.5368
17 C	0.0477	36 O	-0.5368
18 C	0.2050	37 O	-0.5368
19 C	0.1731	38 O	-0.5368

(a) Mulliken

Atom	Charge	Atom	Charge
1 C	0.0105	20 C	0.0105
2 C	0.0100	21 C	0.0100
3 C	-0.0118	22 C	-0.0118
4 C	0.1839	23 C	0.1839
5 C	0.1839	24 C	0.1839
6 C	0.0534	25 H	0.0534
7 C	0.0617	26 H	0.0617
8 C	0.0617	27 H	0.0617
9 C	0.0534	28 H	0.0534
10 C	0.0534	29 H	0.0534
11 C	0.0617	30 H	0.0617
12 C	0.0617	31 H	0.0617
13 C	0.0534	32 H	0.0534
14 C	-0.0935	33 O	-0.0935
15 C	-0.0935	34 O	-0.0935
16 C	-0.2234	35 O	-0.2234
17 C	-0.2234	36 O	-0.2234
18 C	-0.2234	37 O	-0.2234
19 C	-0.2234	38 O	-0.2234

(b) Hirshfeld

Table 9: Charge analysis, PTCDA

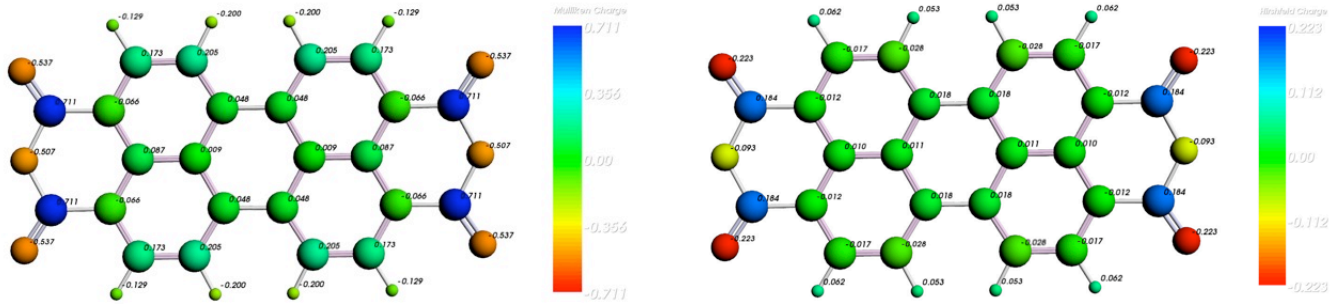

(a) Mulliken (b) Hirshfeld

Figure 14: Charge analysis, PTCDA

C.1.8 Voronoi Charge

Atom	Sphere	RestCell	Total	VDD	Atom	Sphere	RestCell	Total	VDD
1 C	-2.207	-3.763	0.030	0.012	20 C	-2.211	-3.805	-0.016	-0.026
2 C	-2.209	-3.300	0.490	-0.040	21 C	-2.209	-3.264	0.526	-0.037
3 C	-2.209	-3.264	0.526	-0.037	22 C	-2.209	-3.300	0.490	-0.040
4 C	-2.211	-3.805	-0.016	-0.026	23 C	-2.207	-3.763	0.030	0.012
5 C	-2.209	-3.264	0.526	-0.037	24 C	-2.208	-3.793	-0.001	0.017
6 C	-2.209	-3.300	0.490	-0.040	25 C	-2.209	-3.756	0.035	0.002
7 C	-2.207	-3.763	0.030	0.012	26 C	-2.211	-3.805	-0.016	-0.026
8 C	-2.208	-3.793	-0.001	0.017	27 H	-0.121	-1.360	-0.480	0.075
9 C	-2.209	-3.756	0.035	0.002	28 H	-0.118	-1.358	-0.477	0.092
10 C	-2.211	-3.805	-0.016	-0.026	29 C	-2.199	-3.341	0.461	0.196
11 H	-0.121	-1.360	-0.480	0.075	30 H	-0.118	-1.358	-0.477	0.092
12 H	-0.118	-1.358	-0.477	0.092	31 H	-0.121	-1.360	-0.480	0.075
13 C	-2.199	-3.341	0.461	0.196	32 C	-2.199	-3.341	0.461	0.196
14 H	-0.118	-1.358	-0.477	0.092	33 O	-3.349	-4.997	-0.346	-0.092
15 H	-0.121	-1.360	-0.480	0.075	34 O	-3.349	-4.997	-0.346	-0.092
16 C	-2.199	-3.341	0.461	0.196	35 O	-3.348	-5.029	-0.378	-0.236
17 C	-2.207	-3.763	0.030	0.012	36 O	-3.348	-5.029	-0.378	-0.236
18 C	-2.209	-3.300	0.490	-0.040	37 O	-3.348	-5.029	-0.378	-0.236
19 C	-2.209	-3.264	0.526	-0.037	38 O	-3.348	-5.029	-0.378	-0.236

Table 10: Voronoi charge, PTCDA

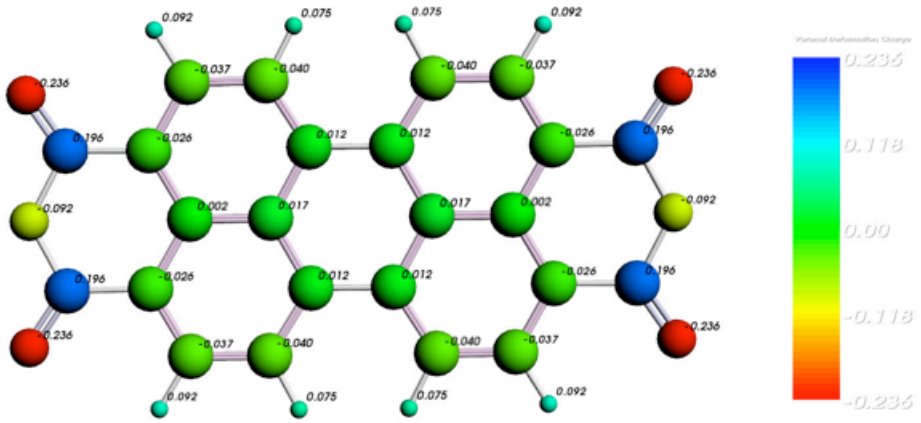

Figure 15: Voronoi deformation density, PTCDA

C.1.9 Electron Density & Electrostatic Potential at Nuclei

Atom	Density	Atom	Density
1 C	124.20239	20 C	124.20706
2 C	124.22324	21 C	124.25458
3 C	124.25458	22 C	124.22324
4 C	124.20706	23 C	124.20239
5 C	124.25458	24 C	124.19289
6 C	124.22324	25 C	124.21954
7 C	124.20239	26 C	124.20706
8 C	124.19289	27 H	0.50458
9 C	124.21954	28 H	0.49683
10 C	124.20706	29 C	124.23495
11 H	0.50458	30 H	0.49683
12 H	0.49683	31 H	0.50458
13 C	124.23495	32 C	124.23495
14 H	0.49683	33 O	307.21298
15 H	0.50458	34 O	307.21298
16 C	124.23495	35 O	307.29970
17 C	124.20239	36 O	307.29970
18 C	124.22324	37 O	307.29970
19 C	124.25458	38 O	307.29970

(a) Electron density

Atom	Potential	Atom	Potential
1 C	3.41705695	20 C	3.42989929
2 C	3.43741295	21 C	3.43819657
3 C	3.43819657	22 C	3.43741295
4 C	3.42989929	23 C	3.41705695
5 C	3.43819657	24 C	3.42151538
6 C	3.43741295	25 C	3.42201979
7 C	3.41705695	26 C	3.42989929
8 C	3.42151538	27 H	1.04983672
9 C	3.42201979	28 H	1.05612269
10 C	3.42989929	29 C	3.33279402
11 H	1.04983672	30 H	1.05612269
12 H	1.05612269	31 H	1.04983672
13 C	3.33279402	32 C	3.33279402
14 H	1.05612269	33 O	7.04007804
15 H	1.04983672	34 O	7.04007804
16 C	3.33279402	35 O	7.10540874
17 C	3.41705695	36 O	7.10540874
18 C	3.43741295	37 O	7.10540874
19 C	3.43819657	38 O	7.10540874

(b) Electrostatic potential

Table 11: Electron density & electrostatic potential at nuclei, PTCDA

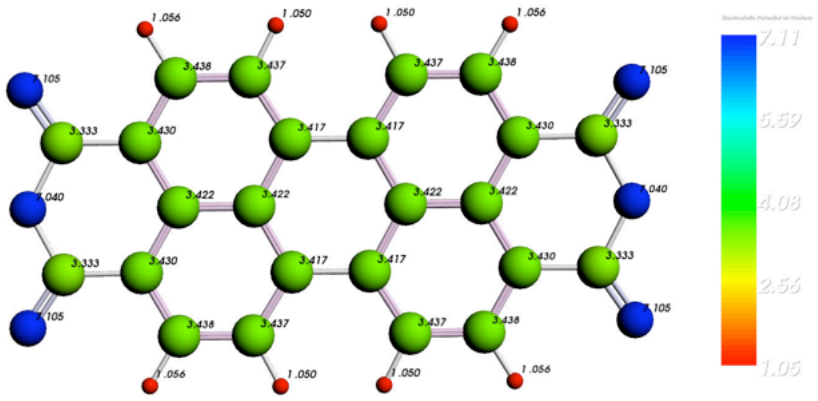

Figure 16: Electrostatic potential, PTCD

C.1.10 Entropy, Internal Energy, Heat Capacity & Moment of Inertia & Dipole and Quadrupole Moment & Polarizability

Temp. = 298.15 K, Pressure = 1 atm	Translational	Rotational	Vibrational	Total
Entropy(cal/mole-K)	43.790	33.294	63.623	140.707
Internal Energy(Kcal/mole)	0.889	0.889	167.622	169.399
Constant Volume Heat Capacity (cal/mole-K)	2.981	2.981	76.211	82.172

(a) Entropy & internal energy & heat capacity

	X	Y	Z
Moments of Inertia	4290.5535	20693.6620	24984.2155
Principal Axis 1	0.0000	1.0000	0.0000
Principal Axis 2	1.0000	0.0000	0.0000
Principal Axis 3	0.0000	0.0000	1.0000

(b) Moment of inertia

	Dipole Moment (Debye)		
Vector	0.00000000	0.00000000	0.00000000
Magnitude	0.00000000		

(c) Dipole moment

	Quadrupole Moment (a.u)				
xx	xy	xz	yy	yz	zz
47.06594961	0.00000000	0.00000000	-93.42866156	0.00000000	46.36271195

(d) Quadrupole moment

	Static Polarizability			
X	Y	Z	Average	Anisotropy
659.432228	0.000000	0.000000	357.26	469.26
0.000000	119.880987	0.000000		
0.000000	0.000000	346.474072		

(e) Polarizability

Table 12: Entropy, internal energy, heat capacity & moment of inertia & dipole and quadrupole moment & polarizability, PTCDA

C.1.11 Isosurfaces

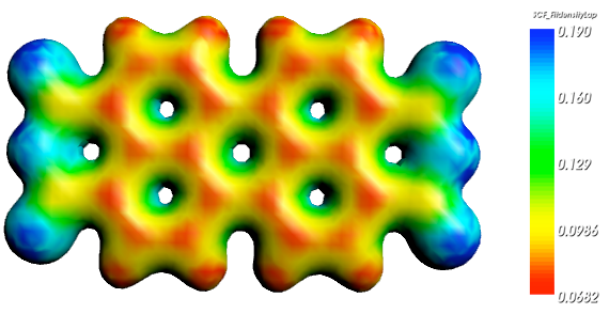

(a) Kinetic energy at density isosurface

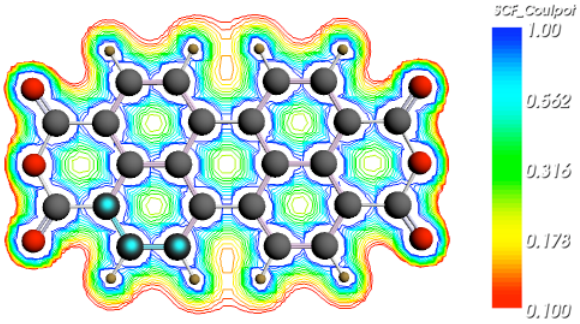

(b) Coulomb potential contours

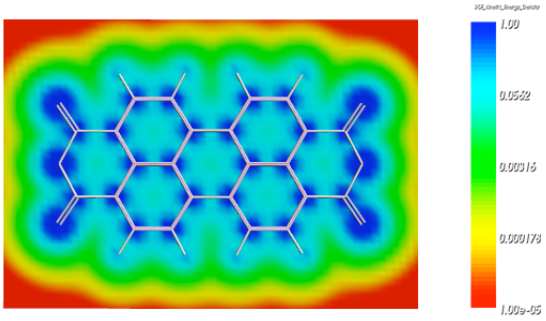

(c) Electron density cut plane

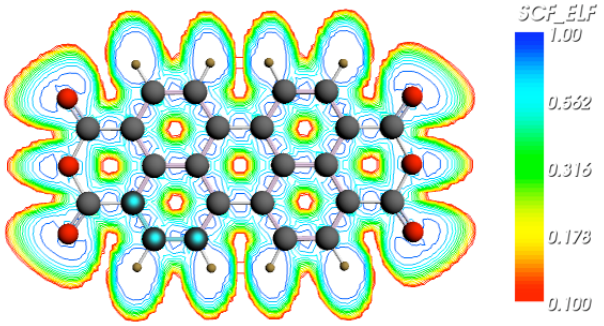

(d) ELF contours

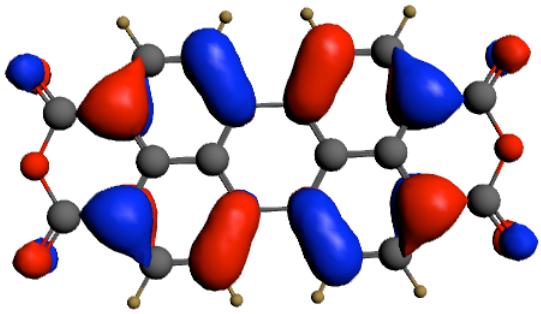

(e) HOMO

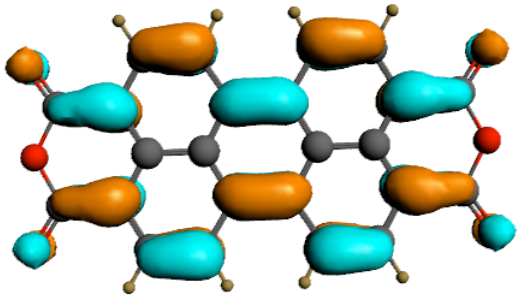

(f) LUMO

Figure 17: Isosurface, PTCDA

C.2 PTCDMe

PTCDMe ($C_{26}H_{14}N_2O_4$) is a moleucle with 46 atoms connected with covalent bonds and a conjugted π-system on the chromophore. It is calculated to be a nonplanar molecule, ($15.0 \times 6.7 \times 1.7$) with 132 normal vibrational modes and 216 valence electroncs. The methyl groups at both ends are bound to the perylene plane by a sp^2-hybridised nitrogen atom. PTCDMe has C_{2v} point group symmetry; two planes of symmetry and a C_2 axis of proper rotation transforms this molecule into itself. It is not a centrosymmetric molecule and all the vibrations change the dipole moment and polarizability at the same time. It also has irreducible representaion as:

$$\Gamma = 44\,A_1 + 23\,A_2 + 22\,B_1 + 43\,B_2 \tag{C.1}$$

It is also calculated to possess a 9.001544 eV zero-point energy and −327.04518406 eV bond energy in the minimum configuration.

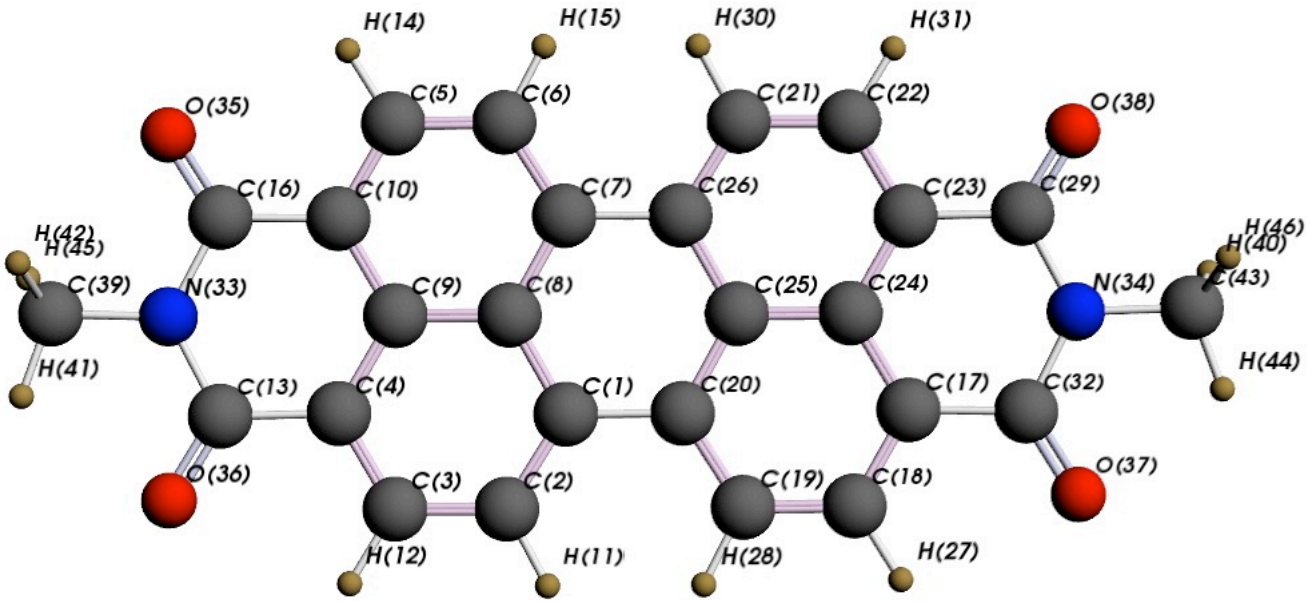

Figure 18: PTCDMe

C.2.1 Optimized Geometry

Atom	X	Y	Z	Atom	X	Y	Z
1 C	0.000000	-0.731827	1.259625	24 C	0.000000	2.858274	0.009959
2 C	0.000000	-1.479330	2.443974	25 C	0.000000	1.428202	0.010988
3 C	0.000000	-2.876003	2.435035	26 C	0.000000	0.731464	-1.237472
4 C	0.000000	-3.571789	1.233616	27 H	0.000000	3.445242	3.362915
5 C	0.000000	-2.872558	-2.416405	28 H	0.000000	0.975895	3.407064
6 C	0.000000	-1.476519	-2.423177	29 C	0.000000	5.046497	-1.237566
7 C	0.000000	-0.731464	-1.237472	30 H	0.000000	0.971788	-3.385434
8 C	0.000000	-1.428202	0.010988	31 H	0.000000	3.441928	-3.344356
9 C	0.000000	-2.858274	0.009959	32 C	0.000000	5.053453	1.258143
10 C	0.000000	-3.567795	-1.215580	33 N	0.000000	-5.699807	0.006937
11 H	0.000000	-0.975895	3.407064	34 N	0.000000	5.699807	0.006937
12 H	0.000000	-3.445242	3.362915	35 O	0.000000	-5.698822	-2.282709
13 C	0.000000	-5.053453	1.258143	36 O	0.000000	-5.693928	2.309989
14 H	0.000000	-3.441928	-3.344356	37 O	0.000000	5.693928	2.309989
15 H	0.000000	-0.971788	-3.385434	38 O	0.000000	5.698822	-2.282709
16 C	0.000000	-5.046497	-1.237566	39 C	0.000000	-7.168501	-0.035646
17 C	0.000000	3.571789	1.233616	40 H	0.889270	7.514253	-0.576744
18 C	0.000000	2.876003	2.435035	41 H	0.000000	-7.533742	0.994338
19 C	0.000000	1.479330	2.443974	42 H	-0.889270	-7.514253	-0.576744
20 C	0.000000	0.731827	1.259625	43 C	0.000000	7.168501	-0.035646
21 C	0.000000	1.476519	-2.423177	44 H	0.000000	7.533742	0.994338
22 C	0.000000	2.872558	-2.416405	45 H	0.889270	-7.514253	-0.576744
23 C	0.000000	3.567795	-1.215580	46 H	-0.889270	7.514253	-0.576744

Table 13: Optimized geometry, PTCDMe

C.2.2 Vibrational Frequencies

	Freq.		
1	121.89	23	1282.07
2	214.20	24	1290.12
3	317.40	25	1292.18
4	373.47	26	1322.13
5	406.79	27	1349.74
6	435.91	28	1382.41
7	466.95	29	1401.74
8	525.62	30	1440.12
9	561.92	31	1455.94
10	604.96	32	1465.55
11	705.94	33	1502.24
12	779.07	34	1556.96
13	813.22	35	1567.62
14	932.13	36	1579.11
15	956.44	37	1637.08
16	1032.92	38	1674.68
17	1077.96	39	2967.84
18	1142.22	40	3095.73
19	1179.18	41	3123.08
20	1199.80	42	3123.57
21	1230.54	43	3140.42
22	1259.72	44	3142.95

(a) A1

	Freq.
1	17.30
2	68.05
3	81.77
4	119.34
5	161.44
6	187.76
7	262.75
8	278.17
9	429.82
10	461.07
11	576.79
12	615.00
13	724.72
14	731.48
15	796.32
16	831.08
17	835.40
18	962.16
19	963.54
20	1112.53
21	1440.07
22	3041.60

(b) B1

	Freq.		
1	232.31	23	1251.90
2	353.18	24	1325.68
3	384.42	25	1344.83
4	391.47	26	1358.45
5	404.29	27	1388.32
6	428.61	28	1391.87
7	499.18	29	1421.30
8	563.47	30	1445.44
9	591.20	31	1456.34
10	690.30	32	1519.53
11	698.57	33	1560.52
12	790.66	34	1583.70
13	861.61	35	1593.94
14	895.72	36	1637.87
15	1008.13	37	1671.00
16	1011.00	38	2967.79
17	1047.11	39	3095.72
18	1124.54	40	3117.60
19	1155.02	41	3119.23
20	1174.59	42	3130.92
21	1210.44	43	3132.28
22	1218.16		

(c) B2

	Freq.
1	5.19
2	62.36
3	81.67
4	91.86
5	127.31
6	151.59
7	246.41
8	300.03
9	356.12
10	449.94
11	514.71
12	640.89
13	643.67
14	731.84
15	742.81
16	812.11
17	830.15
18	840.70
19	953.82
20	954.63
21	1112.53
22	1440.07
23	3041.59

(d) A2

Table 14: Vibrational frequencies, PTCDMe

C.2.3 Infrared Intensities

	Freq.	Dipole Str.	IR Int.		Freq.	Dipole Str.	IR Int.
1	232.31	0.04	0.00	23	1251.90	13.23	4.15
2	353.18	61.42	5.44	24	1325.68	1651.14	548.66
3	384.42	9.01	0.87	25	1344.83	203.08	68.46
4	391.47	83.52	8.19	26	1358.45	2.70	0.92
5	404.29	1179.45	119.52	27	1388.32	207.45	72.19
6	428.61	36.72	3.95	28	1391.87	613.23	213.94
7	499.18	162.70	20.36	29	1421.30	637.04	226.95
8	563.47	0.01	0.00	30	1445.44	0.01	0.00
9	591.20	154.74	22.93	31	1456.34	3.31	1.21
10	690.30	0.90	0.16	32	1519.53	0.57	0.22
11	698.57	16.75	2.93	33	1560.52	410.12	160.42
12	790.66	64.19	12.72	34	1583.70	1116.13	443.06
13	861.61	15.11	3.26	35	1593.94	1.40	0.56
14	895.72	16.77	3.77	36	1637.87	0.01	0.00
15	1008.13	454.05	114.74	37	1671.00	1718.61	719.83
16	1011.00	34.83	8.83	38	2967.79	82.83	61.62
17	1047.11	9.46	2.48	39	3095.72	8.69	6.75
18	1124.54	34.40	9.70	40	3117.60	3.68	2.88
19	1155.02	8.00	2.32	41	3119.23	2.52	1.97
20	1174.59	1.63	0.48	42	3130.92	2.20	1.73
21	1210.44	0.50	0.15	43	3132.28	2.26	1.77
22	1218.16	9.32	2.85				

(a) B2

	Freq.	Dipole Str.	IR Int.
1	17.30	42.78	0.19
2	68.05	5.32	0.09
3	81.77	332.61	6.82
4	119.34	170.43	5.10
5	161.44	1.18	0.05
6	187.76	248.24	11.68
7	262.75	0.01	0.00
8	278.17	7.53	0.53
9	429.82	0.01	0.00
10	461.07	2.08	0.24
11	576.79	10.94	1.58
12	615.00	0.01	0.00
13	724.72	193.64	35.18
14	731.48	30.45	5.58
15	796.32	161.70	32.28
16	831.08	5.27	1.10
17	835.40	135.03	28.27
18	962.16	0.76	0.18
19	963.54	9.67	2.34
20	1112.53	2.05	0.57
21	1440.07	53.08	19.16
22	3041.60	14.39	10.97

(b) B1

	Freq.	Dipole Str.	IR Int.		Freq.	Dipole Str.	IR Int.
1	121.89	37.67	1.15	23	1282.07	12.60	4.05
2	214.20	0.00	0.00	24	1290.12	2.66	0.86
3	317.40	71.30	5.67	25	1292.18	10.60	3.43
4	373.47	90.18	8.44	26	1322.13	6.09	2.02
5	406.79	19.19	1.96	27	1349.74	0.74	0.25
6	435.91	116.84	12.77	28	1382.41	1.03	0.36
7	466.95	0.00	0.00	29	1401.74	8.21	2.88
8	525.62	0.02	0.00	30	1440.12	2.29	0.82
9	561.92	0.01	0.00	31	1455.94	44.13	16.10
10	604.96	0.45	0.07	32	1465.55	0.97	0.36
11	705.94	0.00	0.00	33	1502.24	115.49	43.49
12	779.07	25.90	5.06	34	1556.96	0.00	0.00
13	813.22	0.01	0.00	35	1567.62	0.01	0.00
14	932.13	0.08	0.02	36	1579.11	5.70	2.25
15	956.44	1.07	0.26	37	1637.08	2135.80	876.41
16	1032.92	632.46	163.75	38	1674.68	0.99	0.41
17	1077.96	0.01	0.00	39	2967.84	2.79	2.07
18	1142.22	81.03	23.20	40	3095.73	1.68	1.30
19	1179.18	94.14	27.83	41	3123.08	1.16	0.91
20	1199.80	0.82	0.25	42	3123.57	2.06	1.61
21	1230.54	0.01	0.00	43	3140.42	0.11	0.09
22	1259.72	648.65	204.81	44	3142.95	0.20	0.16

(c) A1

Table 15: IR intensities, PTCDMe

C.2.4 Orbital Energies and UV/Vis Spectrum

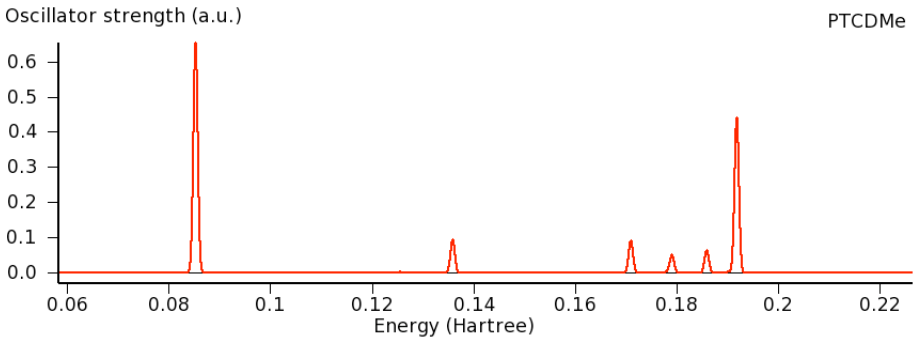

Figure 19: UV/Vis spectrum, PTCDMe

	Energy		
1	-520.35	24	-21.64
2	-520.33	25	-20.25
3	-391.45	26	-19.42
4	-280.61	27	-18.53
5	-280.54	28	-18.24
6	-278.65	29	-18.00
7	-278.64	30	-16.22
8	-278.51	31	-15.54
9	-278.49	32	-15.21
10	-278.24	33	-14.93
11	-278.21	34	-13.82
12	-278.11	35	-13.78
13	-278.10	36	-13.04
14	-278.09	37	-13.01
15	-278.08	38	-12.36
16	-277.88	39	-12.17
17	-29.23	40	-12.02
18	-28.70	41	-11.64
19	-26.02	42	-11.13
20	-25.57	43	-10.55
21	-24.02	44	-10.27
22	-23.46	45	-8.25
23	-21.87	46	-7.72

(a) A1

	Energy
1	-13.47
2	-11.79
3	-11.31
4	-10.74
5	-9.61
6	-8.12
7	-7.88
8	-7.75
9	-6.33

(b) A2

	Energy
1	-13.49
2	-12.45
3	-11.39
4	-11.20
5	-10.49
6	-9.50
7	-8.09
8	-7.97
9	-7.83

(c) B1

	Energy		
1	-520.35	23	-21.26
2	-520.33	24	-20.57
3	-391.45	25	-19.75
4	-280.61	26	-18.52
5	-280.54	27	-17.56
6	-278.64	28	-17.44
7	-278.63	29	-16.84
8	-278.51	30	-15.49
9	-278.49	31	-14.58
10	-278.24	32	-14.35
11	-278.21	33	-13.35
12	-278.11	34	-13.12
13	-278.10	35	-12.58
14	-278.09	36	-12.49
15	-278.08	37	-12.34
16	-277.88	38	-11.63
17	-29.23	39	-11.62
18	-28.70	40	-11.14
19	-26.01	41	-11.05
20	-24.87	42	-9.86
21	-23.41	43	-8.26
22	-22.05	44	-7.72

(d) B2

Table 16: Orbital energies, PTCDMe

C.2.5 Excitation Energies

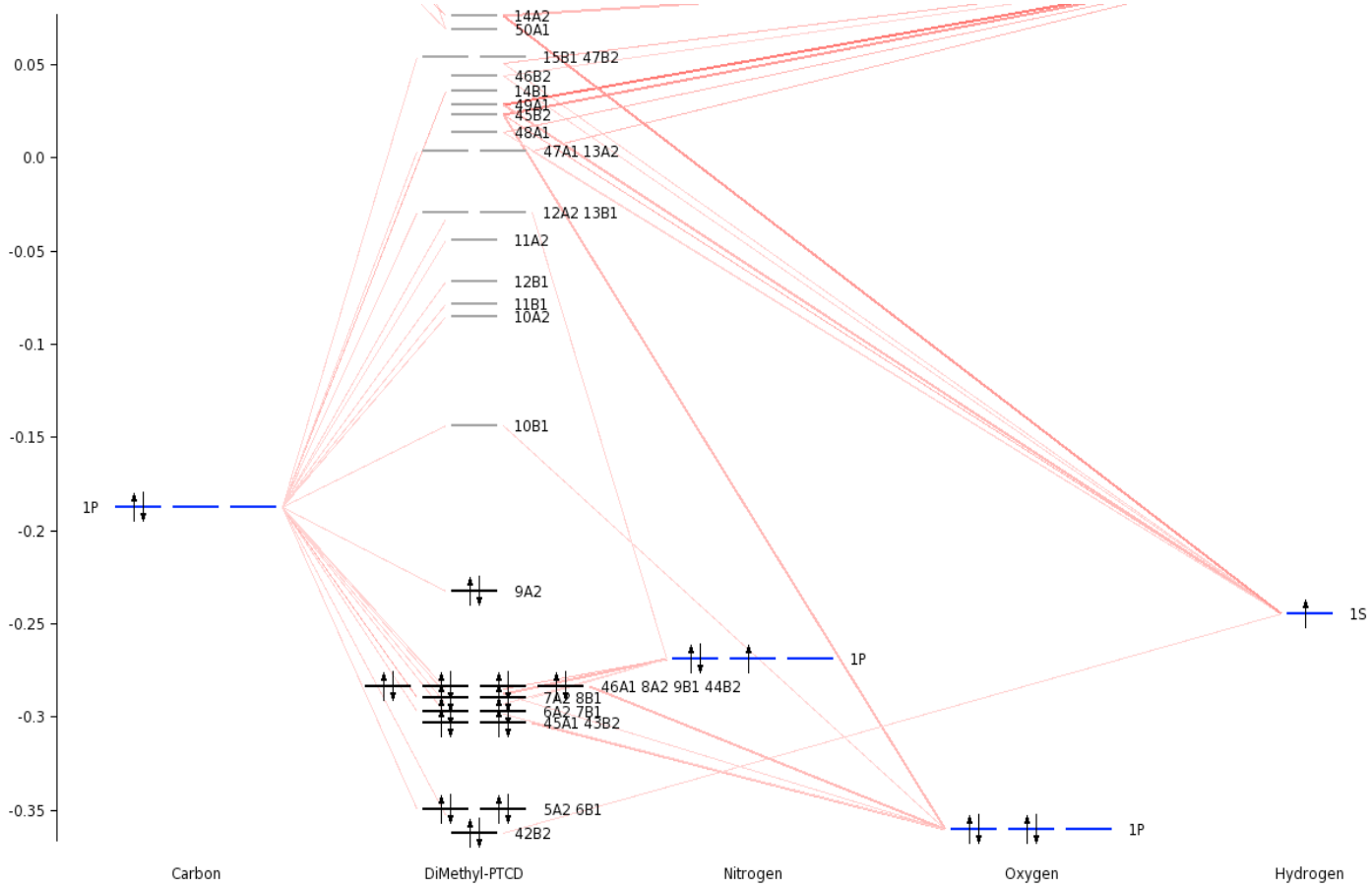

Figure 20: Excitation energies, PTCDMe

The most transition, with an oscillator strength of 0.65, happens at 514.0 nm which has 98.2% contribution from HOMO→LUMO and corresponds to the $\pi \rightarrow \pi^*$ transtion. HOMO (-6.32 eV) has A_2 symmetry, LUMO (-3.91 eV) has B_1 symmetry and the transition dipole moment between them has $A_2 \otimes B_1 = B_2$ symmetry, which is verified by the calculation of ADF.

The HOMO $\longrightarrow$ (LUMO + 4) transition happens at 241 nm which corresponds to the UV transition in this molecule.

C.2.6 IR Spectrum

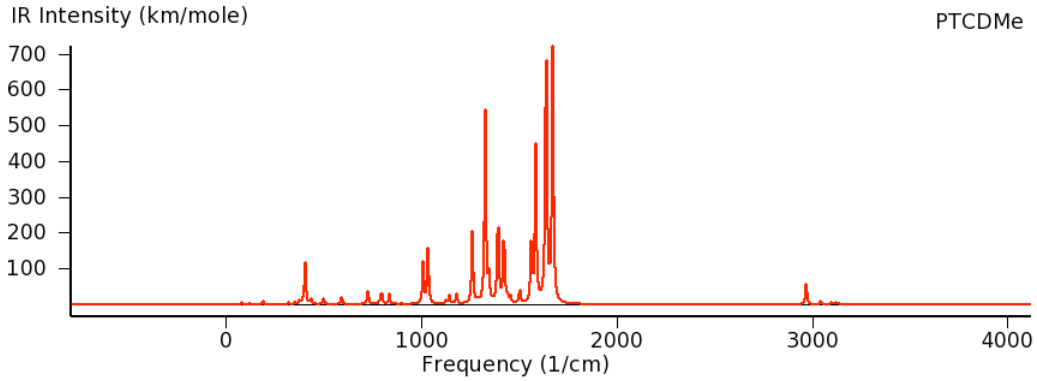

Figure 21: Infrared Spectrum, PTCDMe

2968: C–H in the methyl groups stretching, chromophore hardly moving

1671: C=O symmetric stretching, chromophore and methyl groups hardly moving

1637: C=O antisymmetric stretching, chromophore and methyl groups hardly moving

1584: chromophore stretching, C–H in the chromophore scissoring, methyl groups hardly moving

1561: chromophore vigorously deforming, C–H in the chromophore rocking, methyl groups hardly moving

1421: C–N–C symmetric stretching, chromophore slightly deforming, C–H in the chromophore rocking, C–H in the methyl groups wagging

1392: C–C stretching, C–H in the methyl groups wagging vigorously, C–H in the chromophore rocking, chromophore hardly moving

1326: C–N–C symmetric stretching, C–C stretching, C–H in the chromophore scissoring, C–H in the methyl groups wagging

1260: C–N–C antisymmetric stretching, C–H in the methyl groups twisting C–H in the chromophore scissoring

1033: C–N–C antisymmetric stretching, C–H in the methyl groups twisting, chromophore vigorously deforming, C–H in the chromophore rocking

1008: chromophore deforming, C–C stretching, C–H in the chromophore scissoring, methyl groups twisting

404: C–N–C scissoring, chromophore slightly deforming

C.2.7 Normal Raman Spectrum

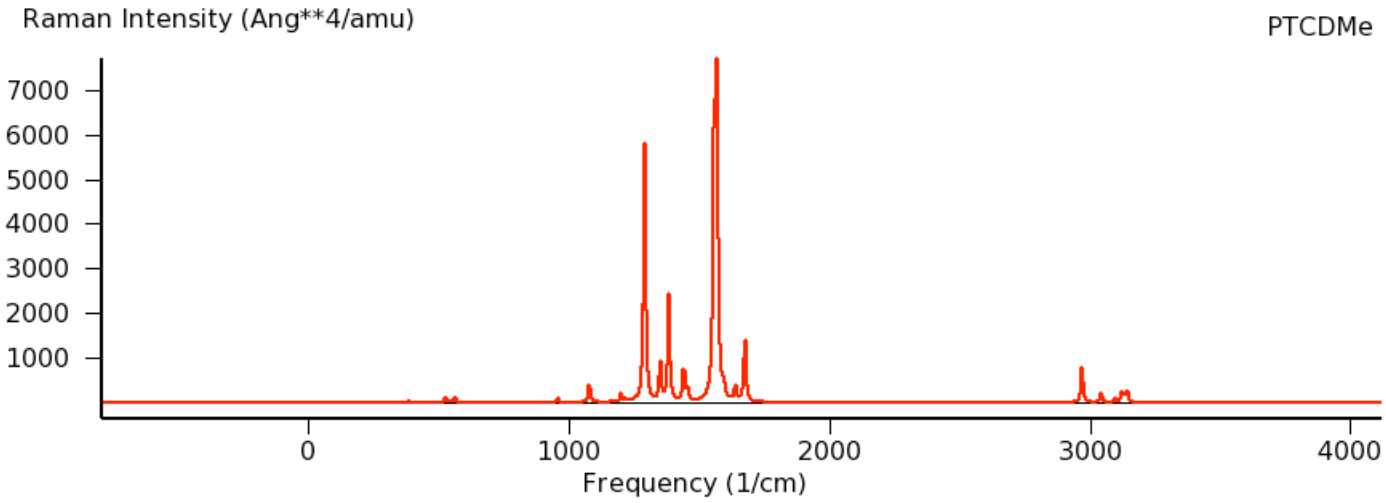

Figure 22: Normal Raman spectrum, PTCDMe

2968: C–H in the methyl group stretching symmetrically, chromophore hardly moving

1675: C=O symmetric stretching, C–N–C scissoring, benzene group at both ends expanding and contracting vigorously, central benzene group hardly moving, methyl group slightly wagging

1568: chromophore symmetric stretching, C–N–C scissoring, methyl group hardly moving

1557: chromophore symmetric stretching, C–H in the chromophore scissoring, methyl group hardly moving

1382: chromophore symmetric stretching, C–H in the methyl group wagging and C–H in the ring scissoring

1290: The central benzene expanding and contracting, C–H on each corner scissoring

C.2.8 Normal Raman Intensities & Depolarization Ratio

	Freq.	Int.	Ratio		Freq.	Int.	Ratio
1	122.12	0.01	0.53	23	1282.12	228.23	0.36
2	214.40	2.50	0.64	24	1290.12	5583.48	0.27
3	317.51	0.03	0.46	25	1292.21	175.06	0.26
4	373.52	0.05	0.25	26	1322.13	0.10	0.70
5	406.90	1.16	0.28	27	1349.73	985.06	0.24
6	435.97	0.33	0.27	28	1382.44	2403.06	0.30
7	466.99	0.12	0.67	29	1401.65	47.40	0.11
8	525.66	172.92	0.13	30	1440.13	896.50	0.28
9	561.98	137.54	0.15	31	1455.94	214.55	0.33
10	605.02	0.17	0.17	32	1465.55	6.04	0.40
11	706.00	16.98	0.38	33	1502.29	0.97	0.26
12	779.07	0.06	0.48	34	1556.98	7660.15	0.39
13	813.26	2.53	0.25	35	1567.67	6752.87	0.34
14	932.12	0.73	0.11	36	1579.10	24.04	0.31
15	956.49	129.89	0.25	37	1637.15	0.55	0.56
16	1032.88	0.72	0.72	38	1674.73	1685.03	0.24
17	1078.01	524.48	0.31	39	2967.89	900.42	0.14
18	1142.22	0.06	0.71	40	3095.64	15.78	0.74
19	1179.26	1.32	0.18	41	3123.07	114.31	0.12
20	1199.85	204.66	0.21	42	3123.63	51.07	0.11
21	1230.57	0.20	0.62	43	3140.44	182.01	0.26
22	1259.72	5.46	0.13	44	3142.99	134.49	0.29

(a) A1

	Freq.	Int.	Ratio
1	-4.23		
2	62.44	1.40	0.74
3	81.76	0.03	0.72
4	91.85	1.97	0.72
5	127.33	1.88	0.75
6	151.58	1.08	0.30
7	246.33	0.01	0.14
8	300.02	0.01	0.70
9	356.10	7.74	0.45
10	449.90	0.66	0.69
11	514.71	0.01	0.22
12	640.87	0.10	0.72
13	643.66	4.67	0.28
14	731.83	0.46	0.75
15	742.82	0.05	0.69
16	812.07	0.86	0.68
17	830.14	0.01	0.02
18	840.69	4.04	0.75
19	953.84	0.85	0.75
20	954.70	2.61	0.74
21	1112.58	0.44	0.64
22	1440.04	21.53	0.75
23	3041.56	214.83	0.75

(b) A2

	Freq.	Int.	Ratio
1	17.67	0.07	0.15
2	68.19	0.73	0.74
3	81.84	0.06	0.53
4	119.30	0.02	0.31
5	161.43	0.09	0.28
6	187.77	3.46	0.25
7	262.75	0.10	0.40
8	278.09	1.87	0.26
9	429.82	1.66	0.74
10	461.04	0.85	0.29
11	576.77	0.11	0.21
12	614.99	1.40	0.34
13	724.71	2.30	0.32
14	731.49	0.01	0.71
15	796.29	0.07	0.40
16	831.10	0.97	0.62
17	835.38	0.12	0.20
18	962.20	2.04	0.29
19	963.59	0.09	0.37
20	1112.58	7.88	0.26
21	1440.04	0.72	0.75
22	3041.56	31.91	0.74

(c) B1

	Freq.	Int.	Ratio		Freq.	Int.	Ratio
1	232.51	17.77	0.75	23	1251.89	40.66	0.74
2	353.12	1.74	0.75	24	1325.68	0.10	0.45
3	384.49	40.18	0.75	25	1344.89	0.14	0.42
4	391.74	0.04	0.26	26	1358.45	21.52	0.75
5	404.40	0.14	0.58	27	1388.31	0.15	0.55
6	428.69	0.68	0.71	28	1391.78	0.99	0.66
7	499.23	0.11	0.26	29	1421.29	2.90	0.74
8	563.49	11.03	0.75	30	1445.47	72.71	0.75
9	591.23	0.01	0.16	31	1456.34	14.16	0.75
10	690.34	0.29	0.38	32	1519.56	2.51	0.74
11	698.64	0.06	0.34	33	1560.54	0.25	0.73
12	790.67	0.02	0.59	34	1583.74	0.02	0.75
13	861.60	11.09	0.74	35	1593.95	289.84	0.75
14	895.80	0.11	0.54	36	1637.93	403.50	0.75
15	1008.15	1.03	0.56	37	1671.06	0.31	0.70
16	1010.98	0.16	0.56	38	2967.83	11.92	0.75
17	1047.12	1.11	0.73	39	3095.63	63.19	0.75
18	1124.62	0.03	0.15	40	3117.62	51.78	0.74
19	1155.07	6.61	0.73	41	3119.28	70.33	0.74
20	1174.61	2.38	0.74	42	3130.93	40.63	0.74
21	1210.49	0.04	0.72	43	3132.32	36.26	0.75
22	1218.20	53.28	0.75				

(d) B2

Table 17: Raman intensities & depolarization ratio, PTCDMe

C.2.9 Resonance Raman Intensities

	A1	514	244		A1	514	244
1	124.1	23.2	0.3	23	1282.0	54522.6	7630.4
2	214.2	5429.1	8.1	24	1293.1	24033.8	286.9
3	314.2	25.9	61.5	25	1293.9	420336.0	91.3
4	354.9	30.7	0.6	26	1326.2	87.6	35.6
5	386.2	268.5	121.4	27	1342.5	117385.0	381.4
6	441.5	41.2	0.8	28	1379.4	53086.1	6864.4
7	471.8	2083.0	471.7	29	1418.4	8656.4	80378.2
8	531.6	16795.7	1807.9	30	1445.1	80910.1	603.1
9	562.9	43869.3	5543.8	31	1462.1	1228.7	191.9
10	617.0	0.4	15.7	32	1466.3	1953.1	2.9
11	721.7	4423.7	92.2	33	1501.0	827.8	50.2
12	796.7	28.9	12.1	34	1551.3	567505.0	196982.0
13	825.1	2407.9	542.4	35	1562.7	654586.0	71933.6
14	930.6	1978.0	121.2	36	1575.2	317.2	50.8
15	955.9	15192.5	4006.6	37	1645.7	724.1	370.6
16	1035.7	750.2	48.1	38	1687.6	2388.8	18482.4
17	1074.4	66.8	2808.4	39	3018.4	571.9	2351.2
18	1148.1	69.7	12.7	40	3153.4	68.0	605.3
19	1183.4	5.6	5.4	41	3174.1	842.1	180.7
20	1201.1	15701.7	5561.2	42	3175.1	503.7	143.0
21	1229.3	302.8	287.1	43	3190.2	1004.7	80.0
22	1263.6	827.3	879.0	44	3191.3	586.5	853.4

(a) A1

	A2	514	244
1	-5.2	0.7	2.4
2	15.8	0.0	1.6
3	85.8	33.3	0.0
4	91.5	0.3	0.3
5	115.7	0.2	0.1
6	151.9	5.1	0.1
7	274.9	0.3	0.5
8	306.7	0.0	0.0
9	376.1	6.2	6.7
10	460.0	55.3	0.8
11	521.4	0.1	0.0
12	632.6	0.0	28.5
13	662.5	58.8	0.2
14	738.8	18.3	0.0
15	743.6	1.1	0.3
16	830.9	4.2	60.7
17	835.0	0.1	0.0
18	861.1	121.1	78.0
19	943.7	311.7	0.1
20	944.2	6.0	48.9
21	1114.6	0.9	0.0
22	1450.1	7.9	44.0
23	3104.9	25.6	246.3

(b) A2

	B1	514	244
1	-6.3	0.1	0.2
2	41.9	0.0	0.1
3	69.6	0.3	0.8
4	112.7	0.0	0.1
5	164.1	0.0	0.1
6	194.0	0.0	0.1
7	269.9	0.0	0.0
8	320.6	0.0	0.1
9	436.5	6.7	10.2
10	469.2	0.0	0.3
11	598.6	0.0	0.0
12	622.5	0.1	0.1
13	726.4	0.1	5.3
14	747.0	0.0	0.0
15	814.6	0.0	0.1
16	830.7	0.8	4.2
17	846.1	0.0	0.1
18	951.6	0.0	6.5
19	951.7	0.0	0.1
20	1114.6	0.0	0.4
21	1450.1	0.8	6.4
22	3104.9	43.2	12.6

(c) B1

	B2	514	244
1	228.7	78.0	53.2
2	340.4	20.8	29.6
3	375.5	1.8	0.2
4	390.1	259.9	312.4
5	403.6	3.9	1.5
6	431.1	34.5	24.0
7	505.9	6.2	0.2
8	580.3	135.7	125.8
9	605.3	1.7	0.0
10	711.1	2.1	4.6
11	712.7	37.9	0.1
12	803.8	5.3	0.0
13	873.1	389.4	170.9
14	898.1	0.4	0.3
15	1009.2	0.9	115.0
16	1021.8	315.2	41.3
17	1050.1	391.3	55.0
18	1132.9	12.8	0.2
19	1162.3	575.7	187.6
20	1183.8	1.5	35.8
21	1216.2	124.5	35.0
22	1220.8	29.0	3492.5

	B2	514	244
23	1259.6	26.5	4.5
24	1318.7	299.1	18.8
25	1347.2	29.5	148.5
26	1359.7	1051.8	4113.7
27	1397.6	17.4	1861.9
28	1408.3	2.2	10.2
29	1424.4	120.1	2.0
30	1444.2	325.8	3428.0
31	1465.9	19.0	151.0
32	1520.3	87.0	2760.2
33	1555.1	3.5	0.1
34	1583.2	0.0	1.1
35	1590.9	36082.7	5709.4
36	1646.2	22548.8	5727.4
37	1684.9	3.0	25.7
38	3018.4	62.1	3.1
39	3153.4	53.1	0.1
40	3169.5	6.3	1.0
41	3169.7	280.0	79.2
42	3181.4	169.7	12.0
43	3181.7	131.8	7.8

(d) B2

Table 18: Resonance Raman intensities at 244 & 514.5 nm , PTCDMe

C.2.10 Resonance Raman Spectra

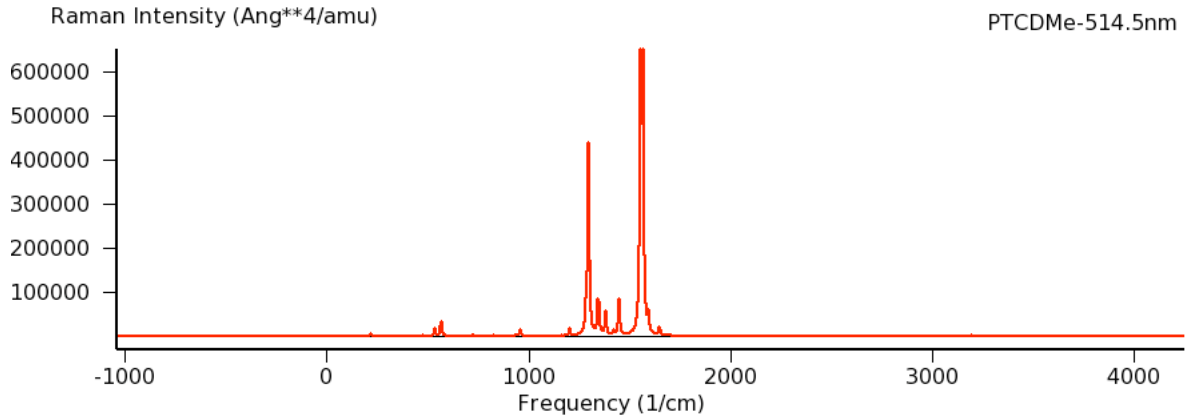

(a) 514.5 nm

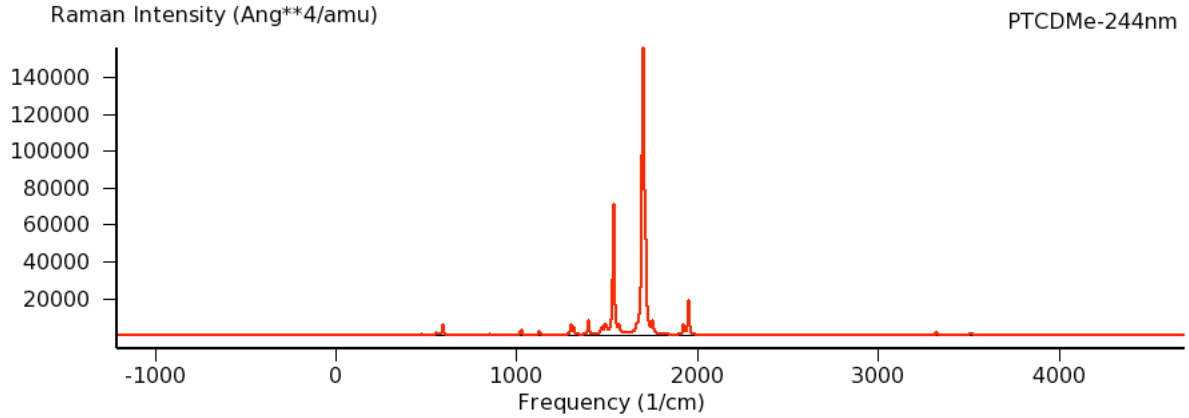

(b) 244 nm

Figure 23: Calculated RRS, broaden with a Lorentzian having a width of 9 cm-1, PTCDMe

C.2.11 Mulliken & Hirshfeld Charge

Atom	Charge	Atom	Charge
1 C	0.0130	24 C	0.1545
2 C	-0.0336	25 C	-0.0593
3 C	-0.0233	26 C	-0.0593
4 C	-0.0097	27 H	0.0494
5 C	-0.0233	28 H	0.0550
6 C	-0.0334	29 H	0.0551
7 C	0.0128	30 H	0.0494
8 C	0.0069	31 H	0.0550
9 C	0.0088	32 H	0.0494
10 C	-0.0100	33 H	0.0494
11 C	0.1545	34 H	0.0551
12 C	0.1524	35 H	0.0519
13 C	-0.0097	36 H	0.0456
14 C	-0.0233	37 H	0.0519
15 C	-0.0336	38 H	0.0456
16 C	0.0130	39 H	0.0519
17 C	-0.0334	40 H	0.0519
18 C	-0.0233	41 N	-0.0259
19 C	-0.0100	42 N	-0.0259
20 C	0.0088	43 O	-0.2443
21 C	0.0069	44 O	-0.2426
22 C	0.0128	45 O	-0.2426
23 C	0.1524	46 O	-0.2443

(a) Hirshfeld

Atom	Charge	Atom	Charge
1 C	-0.0112	24 C	0.0341
2 C	0.2328	25 C	-0.0050
3 C	0.2132	26 C	-0.0118
4 C	-0.1031	27 H	-0.1359
5 C	0.2142	28 H	-0.1899
6 C	0.2342	29 C	0.6061
7 C	-0.0118	30 H	-0.1896
8 C	-0.0050	31 H	-0.1376
9 C	0.0341	32 C	0.6079
10 C	-0.1063	33 N	-0.3936
11 H	-0.1899	34 N	-0.3936
12 H	-0.1359	35 O	-0.5489
13 C	0.6079	36 O	-0.5515
14 H	-0.1376	37 O	-0.5515
15 H	-0.1896	38 O	-0.5489
16 C	0.6061	39 C	0.5883
17 C	-0.1031	40 H	-0.1099
18 C	0.2132	41 H	-0.1265
19 C	0.2328	42 H	-0.1099
20 C	-0.0112	43 C	0.5883
21 C	0.2342	44 H	-0.1265
22 C	0.2142	45 H	-0.1099
23 C	-0.1063	46 H	-0.1099

(b) Mulliken

Table 19: Charge analysis, PTCDMe

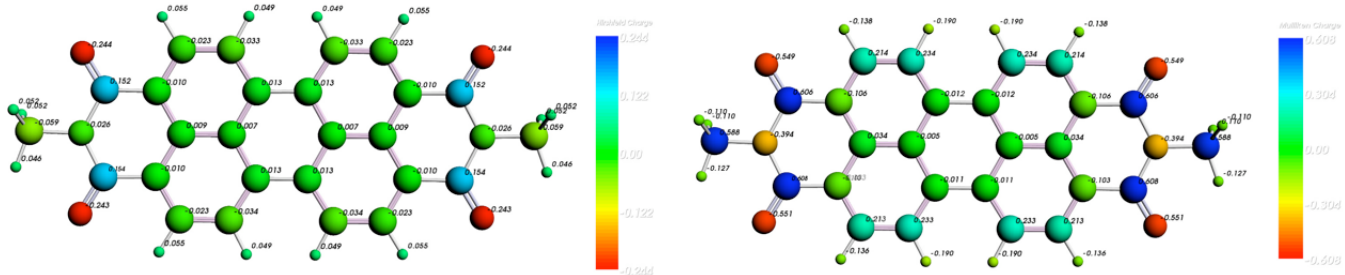

(a) Hirshfeld (b) Mulliken

Figure 24: Charge analysis, PTCDMe

C.2.12 Voronoi Charge

Atom	Sphere	RestCell	Total	VDD	Atom	Sphere	RestCell	Total	VDD
1 C	-2.207	-3.768	0.025	0.007	24 C	-2.209	-3.774	0.017	0.012
2 C	-2.209	-3.305	0.486	-0.047	25 C	-2.208	-3.790	0.002	0.008
3 C	-2.209	-3.280	0.511	-0.033	26 C	-2.207	-3.768	0.025	0.007
4 C	-2.210	-3.790	0.001	-0.029	27 H	-0.119	-1.367	-0.486	0.082
5 C	-2.209	-3.281	0.510	-0.032	28 H	-0.121	-1.363	-0.484	0.067
6 C	-2.209	-3.306	0.485	-0.047	29 C	-2.200	-3.439	0.361	0.166
7 C	-2.207	-3.768	0.025	0.007	30 H	-0.121	-1.364	-0.485	0.069
8 C	-2.208	-3.790	0.002	0.008	31 H	-0.119	-1.365	-0.484	0.082
9 C	-2.209	-3.774	0.017	0.012	32 C	-2.200	-3.439	0.362	0.170
10 C	-2.210	-3.789	0.001	-0.029	33 N	-3.045	-4.101	-0.146	-0.054
11 H	-0.121	-1.363	-0.484	0.067	34 N	-3.045	-4.101	-0.146	-0.054
12 H	-0.119	-1.367	-0.486	0.082	35 O	-3.396	-5.012	-0.409	-0.272
13 C	-2.200	-3.439	0.362	0.170	36 O	-3.397	-4.989	-0.386	-0.270
14 H	-0.119	-1.365	-0.484	0.082	37 O	-3.397	-4.989	-0.386	-0.270
15 H	-0.121	-1.364	-0.485	0.069	38 O	-3.396	-5.012	-0.409	-0.272
16 C	-2.200	-3.439	0.361	0.166	39 C	-2.206	-2.329	1.465	-0.039
17 C	-2.210	-3.790	0.001	-0.029	40 H	-0.119	-1.329	-0.448	0.062
18 C	-2.209	-3.280	0.511	-0.033	41 H	-0.118	-1.355	-0.473	0.059
19 C	-2.209	-3.305	0.486	-0.047	42 H	-0.119	-1.329	-0.448	0.062
20 C	-2.207	-3.768	0.025	0.007	43 C	-2.206	-2.329	1.465	-0.039
21 C	-2.209	-3.306	0.485	-0.047	44 H	-0.118	-1.355	-0.473	0.059
22 C	-2.209	-3.281	0.510	-0.032	45 H	-0.119	-1.329	-0.448	0.062
23 C	-2.210	-3.789	0.001	-0.029	46 H	-0.119	-1.329	-0.448	0.062

Table 20: Voronoi charge, PTCDMe

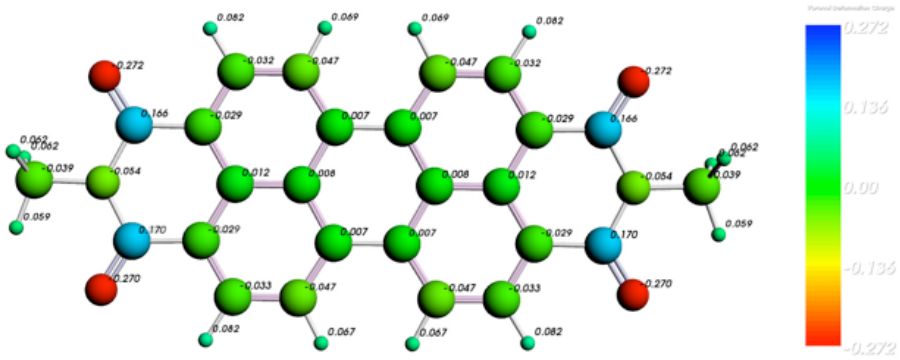

Figure 25: VDD, PTCDMe

C.2.13 Electron Density & Electrostatic Potential at Nuclei

Atom	Density	Atom	Density
1 C	126.52234	24 C	126.52251
2 C	126.53018	25 C	126.50849
3 C	126.56199	26 C	126.51718
4 C	126.52680	27 H	0.49678
5 C	126.56207	28 H	0.50474
6 C	126.53101	29 C	126.55371
7 C	126.51718	30 H	0.50487
8 C	126.50849	31 H	0.49662
9 C	126.52251	32 C	126.55817
10 C	126.52499	33 N	204.78439
11 H	0.50474	34 N	204.78439
12 H	0.49678	35 O	311.49977
13 C	126.55817	36 O	311.49839
14 H	0.49662	37 O	311.49839
15 H	0.50487	38 O	311.49977
16 C	126.55371	39 C	126.41182
17 C	126.52680	40 H	0.49915
18 C	126.56199	41 H	0.49573
19 C	126.53018	42 H	0.49915
20 C	126.52234	43 C	126.41182
21 C	126.53101	44 H	0.49573
22 C	126.56207	45 H	0.49915
23 C	126.52499	46 H	0.49915

(a) Electron density

Atom	Potential	Atom	Potential
1 C	14.71942140	24 C	14.72629608
2 C	14.73839295	25 C	14.72394498
3 C	14.74080638	26 C	14.71968065
4 C	14.73331950	27 H	1.07416721
5 C	14.74123840	28 H	1.06614295
6 C	14.73875956	29 C	14.65490754
7 C	14.71968065	30 H	1.06639573
8 C	14.72394498	31 H	1.07429337
9 C	14.72629608	32 C	14.65230531
10 C	14.73417589	33 N	18.32217791
11 H	1.06614295	34 N	18.32217791
12 H	1.07416721	35 O	22.37108777
13 C	14.65230531	36 O	22.37003734
14 H	1.07429337	37 O	22.37003734
15 H	1.06639573	38 O	22.37108777
16 C	14.65490754	39 C	14.73893983
17 C	14.73331950	40 H	1.09661727
18 C	14.74080638	41 H	1.09549571
19 C	14.73839295	42 H	1.09661727
20 C	14.71942140	43 C	14.73893983
21 C	14.73875956	44 H	1.09549571
22 C	14.74123840	45 H	1.09661727
23 C	14.73417589	46 H	1.09661727

(b) Electrostatic potential

Table 21: Electron density and electrostatic potential, PTCDMe

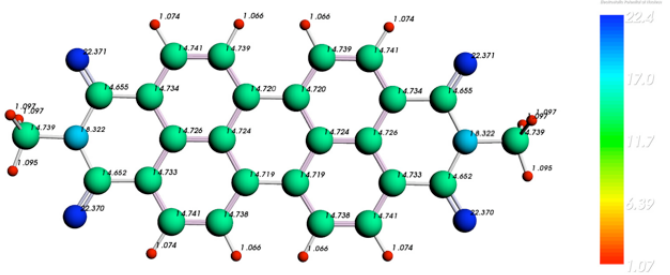

Figure 26: Electrostatic potential, PTCDMe

C.2.14 Entropy, Internal Energy, Heat Capacity & Moment of Inertia & Moment of Inertia & Dipole Moment & Hyperpolarizability

Temp. = 298.15 K Pressure = 1 atm	Trans.	Rota.	Vib.	Total
Entropy (cal/mole-K)	43.982	35.096	71.937	151.015
Internal Energy (Kcal/mole)	0.889	0.889	219.686	221.464
Constant Volume Heat Capacity (cal/mole-K)	2.981	2.981	86.480	92.441

(a) Entropy, internal energy, heat capacity

	X	Y	Z
Moments of Inertia	4371.1699	25797.2482	30145.6493
Principal Axis 1	0.0000	1.0000	0.0000
Principal Axis 2	1.0000	0.0000	0.0000
Principal Axis 3	0.0000	0.0000	1.0000

(b) Moment of inertia

	Dipole Moment (Debye)		
Vector	0.00000000	0.00000000	-0.04834724
Magnitude	0.04834724		

(c) Dipole moment

	Quadrupole Moment (a.u)				
xx	xy	xz	yy	yz	zz
22.13321204	0.00000000	0.00000000	-30.30214895	0.00000000	8.16893691

(d) Quadrupole moment

	Static Polarizability			
X	Y	Z	Average	Anisotropy
776.966072	0.000000	0.000000	431.26	554.54
0.000000	371.861459	0.000000		
0.000000	0.000000	144.958548		

(e) Polarizability

Table 22: Entropy, internal energy, heat capacity & moment of inertia & moment of inertia & dipole moment & hyperpolarizability, PTCDMe

C.2.15 Isosurfaces

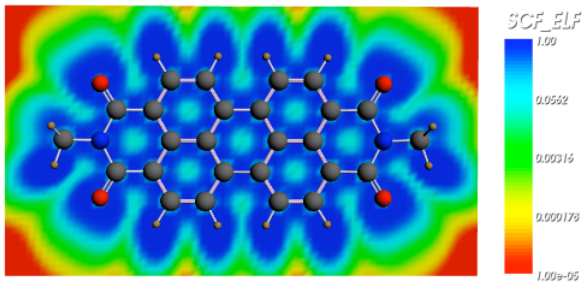

(a) ELF cut plane

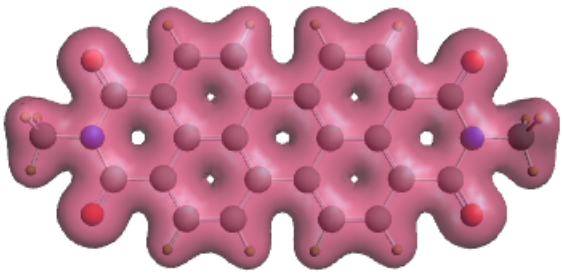

(b) Electron density isosurface

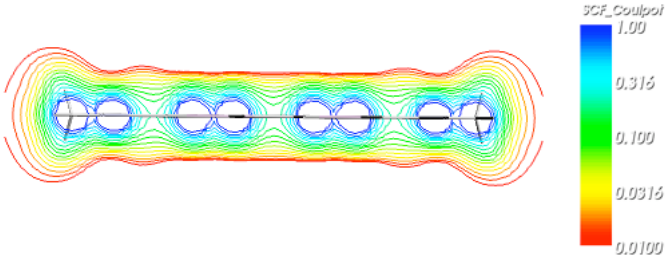

(c) Coulomb potential contours

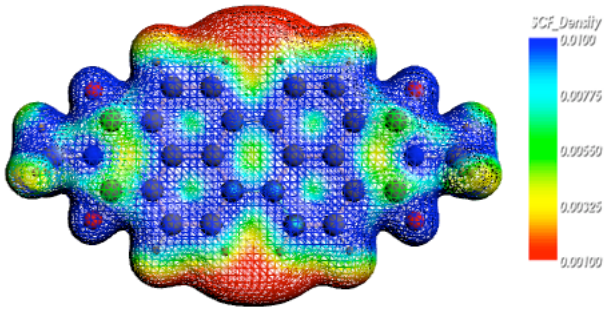

(d) Coulomb potential at density isosurface

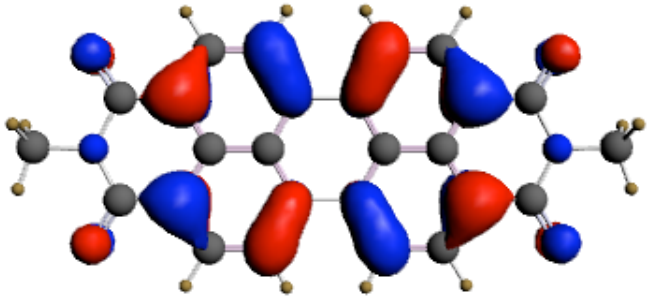

(e) HOMO

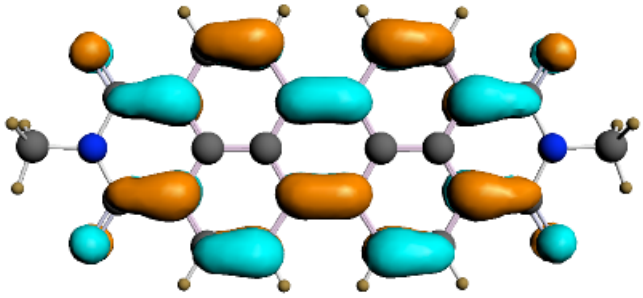

(f) LUMO

Figure 27: Isosurfaces, PTCDMe

C.3 BBIP-PTCD

BBIP-PTCD ($C_{38}H_{22}N_2O_4$), has 66 atoms, 192 vibrational normal modes and 296 valence electrons. It is found to be possessin C_{2h} Point symmetry and hence centerosymmetric, with irreducible representation of:

$$\Gamma = 52\,A_g + 44\,B_g + 45\,A_u + 51\,B_u \tag{C.2}$$

It is also calculated to be be having zero point energy of $13.309827\,eV$ and $-462.61824246\,eV$ of bonding energy.

HOMO (-6.28) eV has A_u symmetry; LUMO (-3.88) eV has B_g symmetry and therefore the HOMO $\longrightarrow$ LUMO transition happens at 516.1 nm.

The HOMO $\longrightarrow$ (LUMO + 4) transition happens at 241 nm which corresponds to the UV transition in this molecule.

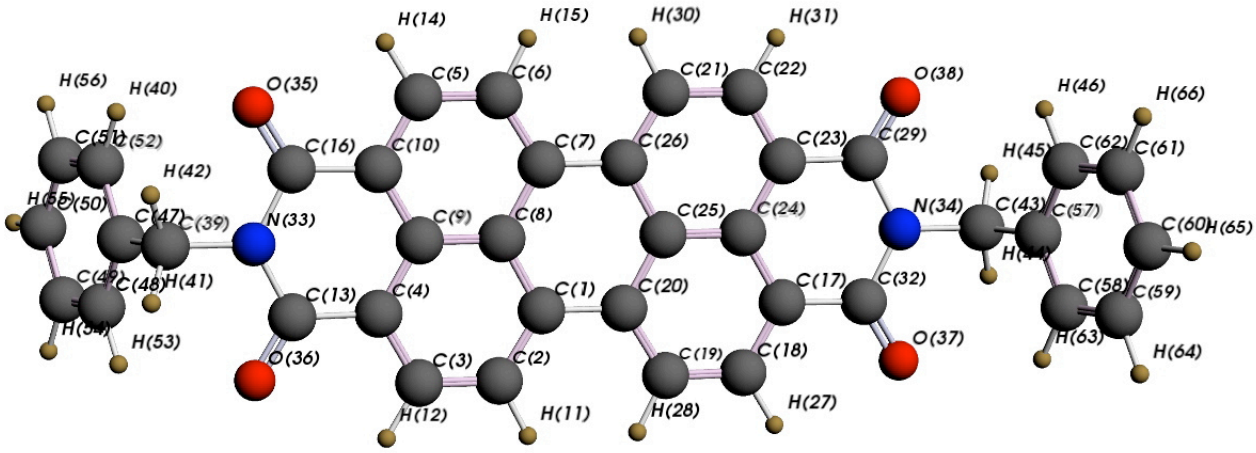

Figure 28: BBIP-PTCD

C.3.1 Optimized Geometry

Atom	X	Y	Z	Atom	X	Y	Z
1 C	-0.146743	-0.717787	1.246891	34 N	1.111990	5.602702	0.000000
2 C	-0.297101	-1.450071	2.430953	35 O	-1.148713	-5.583386	-2.297314
3 C	-0.576039	-2.818665	2.423698	36 O	-1.148713	-5.583386	2.297314
4 C	-0.714558	-3.502963	1.223736	37 O	1.148713	5.583386	2.297314
5 C	-0.576039	-2.818665	-2.423698	38 O	1.148713	5.583386	-2.297314
6 C	-0.297101	-1.450071	-2.430953	39 C	-1.411030	-7.059544	0.000000
7 C	-0.146743	-0.717787	-1.246891	40 H	-0.047145	-8.048309	-2.153569
8 C	-0.286331	-1.401592	0.000000	41 H	-2.011272	-7.241844	0.895671
9 C	-0.572289	-2.804163	0.000000	42 H	-2.011272	-7.241844	-0.895671
10 C	-0.714558	-3.502963	-1.223736	43 C	1.411030	7.059544	0.000000
11 H	-0.195761	-0.954675	3.393138	44 H	2.011272	7.241844	0.895671
12 H	-0.687447	-3.373472	3.353452	45 H	2.011272	7.241844	-0.895671
13 C	-1.002737	-4.957092	1.245457	46 H	0.047145	8.048309	-2.153569
14 H	-0.687447	-3.373472	-3.353452	47 C	-0.180066	-7.949097	0.000000
15 H	-0.195761	-0.954675	-3.393138	48 C	0.389834	-8.378480	1.209868
16 C	-1.002737	-4.957092	-1.245457	49 C	1.512819	-9.211837	1.209489
17 C	0.714558	3.502963	1.223736	50 C	2.078984	-9.627990	0.000000
18 C	0.576039	2.818665	2.423698	51 C	1.512819	-9.211837	-1.209489
19 C	0.297101	1.450071	2.430953	52 C	0.389834	-8.378480	-1.209868
20 C	0.146743	0.717787	1.246891	53 H	-0.047145	-8.048309	2.153569
21 C	0.297101	1.450071	-2.430953	54 H	1.947193	-9.536127	2.156529
22 C	0.576039	2.818665	-2.423698	55 H	2.957079	-10.276085	0.000000
23 C	0.714558	3.502963	-1.223736	56 H	1.947193	-9.536127	-2.156529
24 C	0.572289	2.804163	0.000000	57 C	0.180066	7.949097	0.000000
25 C	0.286331	1.401592	0.000000	58 C	-0.389834	8.378480	1.209868
26 C	0.146743	0.717787	-1.246891	59 C	-1.512819	9.211837	1.209489
27 H	0.687447	3.373472	3.353452	60 C	-2.078984	9.627990	0.000000
28 H	0.195761	0.954675	3.393138	61 C	-1.512819	9.211837	-1.209489
29 C	1.002737	4.957092	-1.245457	62 C	-0.389834	8.378480	-1.209868
30 H	0.195761	0.954675	-3.393138	63 H	0.047145	8.048309	2.153569
31 H	0.687447	3.373472	-3.353452	64 H	-1.947193	9.536127	2.156529
32 C	1.002737	4.957092	1.245457	65 H	-2.957079	10.276085	0.000000
33 N	-1.111990	-5.602702	0.000000	66 H	-1.947193	9.536127	-2.156529

Table 23: Optimized geometry, BBIP-PTCD

C.3.2 Orbital Energies and UV/Vis Spectrum

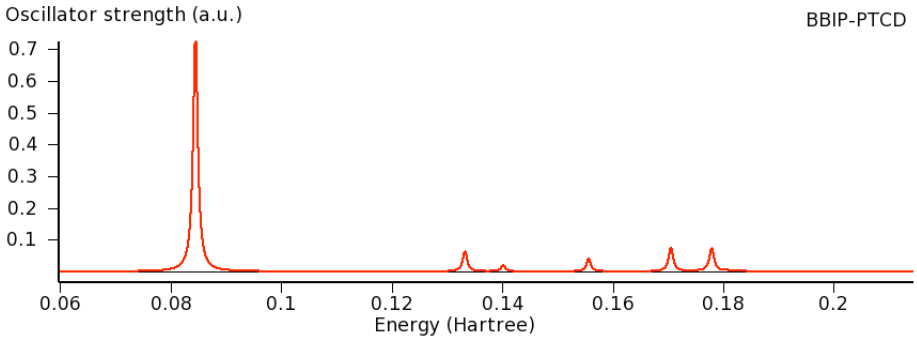

Figure 29: UV/Vis spectrum, BBIP-PTCD

	Ag		
1	-520.39	23	-18.51
2	-391.46	24	-18.22
3	-280.68	25	-16.14
4	-278.65	26	-15.14
5	-278.52	27	-14.92
6	-278.49	28	-14.08
7	-278.24	29	-13.80
8	-278.19	30	-13.30
9	-278.11	31	-12.92
10	-278.10	32	-12.49
11	-277.19	33	-12.28
12	-276.96	34	-12.06
13	-276.93	35	-11.51
14	-276.88	36	-10.83
15	-29.29	37	-10.30
16	-26.06	38	-9.82
17	-25.55	39	-9.60
18	-23.53	40	-8.34
19	-23.17	41	-8.07
20	-21.64	42	-7.83
21	-21.14	43	-7.69
22	-19.58	44	-6.76

(a) Ag

	Au		
1	-520.39	17	-15.53
2	-280.68	18	-13.81
3	-278.65	19	-13.01
4	-278.24	20	-12.59
5	-278.11	21	-12.16
6	-278.10	22	-11.62
7	-276.94	23	-11.43
8	-276.88	24	-11.30
9	-28.76	25	-10.80
10	-24.01	26	-10.53
11	-21.85	27	-9.57
12	-20.22	28	-9.28
13	-19.42	29	-7.74
14	-18.02	30	-6.83
15	-16.53	31	-6.29
16	-16.15		

(b) Au

	Bu		
1	-520.39	23	-17.43
2	-391.46	24	-17.04
3	-280.68	25	-15.90
4	-278.64	26	-14.60
5	-278.52	27	-14.05
6	-278.49	28	-13.46
7	-278.24	29	-13.34
8	-278.19	30	-12.94
9	-278.11	31	-12.61
10	-278.10	32	-12.48
11	-277.19	33	-12.10
12	-276.96	34	-11.63
13	-276.93	35	-11.20
14	-276.88	36	-11.16
15	-29.29	37	-9.83
16	-26.05	38	-9.70
17	-24.86	39	-9.41
18	-23.26	40	-8.34
19	-22.08	41	-8.02
20	-21.25	42	-7.77
21	-20.94	43	-6.76
22	-19.16		

(c) Bu

	Bg		
1	-520.39	16	-15.47
2	-280.68	17	-14.34
3	-278.64	18	-12.78
4	-278.24	19	-12.44
5	-278.11	20	-12.17
6	-278.10	21	-10.40
7	-276.94	22	-10.31
8	-276.88	23	-10.16
9	-28.76	24	-9.62
10	-23.40	25	-9.44
11	-20.57	26	-8.74
12	-20.22	27	-8.18
13	-18.54	28	-7.29
14	-17.57	29	-6.51
15	-16.49	30	-6.23

(d) Bg

Table 24: Orbital energies, BBIP-PTCD

C.3.3 Excitation Energies

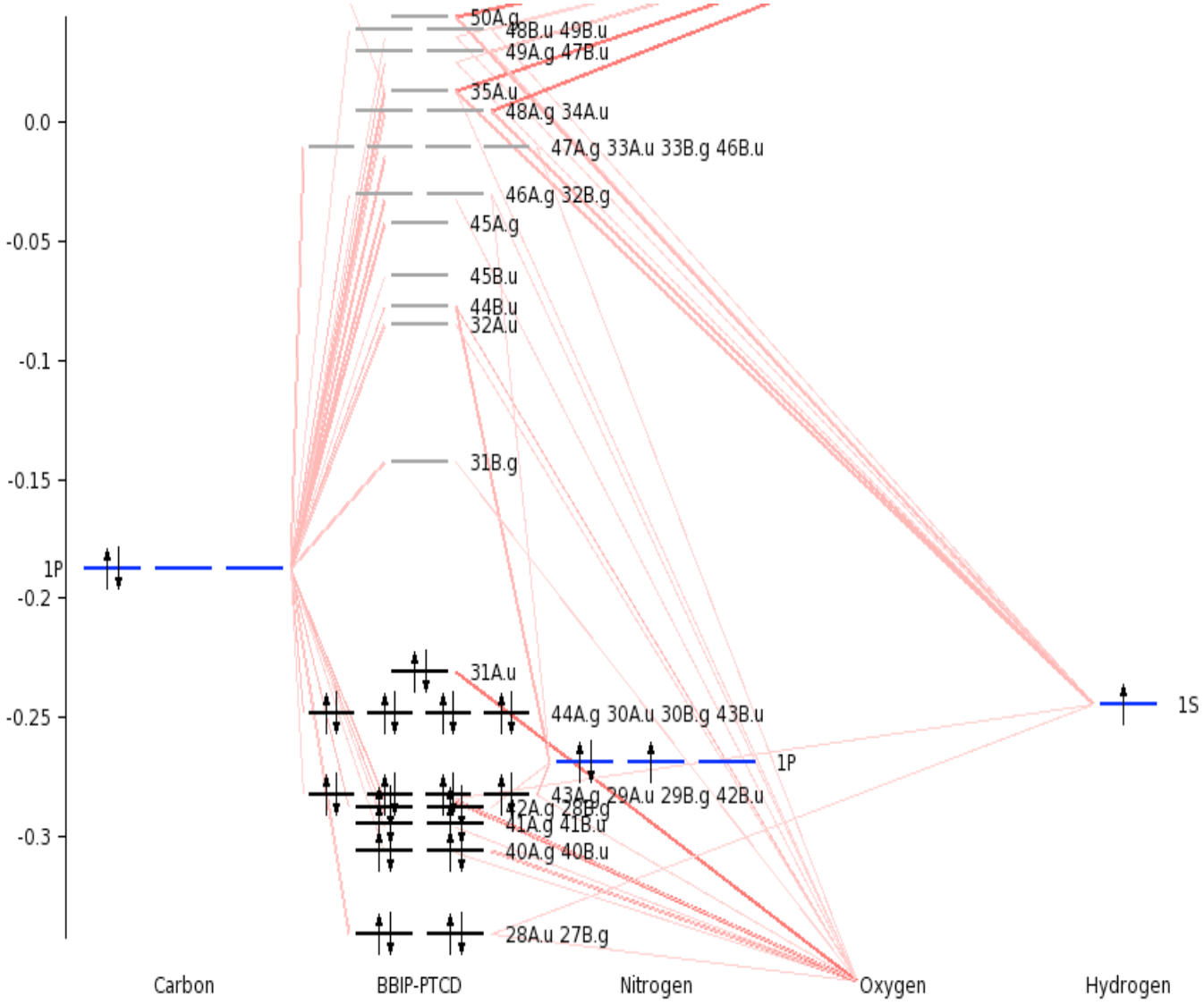

Figure 30: Excitation energies, BBIP-PTCD

C.3.4 Infrared Spectrum

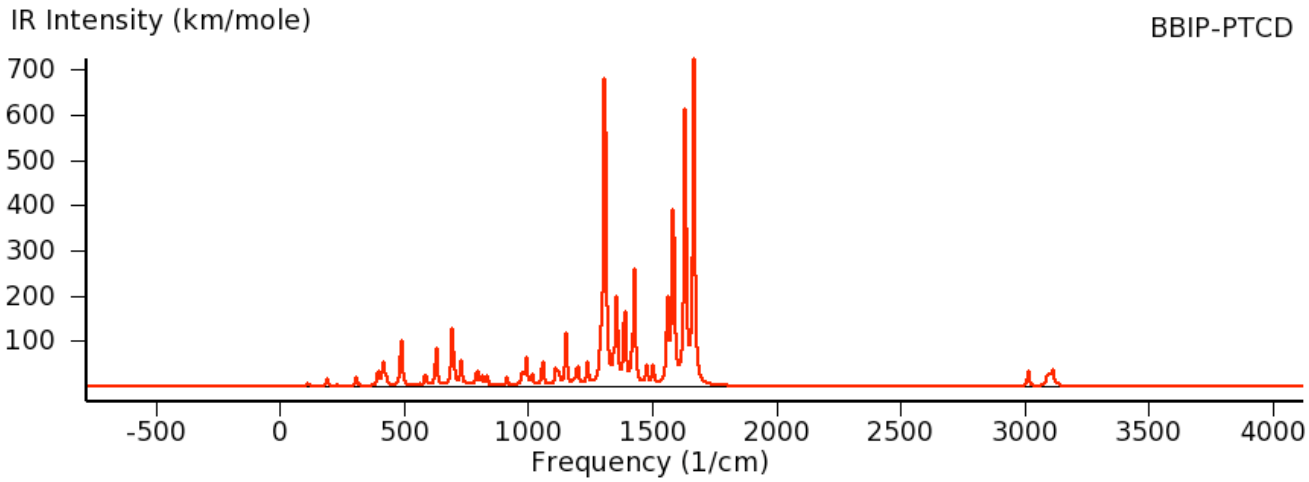

Figure 31: IR spectrum, BBIP-PTCD

488: chromophore deformation, C–N–C scissoring, the benzene groups at both ends wagging

692: benzene at both ends wagging vigorously, chromophore hardly moving

1307: C–N–C symmetric stretching, C–C stretching, C–H in methyl groups wagging, C–H in the chromophore rocking

1355: chromophore slight deformation, C–H in the methyl groups wagging vigorously, C–H in the ring rocking

1425: C–C slight stretching, C–H in methyl groups scissoring, C–H in chromophore rocking

1560: chromophore strong deformation, C–H in the chromophore rocking

1583: C–C strong stretching, C–H in the chromophore rocking

1631: C=O antisymmetric stretching, C–N–C rocking

1666: C=O symmetric stretching, C–N–C scissoring, C–H in the methyl groups scissoring

C.3.5 Vibrational Frequencies

	Ag		
1	10.3	28	953.8
2	74.3	29	972.0
3	119.7	30	988.1
4	159.4	31	1014.9
5	177.1	32	1069.4
6	228.8	33	1151.5
7	306.0	34	1185.9
8	359.6	35	1189.5
9	412.8	36	1272.2
10	450.4	37	1289.2
11	466.4	38	1329.5
12	474.7	39	1364.2
13	529.6	40	1384.8
14	559.2	41	1425.3
15	609.5	42	1439.0
16	653.4	43	1476.0
17	692.1	44	1556.5
18	705.8	45	1566.6
19	733.2	46	1589.7
20	749.8	47	1669.0
21	807.4	48	3012.4
22	812.3	49	3079.2
23	816.8	50	3096.3
24	840.6	51	3110.4
25	907.8	52	3126.4
26	941.9	53	3142.4
27	953.8		

(a) Ag

	Bg		
1	21.2	24	1037.9
2	59.0	25	1057.0
3	87.8	26	1111.3
4	198.2	27	1130.7
5	264.6	28	1161.5
6	267.0	29	1176.5
7	383.9	30	1217.7
8	401.6	31	1289.2
9	411.3	32	1319.3
10	430.8	33	1341.2
11	448.8	34	1358.1
12	563.5	35	1438.9
13	616.6	36	1446.6
14	617.7	37	1519.3
15	686.4	38	1572.0
16	731.7	39	1592.8
17	829.1	40	1631.8
18	830.9	41	3076.2
19	839.1	42	3087.5
20	940.0	43	3102.8
21	955.1	44	3119.9
22	961.5	45	3134.0
23	1037.9		

(b) Bg

	Au		
1	19.9	24	1057.0
2	33.9	25	1110.4
3	59.4	26	1130.7
4	93.7	27	1151.1
5	120.1	28	1180.7
6	230.6	29	1237.8
7	301.6	30	1289.4
8	340.4	31	1291.3
9	401.7	32	1317.7
10	425.8	33	1322.7
11	447.4	34	1343.1
12	515.8	35	1438.9
13	604.0	36	1466.0
14	617.7	37	1501.8
15	641.2	38	1571.9
16	743.9	39	1578.2
17	768.1	40	1630.7
18	829.2	41	3076.2
19	831.0	42	3087.5
20	893.2	43	3102.8
21	953.4	44	3126.6
22	955.1	45	3142.5
23	976.1		

(c) Au

	Bu		
1	5.4	27	971.8
2	33.1	28	988.0
3	106.9	29	991.2
4	169.2	30	1014.8
5	189.2	31	1122.6
6	217.4	32	1151.4
7	307.1	33	1186.7
8	394.9	34	1197.4
9	414.6	35	1307.0
10	462.2	36	1341.6
11	487.5	37	1355.2
12	505.0	38	1387.5
13	561.6	39	1414.9
14	584.5	40	1426.4
15	628.5	41	1475.9
16	691.8	42	1559.9
17	699.4	43	1582.7
18	728.9	44	1589.6
19	748.8	45	1665.6
20	788.9	46	3012.4
21	795.3	47	3079.2
22	812.6	48	3096.3
23	834.0	49	3110.4
24	888.6	50	3119.7
25	913.6	51	3133.9
26	962.6		

(d)

Table 25: Vibrational frequencies, BBIP-PTCD

	Freq.	Dipole	Int.		Freq.	Dipole	Int.		Freq.	Dipole	Int.
1	17.73	26.40	0.12	16	743.83	0.17	0.03	31	1291.84	63.94	20.70
2	34.20	4.38	0.04	17	767.93	30.60	5.89	32	1318.00	33.74	11.15
3	61.86	2.60	0.04	18	829.01	0.12	0.03	33	1322.84	1.30	0.43
4	93.96	0.84	0.02	19	831.25	13.06	2.72	34	1343.08	88.22	29.70
5	120.51	53.43	1.61	20	892.53	4.79	1.07	35	1439.34	10.36	3.74
6	230.93	38.87	2.25	21	952.36	0.01	0.00	36	1465.96	0.00	0.00
7	301.58	0.01	0.00	22	955.29	8.21	1.97	37	1501.16	110.73	41.67
8	340.08	1.71	0.15	23	975.88	115.88	28.35	38	1572.19	27.48	10.83
9	402.16	1.65	0.17	24	1057.49	248.33	65.82	39	1578.16	3.35	1.33
10	425.39	205.40	21.90	25	1110.16	157.62	43.86	40	1630.74	1636.44	668.90
11	446.48	2.76	0.31	26	1131.27	0.03	0.01	41	3076.45	1.16	0.90
12	515.72	0.09	0.01	27	1151.25	285.89	82.50	42	3087.88	21.25	16.45
13	604.09	0.87	0.13	28	1179.30	25.82	7.63	43	3103.10	10.40	8.09
14	617.42	0.01	0.00	29	1237.87	159.63	49.53	44	3124.83	3.16	2.47
15	641.34	0.03	0.00	30	1289.80	147.97	47.84	45	3143.04	0.30	0.24

(a) Au

	Freq.	Dipole	Int.		Freq.	Dipole	Int.		Freq.	Dipole	Int.
1	8.18	10.43	0.02	18	728.97	306.18	55.94	35	1307.02	2721.36	891.55
2	35.63	131.16	1.17	19	749.01	24.65	4.63	36	1340.94	28.47	9.57
3	107.45	261.01	7.03	20	789.10	89.84	17.77	37	1354.91	608.39	206.62
4	169.55	0.19	0.01	21	795.38	125.14	24.95	38	1387.48	568.93	197.86
5	189.62	323.83	15.39	22	812.65	103.08	21.00	39	1414.84	80.37	28.50
6	218.14	12.46	0.68	23	833.61	96.22	20.10	40	1425.25	733.14	261.91
7	307.13	288.84	22.24	24	888.65	6.38	1.42	41	1476.42	107.43	39.76
8	394.66	420.18	41.57	25	913.63	81.67	18.70	42	1559.60	526.62	205.87
9	415.11	507.51	52.81	26	961.66	9.94	2.40	43	1582.54	1211.31	480.49
10	462.32	3.64	0.42	27	972.10	16.00	3.90	44	1589.83	48.81	19.45
11	487.75	993.65	121.48	28	988.35	6.95	1.72	45	1665.61	1713.59	715.41
12	505.09	4.39	0.56	29	991.40	239.24	59.45	46	3012.66	48.12	36.34
13	561.63	19.25	2.71	30	1014.69	106.76	27.15	47	3078.75	0.21	0.16
14	584.65	219.61	32.18	31	1121.83	95.57	26.87	48	3095.86	31.24	24.24
15	628.75	611.11	96.31	32	1151.79	101.81	29.39	49	3110.24	42.59	33.20
16	692.64	662.93	115.09	33	1186.79	13.72	4.08	50	3119.65	7.68	6.00
17	699.70	227.71	39.94	34	1197.18	177.43	53.24	51	3133.02	5.45	4.28

(b) Bu

Table 26: Dipole moment & infrared intensities, BBIP-PTCD

C.3.6 Normal Raman Spectrum

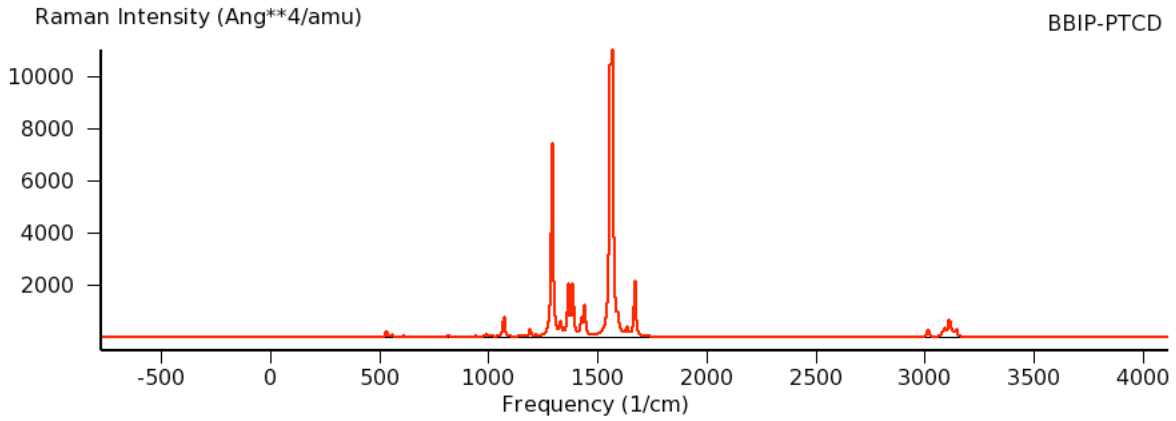

Figure 32: Normal Raman spectrum, BBIP-PTCD

1290: The central benzene in the chromophore expanding and contracting symmetrically with the C–H on each end of the benzene ring scissoring, other benzene groups hardly moving

1364: chromophore symmetrically expanding and contracting, C–H in the methyl groups wagging vigorously, C–H in the chromophore rocking

1385: chromophore symmetric stretching, C–H in the methyl groups wagging, C–H in the chromophore scissoring

1557: chromophore symmetric stretching, C–H in the chromophore scissoring

1566: chromophore symmetric expansion and contraction, C=O slightly stretching, C–H in the chromophore rocking

3110: C–H in the benzene groups at both ends stretches symmetrically, chromophore hardly moves

C.3.7 Normal Raman Intensities and Depolarization Ratio

	Freq.	Int.	Ratio		Freq.	Int.	Ratio		Freq.	Int.	Ratio
1	16.90	18.29	0.64	18	705.92	21.72	0.47	35	1271.44	48.95	0.55
2	75.26	2.10	0.49	19	733.07	0.94	0.43	36	1289.92	8158.81	0.29
3	119.87	1.16	0.73	20	749.99	5.01	0.21	37	1329.21	487.90	0.26
4	159.87	4.96	0.56	21	807.46	16.59	0.04	38	1363.95	1937.22	0.26
5	177.72	24.93	0.68	22	812.51	3.37	0.70	39	1384.69	2106.02	0.33
6	229.15	4.26	0.46	23	816.89	48.30	0.14	40	1423.98	675.92	0.34
7	306.14	3.45	0.71	24	840.63	3.68	0.75	41	1439.05	1124.53	0.29
8	359.62	2.47	0.74	25	907.75	17.15	0.14	42	1476.52	29.58	0.35
9	413.13	6.12	0.39	26	941.84	43.99	0.33	43	1556.66	11772.96	0.38
10	450.63	3.34	0.30	27	952.75	4.05	0.74	44	1566.09	9034.15	0.34
11	466.67	1.17	0.53	28	972.31	6.34	0.21	45	1589.89	169.87	0.46
12	474.96	3.27	0.72	29	988.50	164.16	0.12	46	1669.05	2339.73	0.27
13	529.83	268.49	0.14	30	1014.70	30.85	0.13	47	3012.69	381.00	0.10
14	559.40	84.05	0.22	31	1068.76	1016.94	0.30	48	3078.75	108.12	0.75
15	609.61	45.00	0.18	32	1151.88	30.68	0.70	49	3095.87	113.75	0.46
16	653.49	7.39	0.10	33	1185.87	78.13	0.53	50	3110.26	832.24	0.09
17	692.98	0.81	0.50	34	1189.47	240.47	0.17	51	3124.68	141.08	0.11

(a) Ag

	Freq.	Int.	Ratio		Freq.	Int.	Ratio		Freq.	Int.	Ratio
1	20.58	9.10	0.75	16	731.54	1.32	0.74	31	1319.63	1.04	0.75
2	61.20	18.27	0.75	17	828.64	2.58	0.75	32	1341.17	30.20	0.75
3	88.03	1.73	0.69	18	831.15	1.28	0.75	33	1358.02	14.88	0.73
4	198.75	3.65	0.68	19	838.74	7.76	0.74	34	1439.32	2.69	0.75
5	264.51	0.83	0.75	20	939.33	5.21	0.74	35	1446.12	49.91	0.75
6	266.87	17.79	0.75	21	955.34	0.69	0.60	36	1519.12	2.90	0.73
7	384.00	27.97	0.75	22	960.53	3.66	0.72	37	1572.29	39.71	0.75
8	402.13	0.18	0.73	23	1037.90	0.75	0.73	38	1592.72	339.28	0.75
9	410.75	1.15	0.75	24	1057.48	0.87	0.74	39	1631.88	309.51	0.75
10	430.80	1.48	0.75	25	1111.00	0.89	0.63	40	3076.45	63.00	0.75
11	447.92	0.34	0.72	26	1131.27	10.19	0.75	41	3087.88	256.07	0.75
12	563.80	9.98	0.75	27	1160.65	10.99	0.75	42	3103.09	20.85	0.75
13	616.62	0.24	0.74	28	1177.38	0.54	0.74	43	3119.82	109.05	0.75
14	617.41	7.92	0.75	29	1217.09	69.57	0.75	44	3133.14	62.94	0.75
15	686.23	0.10	0.66	30	1289.51	13.72	0.75				

(b) Bg

Table 27: Raman intensities and depolarization ratio, BBIP-PTCD

C.3.8 Mulliken & Hirshfeld &VDD

Atom	Charge	Atom	Charge	Atom	Charge
1 C	-0.0099	23 C	-0.1055	45 H	-0.1311
2 C	0.2332	24 C	0.0297	46 H	-0.1584
3 C	0.2151	25 C	-0.0047	47 C	-0.0375
4 C	-0.1055	26 C	-0.0099	48 C	0.2155
5 C	0.2151	27 H	-0.1397	49 C	0.1757
6 C	0.2332	28 H	-0.1905	50 C	0.1706
7 C	-0.0099	29 C	0.6312	51 C	0.1757
8 C	-0.0047	30 H	-0.1905	52 C	0.2155
9 C	0.0297	31 H	-0.1397	53 H	-0.1584
10 C	-0.1055	32 C	0.6312	54 H	-0.1823
11 H	-0.1905	33 N	-0.4090	55 H	-0.1767
12 H	-0.1397	34 N	-0.4090	56 H	-0.1823
13 C	0.6312	35 O	-0.5600	57 C	-0.0375
14 H	-0.1397	36 O	-0.5600	58 C	0.2155
15 H	-0.1905	37 O	-0.5600	59 C	0.1757
16 C	0.6312	38 O	-0.5600	60 C	0.1706
17 C	-0.1055	39 C	0.4410	61 C	0.1757
18 C	0.2151	40 H	-0.1584	62 C	0.2155
19 C	0.2332	41 H	-0.1311	63 H	-0.1584
20 C	-0.0099	42 H	-0.1311	64 H	-0.1823
21 C	0.2332	43 C	0.4410	65 H	-0.1767
22 C	0.2151	44 H	-0.1311	66 H	-0.1823

(a) Mulliken

Atom	Charge	Atom	Charge	Atom	Charge
1 C	0.0130	23 C	0.1578	45 H	0.0494
2 C	-0.0337	24 C	0.1578	46 H	0.0549
3 C	-0.0231	25 C	-0.0237	47 C	0.0398
4 C	-0.0080	26 C	-0.0237	48 C	0.0447
5 C	-0.0231	27 H	-0.0005	49 C	0.0447
6 C	-0.0337	28 H	-0.0413	50 C	0.0447
7 C	0.0130	29 C	-0.0439	51 C	0.0447
8 C	0.0072	30 H	-0.0433	52 C	0.0398
9 C	0.0105	31 H	-0.0439	53 H	0.0398
10 C	-0.0080	32 C	-0.0413	54 H	0.0444
11 H	0.1578	33 N	-0.0005	55 H	0.0438
12 H	0.1578	34 N	-0.0413	56 H	0.0444
13 C	-0.0080	35 O	-0.0439	57 C	0.0398
14 H	-0.0231	36 O	-0.0433	58 C	0.0444
15 H	-0.0337	37 O	-0.0439	59 C	0.0438
16 C	0.0130	38 O	-0.0413	60 C	0.0444
17 C	-0.0337	39 C	0.0494	61 C	-0.0260
18 C	-0.0231	40 H	0.0549	62 C	-0.0260
19 C	-0.0080	41 H	0.0549	63 H	-0.2351
20 C	0.0105	42 H	0.0494	64 H	-0.2351
21 C	0.0072	43 C	0.0549	65 H	-0.2351
22 C	0.0130	44 H	0.0494	66 H	-0.2351

(b) Hishfeld

Table 28: Charge analysis, BBIP-PTCD

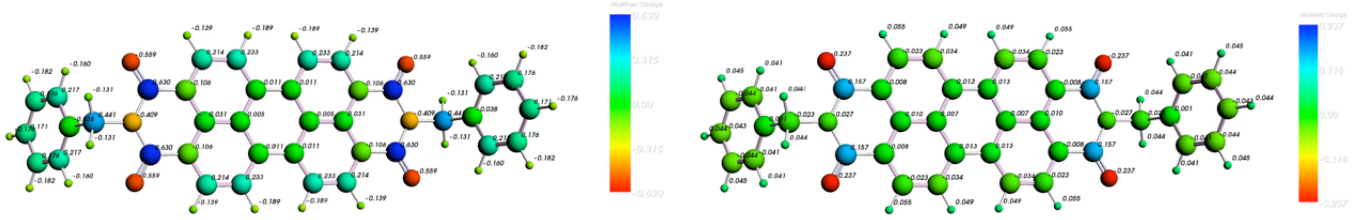

(a) Mulliken (b) Hirshfeld

Figure 33: Charge analysis, BBP-PTCD

C.3.9 Voronoi Charge

Atom	Sphere	RestCell	Total	VDD	Atom	Sphere	RestCell	Total	VDD
1 C	-2.207	-3.768	0.026	0.007	34 N	-3.046	-4.120	-0.166	-0.046
2 C	-2.209	-3.305	0.486	-0.047	35 O	-3.401	-4.984	-0.385	-0.267
3 C	-2.209	-3.282	0.509	-0.031	36 O	-3.401	-4.984	-0.385	-0.267
4 C	-2.210	-3.788	0.003	-0.027	37 O	-3.401	-4.984	-0.385	-0.267
5 C	-2.209	-3.282	0.509	-0.031	38 O	-3.401	-4.984	-0.385	-0.267
6 C	-2.209	-3.305	0.486	-0.047	39 C	-2.204	-2.737	1.059	-0.025
7 C	-2.207	-3.768	0.026	0.007	40 H	-0.119	-1.378	-0.497	0.054
8 C	-2.208	-3.790	0.002	0.008	41 H	-0.120	-1.373	-0.493	0.072
9 C	-2.208	-3.773	0.019	0.014	42 H	-0.120	-1.373	-0.493	0.072
10 C	-2.210	-3.788	0.003	-0.027	43 C	-2.204	-2.737	1.059	-0.025
11 H	-0.121	-1.364	-0.485	0.067	44 H	-0.120	-1.373	-0.493	0.072
12 H	-0.119	-1.366	-0.484	0.081	45 H	-0.120	-1.373	-0.493	0.072
13 C	-2.200	-3.437	0.364	0.174	46 H	-0.119	-1.378	-0.497	0.054
14 H	-0.119	-1.366	-0.484	0.081	47 C	-2.206	-3.761	0.033	-0.024
15 H	0.121	-1.364	-0.485	0.067	48 C	-2.207	-3.308	0.485	-0.045
16 C	-2.200	-3.437	0.364	0.174	49 C	-2.208	-3.303	0.489	-0.053
17 C	-2.210	-3.788	0.003	-0.027	50 C	-2.207	-3.303	0.490	-0.051
18 C	-2.209	-3.282	0.509	-0.031	51 C	-2.208	-3.303	0.489	-0.053
19 C	-2.209	-3.305	0.486	-0.047	52 C	-2.207	-3.308	0.485	-0.045
20 C	-2.207	-3.768	0.026	0.007	53 H	-0.119	-1.378	-0.497	0.054
21 C	-2.209	-3.305	0.486	-0.047	54 H	-0.120	-1.369	-0.488	0.051
22 C	-2.209	-3.282	0.509	-0.031	55 H	-0.120	-1.369	-0.489	0.051
23 C	-2.210	-3.788	0.003	-0.027	56 H	-0.120	-1.369	-0.488	0.051
24 C	-2.208	-3.773	0.019	0.014	57 C	-2.206	-3.761	0.033	-0.024
25 C	-2.208	-3.790	0.002	0.008	58 C	-2.207	-3.308	0.485	-0.045
26 C	-2.207	-3.768	0.026	0.007	59 C	-2.208	-3.303	0.489	-0.053
27 H	-0.119	-1.366	-0.484	0.081	60 C	-2.207	-3.303	0.490	-0.051
28 H	-0.121	-1.364	-0.485	0.067	61 C	-2.208	-3.303	0.489	-0.053
29 C	-2.200	-3.437	0.364	0.174	62 C	-2.207	-3.308	0.485	-0.045
30 H	-0.121	-1.364	-0.485	0.067	63 H	-0.119	-1.378	-0.497	0.054
31 H	-0.119	-1.366	-0.484	0.081	64 H	-0.120	-1.369	-0.488	0.051
32 C	-2.200	-3.437	0.364	0.174	65 H	-0.120	-1.369	-0.489	0.051
33 N	-3.046	-4.120	-0.166	-0.046	66 H	-0.120	-1.369	-0.488	0.051

Table 29: Voronoi charge, BBIP-PTCD

C.3.10 Electron Density & Electrostatic Potential at Nuclei

Atom	Potential	Atom	Potential	Atom	Potential
1 C	14.71955668	23 C	14.73359831	45 H	1.09737469
2 C	14.73868184	24 C	14.72621055	46 H	1.11179148
3 C	14.74098078	25 C	14.72381509	47 C	14.76839092
4 C	14.73359831	26 C	14.71955668	48 C	14.78228525
5 C	14.74098078	27 H	1.07442203	49 C	14.77942114
6 C	14.73868184	28 H	1.06651722	50 C	14.77887119
7 C	14.71955668	29 C	14.65265096	51 C	14.77942114
8 C	14.72381509	30 H	1.06651722	52 C	14.78228525
9 C	14.72621055	31 H	1.07442203	53 H	1.11179148
10 C	14.73359831	32 C	14.65265096	54 H	1.10881719
11 H	1.06651722	33 N	18.32441014	55 H	1.10825647
12 H	1.07442203	34 N	18.32441014	56 H	1.10881719
13 C	14.65265096	35 O	22.36982262	57 C	14.76839092
14 H	1.07442203	36 O	22.36982262	58 C	14.78228525
15 H	1.06651722	37 O	22.36982262	59 C	14.77942114
16 C	14.65265096	38 O	22.36982262	60 C	14.77887119
17 C	14.73359831	39 C	14.73040321	61 C	14.77942114
18 C	14.74098078	40 H	1.11179148	62 C	14.78228525
19 C	14.73868184	41 H	1.09737469	63 H	1.11179148
20 C	14.71955668	42 H	1.09737469	64 H	1.10881719
21 C	14.73868184	43 C	14.73040321	65 H	1.10825647
22 C	14.74098078	44 H	1.09737469	66 H	1.10881719

(a) Electrostatic potential

Atom	Density	Atom	Density	Atom	Density
1 C	126.52016	23 C	126.5192	45 H	0.50119
2 C	126.52661	24 C	126.51534	46 H	0.49764
3 C	126.5506	25 C	126.50161	47 C	126.50974
4 C	126.5192	26 C	126.52016	48 C	126.53435
5 C	126.5506	27 H	0.49689	49 C	126.52268
6 C	126.52661	28 H	0.50484	50 C	126.52094
7 C	126.52016	29 C	126.55043	51 C	126.52268
8 C	126.50161	30 H	0.50484	52 C	126.53435
9 C	126.51534	31 H	0.49689	53 H	0.49764
10 C	126.5192	32 C	126.55043	54 H	0.49995
11 H	0.50484	33 N	204.81878	55 H	0.4999
12 H	0.49689	34 N	204.81878	56 H	0.49995
13 C	126.55043	35 O	311.49717	57 C	126.50974
14 H	0.49689	36 O	311.49717	58 C	126.53435
15 H	0.50484	37 O	311.49717	59 C	126.52268
16 C	126.55043	38 O	311.49717	60 C	126.52094
17 C	126.5192	39 C	126.41597	61 C	126.52268
18 C	126.5506	40 H	0.49764	62 C	126.53435
19 C	126.52661	41 H	0.50119	63 H	0.49764
20 C	126.52016	42 H	0.50119	64 H	0.49995
21 C	126.52661	43 C	126.41597	65 H	0.4999
22 C	126.5506	44 H	0.50119	66 H	0.49995

(b) Electron density

Table 30: Electron density, BBIP-PTCD

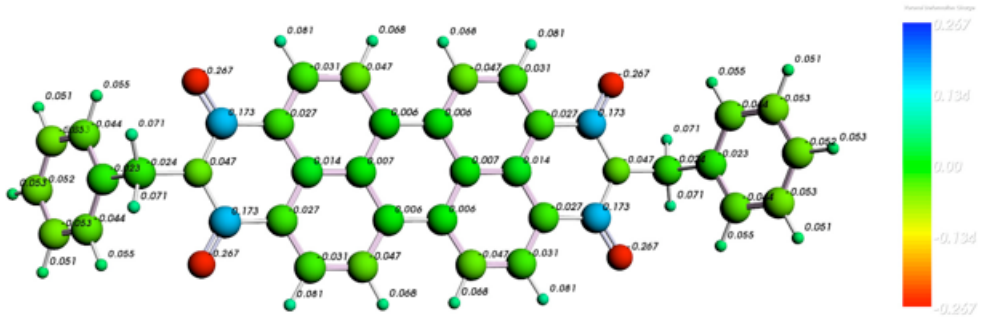

(a) VDD

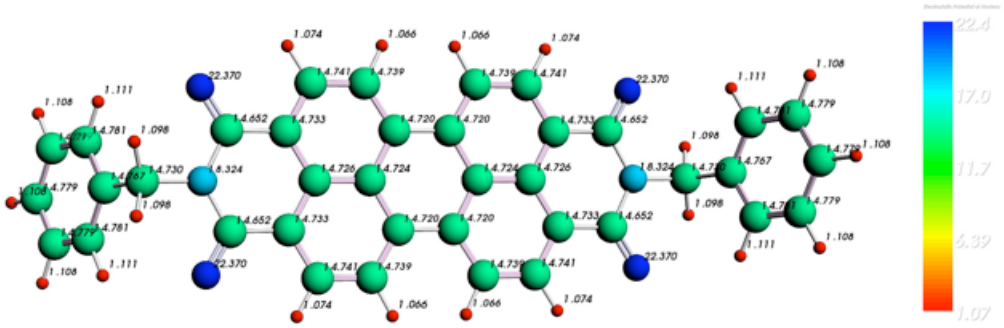

(b) Electrostatic Potential

Figure 34: VDD & electrostatic potential, BBIP-PTCD

C.3.11 Entropy, Internal Energy, Heat Capacity & Moment of Inertia & Moment of Inertia & Dipole Moment & Hyperpolarizability

Temp. = 298.15 K, Pressure = 1 atm	Translational	Rotational	Vibrational	Total
Entropy(cal/mole-K)	44.907	37.382	105.622	187.911
Internal Energy(Kcal/mole)	0.889	0.889	323.791	325.568
Constant Volume Heat Capacity (cal/mole-K)	2.981	2.981	121.720	127.682

(a) Entropy, internal energy and heat capacity

	X	Y	Z
Moments of Inertia	7173.2583	67404.8139	70224.8790
Principal Axis 1	0.0038	0.0000	1.0000
Principal Axis 2	1.0000	0.0000	-0.0038
Principal Axis 3	0.0000	1.0000	0.0000

(b) Moment of inertia

	Dipole Moment (Debye)		
Vector	0.00000000	0.00000000	0.00000000
Magnitude	0.00000000		

(c) Dipole moment

	Quadrupole Moment (a.u)				
xx	xy	xz	yy	yz	zz
19.49854176	-18.79105343	0.00000000	-34.26670226	0.00000000	14.76816050

(d) Quadrupole moment

	Static Polarizability			
X	Y	Z	Average	Anisotropy
34.406865	983.119898	0.000000	588.26	1135.2
0.000000	0.000000	485.466551		
296.199974	32.676753	0.000000		

(e) Polarizability

	Static HyperPolarizability (nonzero component)					
zzz	yyz	xxz	yzy	zyy	xzx	zxx
-15.898	19.527	11.018	19.527	19.527	11.018	11.018

(f) Hyperpolarizability

Table 31: Entropy, internal energy, heat capacity & moment of inertia & dipole and quadrupole moment & polarizability, BBIP-PTCD

C.3.12 Isosurfaces

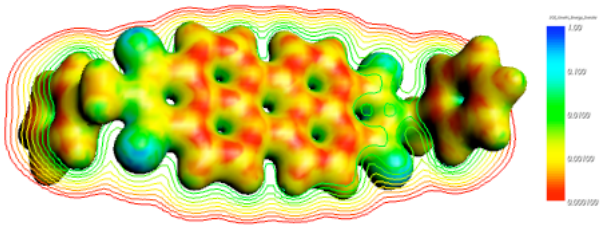

(a) Kinetic energy at density isosurface

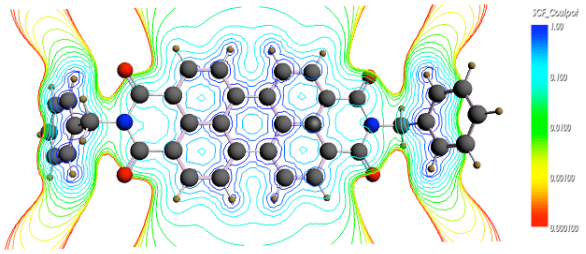

(b) Coulomb potential contours

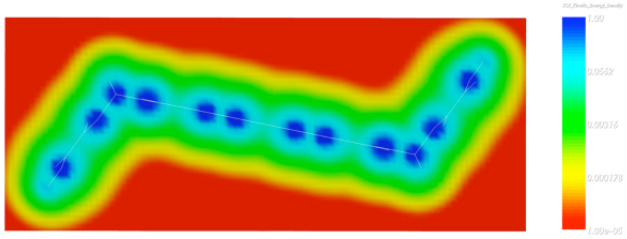

(c) Kinetic energy cut plane

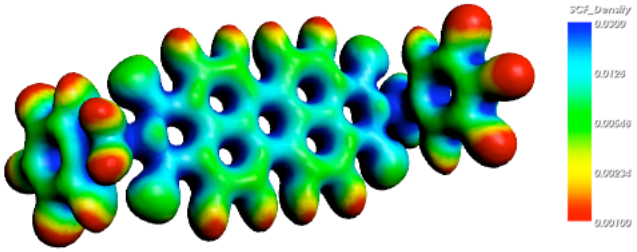

(d) ELF at density isosurface

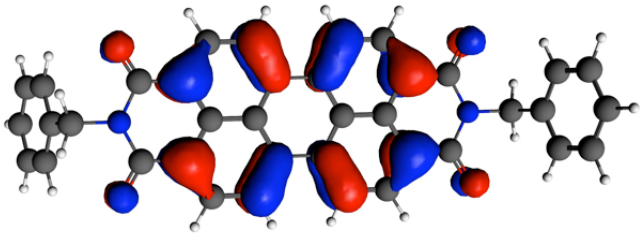

(e) HOMO

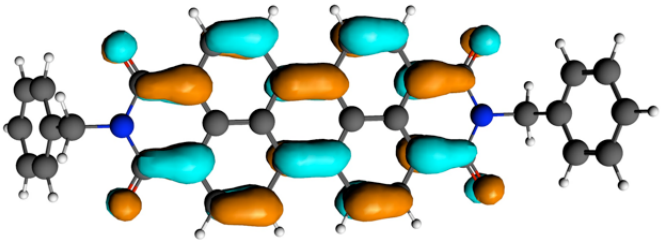

(f) LUMO

Figure 35: Isosurface, BBIP-PTCD

References

[1] J.R. Sheats, H. Antoniadis, M. Hueschen, W. Leonard, J. Miller, R. Moon, D. Roitman, A. Stocking, *Organic Electroluminescent Devices*, Chem. Rev., Science, V. 273, No. 5277, pp.884-888 (1996).

[2] G. Herzberg, *Molecular Spectra and Molecular Structure II. Infrared and Raman Spectra of Polyatomic Molecules,* Van Nostrand Reinhold Company (1945).

[3] K. Burke, J.P.Perdew, Y.Wang, in *Electronic Density Functional Theory: Recent Progress and New Directions*, J. F. Dobson, G. Vignale, M. P. Das, ed., Plenum Press, New York (1998).

[4] C.V. Raman, *A Change of Wavelength in Light Scattering*, Nature, V.121, p.619 (1928).

[5] C.V. Raman, K.S. Krishnan, *A New Type of Secondary Radiation*, Nature, V.121, p.501 (1928).

[6] E.B. Wilson, J.C. Decius, P.C. Cross, *Molecular Vibrations; The Theory of Infrared and Raman Vibrational Spectra*, McGraw-Hill (1955).

[7] J.J. Sakurai, *Modern Quantum Mechanics*, Addison-Wesley, p.333 (1994).

[8] J. Neugebauer, M. Reiher, C. Kind, B.A. Hess, *Quantum Chemical Calculation of Vibrational Spectra of Large Molecules; Raman and IR Spectra for Buckminsterfullerene*, J. Comput. Chem., V.23, pp.895-910 (2002).

[9] D.J. Willock, *Molecular Symmetry*, John Wiley & Sons (2009).

[10] D.J. Griffiths, *Introduction to Quantum Mechanics*, Pearson Education International, 2nd ed., p.349 (2005).

[11] E. Smith, G. Dent, *Modern Raman Spectroscopy*, John Wiley & Sons (2005).

[12] L. Rayleigh, *On the Light From the Sky; its Polarization and Colour*, Philos. Mag., V.41, pp.107-120 (1871).

[13] A.M. Kelley, *Hyper-Raman Scattering by Molecular Vibrations*, Ann. Rev. Phys. Chem., V.61, pp.41-61 (2010).

[14] P.P. Shorygin, L.L. Krushinskij, *Early Days and Later Development of Resonance Raman Spectroscopy,* J. Raman Spectrosc. V.28, pp.383-388 (1997).

[15] S.A. Asher, *UV Resonance Raman Studies of Molecular Structure and Dynamics*, Ann. Rev. Phys. Chem., V.39, pp.537-588 (1988).

[16] G. Placzek, *Rayleigh Scattering and Raman Effect*, Handbook of Radiology, pp.205-374 (1934).

[17] P.F. Bernath, *Spectra of Atoms and Molecules*, Oxford University Press, 2nd ed., p.301 (2005).

[18] J.J. Sakurai, *Advanced Quantum Mechanics*, Pearson Education, p.50 (1967).

[19] P.A.M. Dirac, *The Quantum Theory of Dispersion*, Proc. Roy. Soc. Lond. A, V.114, No.769, pp.710-728 (1927).

[20] A.B. Myers, *Resonance Raman Intensity Analysis of Excited-State Dynamics*, Acc. Chem. Res., V.30, pp.519-527 (1997).

[21] T.Venkatarayudu, *The Rule of Mutual Exclusion,* J. Chem. Phys., V.22, p.1269 (1954).

[22] D.J. Griffiths, *Introduction to Quantum Mechanics*, Pearson Education International, 2nd ed., p.256 (2005).

[23] G.Herzberg, E.Teller, *Vibrational Structure of Electronic Transitions for Polyatomic Molecules*, Z. Phys. Chem. B, V.21, pp.410-446 (1933).

[24] A.C. Albrecht, *On the Theory of Raman Intensities*, J. Chem. Phys., V.34, p.1476 (1961).

[25] D.A. Long, *The Raman Effect; A Unified Treatment of the Theory of Raman Scattering by Molecules,* Wiley & Sons (2001), p.72.

[26] J. Neugebauer, M. Reiher, C. Kind, B.A. Hess, *Quantum Chemical Calculation of Vibrational Spectra of Large Molecules; Raman and IR Spectra for Buckminsterfullerene*, J. Comput. Chem., V.23, pp.895-910 (2002).

[27] L.D. Ziegler, *On the Difference Between Resonance Raman Scattering and Resonance Fluorescence in Molecules: An Experimental View*, Acc. Chem. Res., V.27, No.1, pp.1-8 (1994).

[28] R. Schweitzer-Stenner, *Structure and Dynamics of Biomolecules Probed by Raman Spectroscopy*, J. Raman Spec., V.36, pp.276-278 (2005).

[29] D.A. Long, *The Raman Effect; A Unified Treatment of the Theory of Raman Scattering by Molecules,* Wiley & Sons, p.83 (2001).

[30] D.J. Willock, *Molecular Symmetry,* John Wiley & Sons, p.339 (2009).

[31] S.P.A. Fodor, R.P.Rava, T.R. Hays, T.G. Spiro, *Ultraviolet Resonance Raman Spectroscopy of the Nucleotides with 266-, 240-, 218-, and 200-nm Pulsed Laser Excitation*, J. Am. Chem. Soc. V.107, pp.1520-1529 (1985).

[32] J. Tang, A.C. Albrecht, *Studies in Raman Intensity Theory*, J. Chem. Phys., V.49, pp.1144-1154 (1968).

[33] A.C. Albrecht, M.C. Hutley, *On the Dependence of Vibrational Raman Intensity on the Wavelength of Incident Light,* J. Chem. Phys. V.55, pp.4438-4443 (1971).

[34] M. Harrand, R. Lennuier, Comptes Rendus Academy of Sciences, V.223, p.356 (1946).

[35] L. Jensen, L. Zhao, J. Autschbach, G.C. Schatz, *Theory and Method for Calculating Resonance Raman Scattering from Resonance Polarizability Derivatives*, J. Chem. Phys., V.123, p.174110 (2005).

[36] J. Neugebauer, E.J. Baerends, E. Efremov, F. Ariese, C. Gooijer, *Combined Theoretical and Experimental Deep-UV Resonance Raman Studies of Substituted Pyrenes*, J. Phys. Chem. A, V.109, pp.2100-2106 (2005).

[37] L. Jensen, L. Zhao, J. Autschbach and G.C. Schatz, *Resonance Raman Scattering of Rhodamine 6G as Calculated Using Time-Dependent Density Functional Theory*, J. Phys. Chem. A, V.110, p.5973 (2006).

[38] K.A. Kane, L. Jensen*, Calculation of Absolute Resonance Raman Intensities; Vibronic Theory vs Short-Time Approximation*, J. Phys. Chem. C, V.114, pp.5540-5546 (2010).

[39] P.A.M. Dirac, *Quantum Mechanics of Many-Electron Systems*. Proc. R. Soc. A., V.123, p.714 (1929).

[40] M. Born, J.R. Oppenheimer, *On the Quantum Theory of Molecules*, Ann. Phys., V.84, p.457 (1927).

[41] L.H. Thomas, *The Calculation of Atomic Fields*. Proc. Cambridge Phil. Soc., V.23, p.542-548 (1927).

[42] E. Fermi, *A Statistical Method for the Determination of Some Properties of the Atom and its Application to the Theory of the Periodic System of the Elements*, Z. Phys., V.48, pp.73-79 (1928).

[43] P.A.M. Dirac, *Note on the Exchange Phenomena in the Thomas Atom*, Proc. Cambridge Philos. Soc., V.26, p.376 (1930).

[44] C. von Weizsacker, *On the Theory of Nuclear Masses*, Z. Phys., V.96, p.431 (1935).

[45] D.R. Hartree, *The Wave Mechanics of An atom with Non-Coulombic Central Field; Parts I, II, III,* Proc. Cambridge Phil. Soc., V.24. pp.89-111 (1928).

[46] V. Fock, *Approximation Method for Solving the Quantum Mechanical Multibody Problems*, Z. Phys., V.61, pp.126-148 (1930).

[47] J.C. Slater, *A simplification of the Hartree-Fock method*, Phys. Rev., V.81, p.385 (1951).

[48] A. Szabo, N.S. Ostlund, *Modern Quantum Chemistry*, Mcmillan Publishing Company (1982).

[49] C.D. Sherrill, H.F. Schaefer, *The Configuration Interaction Method, Advances in Highly Correlated Approaches,* Adv. in Quan. Chem., V.34, pp.143-269 (1999).

[50] F. Jensen, *Introduction to Computational Chemistry*. 2nd ed., John Wiley & Sons (2007).

[51] J.C. Slater, Phys. *The Theory of Complex Spectra*, Rev. V.34, p.1293 (1929).

[52] N. Argaman, G. Makov, *Density Functional Theory; An Introduction*, Am. J. Phys., V.68, p.69 (2000).

[53] M.M. Morrell, R.G. Parr, M. Levy, *Calculation of Ionization Potentials From Density Matrices and Natural Functions, and the Long-Range Behavior of Natural Orbitals and Electron Density*, M. J. Chem. Phys., V.62, p.549 (1975).

[54] P. Hohenberg, W. Kohn, *Inhomogeneous Electron Gas,* Phys. Rev. B, V.136, pp.864-871 (1964).

[55] W.Kohn, L.J. Sham, *Self-Consistent Equations Including Exchange and Correlation Effects*, Phys. Rev., V.140, pp.A1133-A1138 (1965).

[56] T. Kato, *On the Eigenfunctions of Many Particle Systems in Quantum Mechanics*, Commun. Pure Appl. Math., V.10, pp.151-171 (1957).

[57] A.D. Becke, *Density Functional Thermochemistry III, The Role of Exact Exchange*. J. Chem. Phys., V.98, p.5648 (1993).

[58] J.P. Perdew, W. Yue, *Accurate and Simple Density Functional for the Electronic Exchange Energy; Generalized Gradient Approximation*. Phys. Rev. B, V.33, p.8822 (1986).

[59] R.G. Parr, W. Yang, *Density Functional Theory of Atoms and Molecules*, Oxford University Press, p.271 (1989).

[60] U.V. Barth, L. Hedin, *A Local Exchange-Correlation Potential for the Spin Polarized Case*, J. Phys. C, V.5, p.1629 (1972).

[61] R.O. Jones, O. Gunnarsson, *Density Functional Formalism; Sources of Error in Local Density Approximations*, Phys. Rev. Lett. V.55, No.1, pp.107-110 (1985).

[62] J.P. Perdew, *Density Functional Approximation for the Correlation Energy of the Inhomogeneous Electron Gas*, Phys. Rev. B, V.33, p.8822 (1986).

[63] A.D. Becke, *Density Functional Exchange Energy Approximation with Correct Asymptotic Behavior,* Phys. Rev. A, V.38, p.3098 (1988).

[64] K. Burke, J. Werschnik, E.K.U. Gross, *Time-Dependent Density Functional Theory, Past, Present, and Future*, J. Chem. Phys., V.123, p.062206 (2005).

[65] R. van Leeuwen, *Key Concepts in Time-Dependent Density Functional Theory*, Int. J. Mod. Phys. B, V.15, p.1969 (2001).

[66] E. Runge, E.K.U. Gross, *Density Functional Theory for Time Dependent Systems*, Phys. Rev. Lett., V.52, p.997 (1984).

[67] E.J. Baerends, J. Autschbach, A. Bérces, C. Bo, P.M. Boerrigter, L. Cavallo, D.P. Chong, L. Deng, R.M. Dickson, D.E. Ellis et al., *Amsterdam Density Functional.*

[68] G. te Velde, F.M. Bickelhaupt, E.J. Baerends, C.F. Guerra, S.J.A. van Gisbergen, J.G. Snijders, T. Ziegler, *Chemistry with ADF*, J. Comput. Chem., V.22, p.931-967 (2001).

[69] S. Heutz, G. Salvan, S.D. Silaghi, T.S. Jones, D.R.T. Zahn, *Raman Scattering as a Probe of Crystallinity in PTCDA and H2Pc Single-layer and Double-layer Thin Film Heterostructures,* J. Phys. Chem. B, V.107, pp.3782-3788 (2003).

[70] K. Akers, R. Aroca, A.M. Hor, R.O Loutfy, *Molecular Organization in Perylenetetracarboxylic Dianhydride Films*, J. Phys. Chem., V.91, pp.2954-2959 (1987).

[71] V. Bulovid, P.E. Burrows, S.R. Forrest, J.A. Cronin, M.E. Thompson, *Study of Localized and Extended Excitons in 3,4,9,10-Perylenetetracarboxylic Dianhydride (PTCDA) I. Spectroscopic Properties of Thin Films and Solutions*, Chemical Physics, V.210, pp.1-12 (1996)

[72] P.J.G. Goulet, N.P.W. Pieczonka, R. Aroca, *Overtones and Combinations in Single-Molecule Surface-Enhanced Resonance Raman Scattering Spectra*, Anal. Chem., V.75, pp.1918-1923 (2003).

[73] K. Akers, R. Aroca, A.M. Hor, R.O Loutfy, *Molecular Organization in Perylenetetracarboxylic di-imide Solid Films,* Spectrochimica Acta, V.44, No.11, p.1129 (1988).

[74] H. Langhals, *Cyclic Carboxylic Imide Structures as Structure Elements of High Stability; Novel Developments in Perylene Dye Chemistry,* Heterocycles, V.40, pp.477-500 (1995).

[75] W. Herbst, K. Hunger, *Industrial Organic Pigments*, 3rd Ed. Wiley-Vch Verlag GmbH & Co. KGaA, p.476 (2004).

[76] J.R. Ostrick, A. Dodabalapur, L. Torsi, A.J. Lovinger, E.W. Kwock, T.M. Miller, M. Galvin, M. Berggren, H.E. Katz, *Conductivity-type Anisotropy in Molecular Solids*, J. Appl. Phys., V.81, No.10, pp.6804-6808 (1997).

[77] C.W. Tang, *Two-layer Organic Photovoltaic Cell,* App. Phys. Lett. V.48, No. 2, pp.183-185 (1986).

[78] S. Ferrere, B.A. Gregg, *New Perylenes for Dye Sensitization of TiO2*, New J. Chem., V.26, pp.1155-1160 (2002).

[79] S. Ferrere, A. Zaban, B.A. Gregg, *Dye Sensitization of Nanocrystalline Tin Oxide by Perylene Derivatives,* J. Phys. Chem. B, V.101, pp.4490-4493 (1997).

[80] E.R. Davidson, D. Feller, *Basis Set Selection for Molecular Calculations*, Chem. Rev., V.86, pp.681-696 (1986).

[81] S.F. Boys, *Electronic Wave Functions. A General Method of Calculation for the Stationary States of Any Molecular System*, Proc. Royal Soc. A, V.200, pp.542-554 (1950).

[82] J.C. Slater, *Atomic Shielding Constants*, Phys. Rev., V.36, p.57-64 (1930).

[83] M. Guell, J.M. Luis, M. Sola, M. Swart, *Importance of the Basis Set for the Spin-State Energetics of Iron Complexes*, J. Phys. Chem. A, V.112, pp.6384-6391 (2008).

[84] F.A. Hamprecht, A.J. Cohen, D.J. Tozer, N.C. Handy, *Development and Assessment of New Exchange Correlation Functionals*, J. of Chem. Phys., V.109, p.6264 (1988).

[85] J. Neugebauer, B.A. Hess, *Fundamental Vibrational Frequencies of Small Polyatomic Molecules from Density Functional Calculations and Vibrational Perturbation Theory,* J. Chem. Phys., V.118, pp.7215-7225 (2003).

[86] P.J. Stephens, F.J. Devlin, C.F. Chabalowski, M. J. Frisch, *Ab Initio Calculation of Vibrational Absorption and Circular Dichroism Spectra Using Density Functional Force Fields*, J. Phys. Chem., V.98, pp.11623-11627 (1994).

[87] O.V. Gritsenko, P.R.T. Schipper, E.J. Baerends, *Approximation of the Exchange-Correlation Kohn-Sham Potential with a Statistical Average of Different Orbital Model Potentials*, Chem. Phys. Letters, V.302, pp.199-207 (1999).

[88] R. van Leeuwen, E.J. Baerends, *Exchange-Correlation Potential with Correct Asymptotic Behavior*, Phys. Rev. A, V.49, p.2421 (1994).

[89] S.J.A. van Gisbergen, V.P. Osinga, O.V. Gritsenko, R. van Leeuwen, J.G. Snijders, E.J. Baerends, *Improved Density Functional Theory Results for Frequency Dependent Polarizabilities, by the Use of an Exchange-Correlation Potential with Correct Asymptotic Behavior*, J. Chem. Phys., V.105, p.3142 (1996).

[90] T.H. Fischer, J.Almlöf, *General Methods for Geometry and Wave Function Optimization*, J. Phys. Chem., V.96, p.9768 (1992).

[91] R.S. Mulliken, *Electronic Population Analysis on LCAO-MO Molecular Wave Functions*, J. Chem. Phys., V.23, pp.1833-1840 (1955).

[92] R. Scholz, A.Y. Kobitski, T.U. Kampen, M. Schreiber, D.R.T. Zahn, G. Jungnickel, M. Elstner, M. Sternberg, T. Frauenheim, *Resonant Raman Spectroscopy of 3,4,9,10-Perylene Tetracarboxylic Dianhydride Epitaxial Films*, Phys. Rev. B, V.61, No.20, pp.13659-13669 (2000).

[93] F.L. Hirshfeld, *Bonded-atom Fragments for Describing Molecular Charge Densities*, Theoretical Chim. Act. V.44, No.2, p.129-138 (1977).

[94] C.F. Guerra, J.W. Handgraaf, E.J. Baerends, F.M. Bickelhaupt, *Voronoi Deformation Density (VDD) Charges. Assessment of the Mulliken, Bader, Hirshfeld, Weinhold and VDD Methods for Charge Analysis*, J, Comput. Chem., V.25, p.189 (2004).

[95] F.D. Proft, C. van Alsenoy, A. Peeters, W. Langenaeker, P. Geerlings, *Atomic Charges, Dipole Moments, and Fukui Functions Using the Hirshfeld Partitioning of the Electron Density,* J. Comput. Chem. V.23, pp.1198-1209 (2002).

[96] S. van Damme, P. Bultinck, S. Fias, *Electrostatic Potentials from Self-Consistent Hirshfeld Atomic Charges*, J. Chem. Theory Comput., V.5, pp.334-340 (2009).

[97] E.R. Davidson, S. Chakravorty, *A Test of the Hirshfeld Definition of Atomic Charges and Moments*, Theor. Chem. Acta., V.83, pp.319-330 (1992)

[98] R. Aroca, *Surface Enhanced Vibrational Spectroscopy*, John Wiley & Sons, p.17 (2006).

[99] L.L. Zhao, L. Jensen, G.C. Schatz, *Pyridine-Ag20 Cluster: A Model System for Studying Surface-Enhanced Raman Scattering*, J. Am. Chem. Soc., V.128, No.9, pp.2911-2919 (2006).

[100] L. Jensen, L.L. Zhao, G.C. Schatz, *Size-Dependence of the Enhanced Raman Scattering of Pyridine Adsorbed on Ag_n (n=2-8,20) Clusters*, J. Phys. Chem. C, V.111, p.4756 (2007).

[101] L.L. Zhao, L. Jensen, G.C. Schatz, *Surface-Enhanced Raman Scattering of Pyrazine at the Junction Between Two Ag-20 Nanoclusters*, Nano Lett., V.6, No.6, pp.1229-1234 (2006).

Vita Auctoris

Amin Torabi was born in 1983 in Tehran, Iran. In 2006, he obtained his Bachelour of Science in Physics from Sharif University of Technology in Tehran, Iran. In 2009, he began his Masters of Science in Physics at the University of Windsor in Ontario, Canada, and hopes to graduate in the fall of 2010.